

EUROPEAN ORGANISATION FOR NUCLEAR RESEARCH (CERN)



Phys. Rev. D 99 (2019) 072001
 DOI: [10.1103/PhysRevD.99.072001](https://doi.org/10.1103/PhysRevD.99.072001)



CERN-EP-2018-232
 13th November 2019

Cross-section measurements of the Higgs boson decaying into a pair of τ -leptons in proton–proton collisions at $\sqrt{s} = 13$ TeV with the ATLAS detector

The ATLAS Collaboration

A measurement of production cross sections of the Higgs boson in proton–proton collisions is presented in the $H \rightarrow \tau\tau$ decay channel. The analysis is performed using 36.1 fb^{-1} of data recorded by the ATLAS experiment at the Large Hadron Collider at a center-of-mass energy of $\sqrt{s} = 13$ TeV. All combinations of leptonic ($\tau \rightarrow \ell\nu\bar{\nu}$ with $\ell = e, \mu$) and hadronic ($\tau \rightarrow \text{hadrons } \nu$) τ decays are considered. The $H \rightarrow \tau\tau$ signal over the expected background from other Standard Model processes is established with an observed (expected) significance of 4.4 (4.1) standard deviations. Combined with results obtained using data taken at 7 and 8 TeV center-of-mass energies, the observed (expected) significance amounts to 6.4 (5.4) standard deviations and constitutes an observation of $H \rightarrow \tau\tau$ decays. Using the data taken at $\sqrt{s} = 13$ TeV, the total cross section in the $H \rightarrow \tau\tau$ decay channel is measured to be $3.77^{+0.60}_{-0.59} (\text{stat.})^{+0.87}_{-0.74} (\text{syst.}) \text{ pb}$, for a Higgs boson of mass 125 GeV assuming the relative contributions of its production modes as predicted by the Standard Model. Total cross sections in the $H \rightarrow \tau\tau$ decay channel are determined separately for vector-boson-fusion production and gluon–gluon-fusion production to be $\sigma_{H \rightarrow \tau\tau}^{\text{VBF}} = 0.28 \pm 0.09 (\text{stat.})^{+0.11}_{-0.09} (\text{syst.}) \text{ pb}$ and $\sigma_{H \rightarrow \tau\tau}^{\text{ggF}} = 3.1 \pm 1.0 (\text{stat.})^{+1.6}_{-1.3} (\text{syst.}) \text{ pb}$, respectively. Similarly, results of a fit are reported in the framework of simplified template cross sections. All measurements are in agreement with Standard Model expectations.

1 Introduction

The ATLAS and CMS collaborations discovered [1, 2] a particle consistent with the Standard Model (SM) [3–5] Higgs boson [6–10] in 2012. Several properties of this particle, such as its coupling strengths, spin and charge-parity (CP) quantum numbers, were studied with 7 and 8 TeV center-of-mass energy (\sqrt{s}) proton–proton collision data delivered by the Large Hadron Collider (LHC) in 2011 and 2012, respectively, referred to as ‘Run 1’. These results rely predominantly on studies of the bosonic decay modes [11–14] and have not shown any significant deviations from the SM expectations.

The coupling of the Higgs boson to the fermionic sector has been established with the observation of the $H \rightarrow \tau\tau$ decay mode with a signal significance of 5.5σ from a combination of ATLAS and CMS results [15–17] using LHC Run-1 data. A measurement performed by the CMS Collaboration with Run-2 data at $\sqrt{s} = 13$ TeV reached a significance of 4.9σ using 35.9 fb^{-1} of integrated luminosity and 5.9σ combined with data from Run 1 [18]. While the Higgs-boson coupling to other fermions such as top quarks [19, 20] and bottom quarks [21, 22] have been observed, only upper limits exist on its coupling to muons [23, 24] and the $H \rightarrow \tau\tau$ decay mode has been the only accessible leptonic decay mode. It was also used to constrain CP violation in the production via vector-boson fusion (VBF) [25] and is unique in that it provides sensitivity to CP violation in the Higgs-boson coupling to leptons [26].

This paper presents cross-section times branching-fraction measurements of Higgs bosons that decay into a pair of τ -leptons in proton–proton (pp) collisions at $\sqrt{s} = 13$ TeV using data collected by the ATLAS experiment in 2015 and 2016, corresponding to an integrated luminosity of 36.1 fb^{-1} . All combinations of leptonic ($\tau \rightarrow \ell\nu\bar{\nu}$ with $\ell = e, \mu$) and hadronic ($\tau \rightarrow \text{hadrons } \nu$) τ decays are considered.¹ The corresponding three analysis channels are denoted by $\tau_{\text{lep}}\tau_{\text{lep}}$, $\tau_{\text{lep}}\tau_{\text{had}}$ and $\tau_{\text{had}}\tau_{\text{had}}$ and are composed of different dominant backgrounds. While $Z \rightarrow \tau\tau$ is a dominant background in all channels, the relative contributions from other backgrounds from top-quark and other vector-boson decays, as well as from misidentified leptonic or hadronic τ decays, vary considerably between the channels. Two analysis categories are defined that are predominantly sensitive to Higgs bosons produced via VBF and gluon–gluon fusion (ggF). A maximum-likelihood fit is performed on data using distributions of the reconstructed di- τ mass in signal regions (SRs), simultaneously with event yields from control regions (CRs) that are included to constrain normalizations of major backgrounds estimated from simulation. The dominant and irreducible $Z \rightarrow \tau\tau$ background is estimated from simulation. This is different from the search for $H \rightarrow \tau\tau$ decays in Run 1 [15], which used the embedding technique [27]. A reliable modeling of this background is therefore of crucial importance for this analysis. Validation regions (VRs) based on $Z \rightarrow \ell\ell$ events are studied, but not included in the fit, to verify as precisely as possible the modeling of the $Z \rightarrow \tau\tau$ background.

The paper is organized as follows. Section 2 describes the ATLAS detector. This is followed in Section 3 by a description of the dataset and Monte Carlo (MC) simulated samples employed by this measurement. Section 4 details the reconstruction of particles and jets. The event selection for each channel and event category as well as signal, control and validation regions are discussed in Section 5. Background estimation techniques and the systematic uncertainties of the analysis are described in Sections 6 and 7, respectively. The signal extraction procedure and the results of the Higgs cross-section measurements in the $H \rightarrow \tau\tau$ decay mode are presented in Section 8. Section 9 gives the conclusions.

¹ Throughout this paper the inclusion of charge-conjugate decay modes is implied. The symbol ℓ is used to denote electrons and muons, also referred to as ‘light leptons’.

2 The ATLAS detector

The ATLAS experiment [28] at the LHC is a multipurpose particle detector with a forward–backward symmetric cylindrical geometry and a near- 4π coverage in solid angle.² It consists of an inner tracking detector surrounded by a thin superconducting solenoid, electromagnetic and hadron calorimeters, and a muon spectrometer. The inner tracking detector covers the pseudorapidity range $|\eta| < 2.5$. It consists of a silicon pixel detector, which has an additional innermost layer (positioned at a radial distance of 3.3 cm from the beam line) that was installed after Run 1 [29, 30], and a silicon microstrip detector surrounding the pixel detector, both covering $|\eta| < 2.5$, followed by a transition radiation straw-tube tracker covering $|\eta| < 2$. The inner tracking detector is immersed in a 2 T axial magnetic field provided by the solenoid. Lead/liquid-argon (LAr) sampling calorimeters provide electromagnetic (EM) energy measurements with high granularity. A hadron (steel/scintillator-tile) calorimeter covers the central pseudorapidity range ($|\eta| < 1.7$). The endcap and forward regions are instrumented with LAr calorimeters for both the EM and hadronic energy measurements up to $|\eta| = 4.9$. The muon spectrometer surrounds the calorimeters and is based on three large air-core toroidal superconducting magnets with eight coils each. The field integral of the toroids ranges between 2.0 and 6.0 T m across most of the detector. The muon spectrometer includes a system of precision tracking chambers and fast detectors for triggering.

Events are selected using a two-level trigger system. The first-level trigger is implemented in hardware and uses a subset of the detector information to filter events that are then processed by a software-based high-level trigger. This further reduces the average recorded collision rate to approximately 1 kHz.

3 Data and simulation samples

The data used in this analysis were taken from pp collisions at the LHC where proton bunches are collided every 25 ns at $\sqrt{s} = 13$ TeV. A combination of several triggers for single light leptons, two light leptons and two hadronically decaying τ -leptons were used to record the data for the analysis, depending on the analysis channel (see Section 5.1). After data quality requirements, the samples used for this measurement consist of 3.2 fb^{-1} of data recorded in 2015, with an average of 14 interactions per bunch crossing, and 32.9 fb^{-1} recorded in 2016, with an average of 25 interactions per bunch crossing.

Samples of signal and background processes were simulated using various MC generators as summarized in Table 1. The signal contributions considered include the following four processes for Higgs-boson production at the LHC: ggF , VBF and associated production of a Higgs boson with a vector boson (VH) or with a top–antitop quark pair ($t\bar{t}H$) where all decay modes for the $H \rightarrow \tau\tau$ process are included. Other Higgs production processes such as associated production with a bottom–antibottom quark pair and with a single top quark are found to be negligible. Higgs decays into WW are considered background and simulated similarly for these production processes. The mass of the Higgs boson was assumed to be 125 GeV [31].

² The ATLAS Collaboration uses a right-handed coordinate system with its origin at the nominal interaction point (IP) in the center of the detector and the z -axis along the beam pipe. The x -axis points from the IP to the center of the LHC ring, and the y -axis points upwards. Cylindrical coordinates (r, ϕ) are used in the transverse plane, ϕ being the azimuthal angle around the z -axis. The pseudorapidity is defined in terms of the polar angle θ as $\eta = -\ln \tan(\theta/2)$. Angular distance is measured in units of $\Delta R \equiv \sqrt{(\Delta\eta)^2 + (\Delta\phi)^2}$.

Table 1: Monte Carlo generators used to describe all signal and background processes together with the corresponding PDF set and the model of parton showering, hadronization and underlying event (UEPS). In addition, the order of the total cross-section calculation is given. The total cross section for VBF production is calculated at approximate NNLO QCD. More details are given in the text.

Process	Monte Carlo generator	PDF	UEPS	Cross-section order
ggF	POWHEG-Box v2	PDF4LHC15 NNLO	PYTHIA 8.212	$N^3\text{LO}$ QCD + NLO EW
VBF	POWHEG-Box v2	PDF4LHC15 NLO	PYTHIA 8.212	$\sim\text{NNLO}$ QCD + NLO EW
VH	POWHEG-Box v2	PDF4LHC15 NLO	PYTHIA 8.212	NNLO QCD + NLO EW
$t\bar{t}H$	MG5_aMC@NLO v2.2.2	NNPDF30LO	PYTHIA 8.212	NLO QCD + NLO EW
$W/Z + \text{jets}$	SHERPA 2.2.1	NNPDF30NNLO	SHERPA 2.2.1	NNLO
$VV/V\gamma^*$	SHERPA 2.2.1	NNPDF30NNLO	SHERPA 2.2.1	NLO
$t\bar{t}$	POWHEG-Box v2	CT10	PYTHIA 6.428	NNLO+NNLL
Wt	POWHEG-Box v1	CT10F4	PYTHIA 6.428	NLO

Higgs production by ggF was simulated with the POWHEG-Box v2 [32–35] NNLOPS program [36] at next-to-leading-order (NLO) accuracy in quantum chromodynamics (QCD) using the MiNLO approach [37], and reweighted to next-to-next-to-leading order (NNLO) in QCD in the Higgs rapidity. The VBF and VH production processes were simulated at NLO accuracy in QCD using PowHEG-Box with the MiNLO approach. The $t\bar{t}H$ production process was simulated with MADGRAPH5_aMC@NLO v2.2.2 [38] at NLO accuracy in QCD. For these signal samples, the simulation was interfaced to the PYTHIA 8.212 [39] model of parton showering, hadronization and underlying event (UEPS). To estimate the impact of UEPS uncertainties, the ggF , VBF and VH samples were also simulated with the HERWIG 7.0.3 [40, 41] UEPS model. The PDF4LHC15 [42] parameterization of the parton distribution functions (PDFs) was used for these production processes. The AZNLO [43] set of tuned parameters was used, with the CTEQ6L1 [44] PDF set, for the modeling of non-perturbative effects. For the $t\bar{t}H$ production process the NNPDF30LO [45] PDF parametrization was used in the matrix element and the NNPDF23LO [46] PDF parametrization for the UEPS model with the A14 [47] set of tuned parameters for the modeling of non-perturbative effects. PHOTOS++ version 3.52 [48] was used for QED emissions from electroweak (EW) vertices and charged leptons.

The overall normalization of the ggF process is taken from a next-to-next-to-next-to-leading-order ($N^3\text{LO}$) QCD calculation with NLO EW corrections included [49–52]. Production by VBF is normalized to an approximate-NNLO QCD cross section with NLO EW corrections included [53–55]. The VH samples are normalized to cross sections calculated at NNLO in QCD, with NLO EW corrections included [56–58]. The $t\bar{t}H$ process is normalized to a cross section calculated at NLO in QCD with NLO EW corrections applied [59–64].

Background samples of EW production of W/Z bosons from VBF, W/Z -boson production with associated jets and diboson production processes were simulated with the SHERPA 2.2.1 [65] generator. Matrix elements were calculated using the Comix [66] and OpenLoops [67] matrix-element generators and merged with the SHERPA UEPS model [68] using the ME+PS@NLO prescription [69]. For W and Z production with associated jets the matrix elements were calculated for up to two partons at NLO and four partons at LO precision. Their inclusive cross sections are normalized to NNLO calculations from FEWZ [70, 71]. In particular, the dominant $Z \rightarrow \tau\tau$ background is estimated using these simulations of Z -boson production. For diboson production, the matrix elements were calculated for up to one additional parton at NLO and up to three additional partons at LO precision. For all samples the NNPDF30NNLO [45]

PDF set was used together with the **SHERPA** UEPS model.

The impact of UEPS uncertainties, and other modeling uncertainties such as LO/NLO precision comparison for leading jets, on the main background from $Z \rightarrow \tau\tau$ is studied in an alternative sample which was simulated using **MADGRAPH5_aMC@NLO** 2.2.2 [38] at leading order interfaced to the **PYTHIA** 8.186 UEPS model. The A14 set of tuned parameters [47] was used together with the NNPDF23LO PDF set [46].

For the generation of $t\bar{t}$ production, the **POWHEG-Box** v2 [32–34, 72] generator with the CT10 PDF sets in the matrix element calculations was used. The predicted $t\bar{t}$ cross section was calculated with the **Top++2.0** program to NNLO in perturbative QCD, including soft-gluon resummation to next-to-next-to-leading-log order [73]. Single top-quark production of Wt was simulated using the **POWHEG-Box** v1 [74, 75] generator. This generator uses the four-flavor scheme for the NLO matrix-element calculations together with the fixed four-flavor PDF set CT10F4. For all top-quark production processes, top-quark spin correlations were preserved, using **MadSpin** [76] for the t-channel. The parton shower, hadronization, and the underlying event were simulated using **PYTHIA** 6.428 [77] with the CTEQ6L1 PDF set and the corresponding Perugia 2012 set of tuned parameters [78]. The top mass was assumed to be 172.5 GeV. The **EvtGen** v.1.2.0 program [79] was used for the properties of b - and c -hadron decays.

For all samples, a full simulation of the ATLAS detector response [80] using the **GEANT4** program [81] was performed. The effect of multiple pp interactions in the same and neighboring bunch crossings (pileup) was included by overlaying minimum-bias events simulated with **PYTHIA** 8.186 using the MSTW2008LO PDF [82] and the A2 [83] set of tuned parameters on each generated signal and background event. The number of overlaid events was chosen such that the distribution of the average number of interactions per pp bunch crossing in the simulation matches that observed in data.

4 Object reconstruction

Electron candidates are reconstructed from energy deposits in the electromagnetic calorimeter associated with a charged-particle track measured in the inner detector. The electron candidates are required to pass the ‘loose’ likelihood-based identification selection of Refs. [84, 85], to have transverse momentum $p_T > 15$ GeV and to be in the fiducial volume of the inner detector, $|\eta| < 2.47$. The transition region between the barrel and endcap calorimeters ($1.37 < |\eta| < 1.52$) is excluded. The trigger efficiency for single electrons selected in the analysis ranges between 90% and 95% [86]. Electron candidates are ignored if they share their reconstructed track with a muon candidate defined below or if their angular distance from a jet is within $0.2 < \Delta R < 0.4$.

Muon candidates are constructed by matching an inner detector track with a track reconstructed in the muon spectrometer [87]. The muon candidates are required to have $p_T > 10$ GeV and $|\eta| < 2.5$ and to pass the ‘loose’ muon identification requirements of Ref. [87]. The trigger efficiency for single muons selected in the analysis is close to 80% (70%) in the barrel in the 2016 (2015) dataset and 90% in the endcaps [86]. Muon candidates are ignored if their angular distance from a jet is $\Delta R < 0.4$ with the following exceptions: If $\Delta R < 0.2$ or the muon track is associated with the jet, and if the jet has either less than three tracks or less than twice the transverse momentum of the muon candidate, the jet is removed instead. This recovers efficiency for muons that radiate a hard bremsstrahlung photon in the calorimeter.

In the $\tau_{\text{lep}}\tau_{\text{lep}}$ and $\tau_{\text{lep}}\tau_{\text{had}}$ signal regions, events are selected only if the selected electron and muon candidates satisfy their respective ‘medium’ identification criteria. The reconstruction and identification

efficiency for muons with the ‘medium’ identification requirement has been measured in $Z \rightarrow \mu\mu$ events [87]. It is well above 98% over the full phase space, except for $|\eta| < 0.1$ where the reconstruction efficiency is about 70%. The combined identification and reconstruction efficiency for ‘medium’ electrons ranges from 80% to 90% in the p_T range of 10 GeV to 80 GeV as measured in $Z \rightarrow ee$ events [85]. In addition, the electrons and muons must satisfy the ‘gradient’ isolation criterion, which requires that there are no additional high- p_T tracks in a cone around the track and no significant energy deposits in a cone around the calorimeter clusters of the object after correcting for pileup. The size of the respective cones depends on the p_T of the light lepton. This isolation requirement rejects about 10% of light leptons for low p_T and less than 1% for $p_T > 60$ GeV [85, 87].

Jets are reconstructed from topological clusters in the calorimeter using the anti- k_t algorithm [88, 89], with a radius parameter value $R = 0.4$, and have $p_T > 20$ GeV and $|\eta| < 4.9$. To reject jets from pileup a ‘Jet Vertex Tagger’ (JVT) [90] algorithm is used for jets with $p_T < 50$ GeV and $|\eta| < 2.4$. It employs a multivariate technique that relies on jet-tracking and calorimeter-cluster-shape variables to determine the likelihood that the jet originates from pileup. Similarly, pileup jets in the forward region are suppressed with a ‘forward JVT’ [91] algorithm, relying in this case only on calorimeter-cluster-shape variables, which is applied to all jets with $p_T < 50$ GeV and $|\eta| > 2.5$. In the pseudorapidity range $|\eta| < 2.5$, b -jets are selected using a multivariate algorithm [92, 93]. A working point is chosen that corresponds to an efficiency of approximately 85% for b -jets and rejection factors of 2.8 and 28 for c -jets and light-flavor jets, respectively, in simulated $t\bar{t}$ events. A jet is ignored if it is within $\Delta R = 0.2$ of an electron or hadronically decaying τ candidate.

Leptonic τ decays are reconstructed as electrons and muons. The reconstruction of the visible decay products of hadronic τ decays ($\tau_{\text{had-vis}}$) [94] starts with a reconstructed jet that has $p_T > 10$ GeV and $|\eta| < 2.5$. As in the case of electron reconstruction the transition region between the barrel and endcap calorimeters is excluded. To discriminate $\tau_{\text{had-vis}}$ from jets initiated by light-quarks or gluons, an identification algorithm using multivariate techniques is applied to $\tau_{\text{had-vis}}$ candidates. They have to pass the ‘loose’ identification requirement of Ref. [94]. In addition, the $\tau_{\text{had-vis}}$ candidates are required to have $p_T > 20$ GeV, to have one or three associated tracks and an absolute electric charge of one. Their energy is reconstructed by multivariate regression techniques using information about the associated tracks and calorimeter clusters, as well as the average number of collisions recorded. The trigger efficiency per $\tau_{\text{had-vis}}$ selected in the analysis is 95% and 85% for 1-prong and 3-prong τ -leptons, respectively [95]. The $\tau_{\text{had-vis}}$ candidates are ignored if they are within $\Delta R = 0.2$ of a muon or electron candidate or if they have a high likelihood score of being an electron [85]. The requirement on the likelihood score corresponds to a $\tau_{\text{had-vis}}$ efficiency measured in $Z \rightarrow \tau\tau$ decays of 95% [94].

In the $\tau_{\text{lep}}\tau_{\text{had}}$ signal regions, events are selected only if the $\tau_{\text{had-vis}}$ candidate passes the ‘medium’ identification requirement, corresponding to an efficiency of 55% and 40% for real 1-prong and 3-prong $\tau_{\text{had-vis}}$, respectively [94]. In addition, if a 1-prong $\tau_{\text{had-vis}}$ candidate and an electron candidate are selected, a dedicated multivariate algorithm to reject electrons misidentified as $\tau_{\text{had-vis}}$ is applied to suppress $Z \rightarrow ee$ events. In the $\tau_{\text{had}}\tau_{\text{had}}$ signal regions, both selected $\tau_{\text{had-vis}}$ candidates have to fulfill the ‘tight’ identification requirement, which corresponds to a selection efficiency of 45% for real 1-prong $\tau_{\text{had-vis}}$ and 30% for real 3-prong $\tau_{\text{had-vis}}$ [94].

The missing transverse momentum vector is calculated as the negative vectorial sum of the p_T of the fully calibrated and reconstructed physics objects [96]. This procedure includes a soft term, which is calculated from the inner detector tracks that originate from the vertex associated with the hard-scattering process and that are not associated with any of the reconstructed objects. The missing transverse momentum (E_T^{miss}) is defined as the magnitude of this vector.

The Higgs-boson candidate is reconstructed from the visible decay products of the τ -leptons and from the E_T^{miss} , which is assumed to originate from the final-state neutrinos. The di- τ invariant mass ($m_{\tau\tau}^{\text{MMC}}$) is determined using the missing-mass calculator (MMC) [97]. The standard deviation of the reconstructed di- τ mass is 17.0 GeV, 15.3 GeV and 14.7 GeV for signal events selected in the $\tau_{\text{lep}}\tau_{\text{lep}}$, $\tau_{\text{lep}}\tau_{\text{had}}$ and $\tau_{\text{had}}\tau_{\text{had}}$ channels, respectively. The p_T of the Higgs-boson candidate ($p_T^{\tau\tau}$) is computed as the vector sum of the transverse momenta of the visible decay products of the τ -leptons and the missing transverse momentum vector.

5 Event selection and categorization

In addition to data quality criteria that ensure that the detector was functioning properly, events are rejected if they contain reconstructed jets associated with energy deposits that can arise from hardware problems, beam-halo events or cosmic-ray showers. Furthermore, events are required to have at least one reconstructed primary vertex with at least two associated tracks with $p_T > 0.5$ GeV, which rejects non-collision events originating from cosmic rays or beam-halo events. The primary vertex is chosen as the pp vertex candidate with the highest sum of the squared transverse momenta of all associated tracks.

The triggers and event selection for the three analysis channels are described in Section 5.1. Selected events are categorized into exclusive signal regions, with enhanced signal-to-background ratios. In addition, control regions are defined where a specific background is dominant, and thus a CR facilitates the adjustment of the simulated prediction of a background contribution to match the observed data. The signal and control regions are included in the fit described in Section 8. They are described in Section 5.2 together with validation regions (VRs) used to validate the simulation of the dominant $Z + \text{jets}$ background.

5.1 Event selection

Depending on the trigger, transverse momentum requirements are applied to selected electron, muon, and $\tau_{\text{had-vis}}$ candidates. They are summarized in Table 2 and their per-object efficiencies are given in Section 4. Due to the increasing luminosity and the different pileup conditions, the p_T thresholds of the triggers were increased during data-taking in 2016, which is taken into account in the p_T requirements of the event selection. In the $\tau_{\text{lep}}\tau_{\text{lep}}$ channel, the triggers for multiple light leptons are used only if the highest- p_T light lepton does not pass the corresponding single-light-lepton trigger p_T requirement. This ensures that each trigger selects an exclusive set of events.

All channels require the exact number of identified ‘loose’ leptons, i.e. electrons, muons and $\tau_{\text{had-vis}}$, as defined in Section 4, corresponding to their respective final state. Events with additional ‘loose’ leptons are rejected. The two leptons are required to be of opposite charge and they have to fulfill the p_T requirements of the respective trigger shown in Table 2. The selected $\tau_{\text{had-vis}}$ in the $\tau_{\text{lep}}\tau_{\text{had}}$ channel is required to have $p_T > 30$ GeV.

The event selection for the three analysis channels is summarized in Table 3. Only events with $E_T^{\text{miss}} > 20$ GeV are selected to reject events without neutrinos. In the $\tau_{\text{lep}}\tau_{\text{lep}}$ channel with two same-flavor (SF) light leptons this requirement is further tightened to suppress the large $Z \rightarrow \ell\ell$ background. For the same reason, requirements are tightened on the invariant mass of two light leptons ($m_{\ell\ell}$) and a requirement is introduced on the E_T^{miss} calculated only from the physics objects without the soft track term ($E_T^{\text{miss, hard}}$).

Table 2: Summary of the triggers used to select events for the three analysis channels during 2015 and 2016 data-taking and the corresponding p_T requirements applied in the analysis. For the electron+muon trigger the first number corresponds to the electron p_T requirement, the second to the muon p_T requirement. For the $\tau_{\text{had}}\tau_{\text{had}}$ channel, at least one high- p_T jet in addition to the two $\tau_{\text{had-vis}}$ candidates is required for the 2016 dataset (see Section 5.1).

Analysis channel	Trigger	Analysis p_T requirement [GeV]	
		2015	2016
$\tau_{\text{lep}}\tau_{\text{lep}} \& \tau_{\text{lep}}\tau_{\text{had}}$	Single electron	25	27
	Single muon	21	27
$\tau_{\text{lep}}\tau_{\text{lep}}$	Dielectron	15 / 15	18 / 18
	Dimuon	19 / 10	24 / 10
	Electron+muon	18 / 15	18 / 15
$\tau_{\text{had}}\tau_{\text{had}}$	Di- $\tau_{\text{had-vis}}$	40 / 30	40 / 30

Requirements on the angular distance between the visible decay products of the two selected τ -lepton decays ($\Delta R_{\tau\tau}$) and their pseudorapidity difference ($|\Delta\eta_{\tau\tau}|$) are applied in all channels to reject non-resonant background events. Requirements are applied to the fractions of the τ -lepton momenta carried by each visible decay product $x_i = p_i^{\text{vis}} / (p_i^{\text{vis}} + p_i^{\text{miss}})$, where p_i^{vis} and p_i^{miss} are the visible and missing momenta of the i th τ lepton, ordered in descending p_T , calculated in the collinear approximation [98], to suppress events with E_T^{miss} that is incompatible with a di- τ decay. Low transverse mass (m_T), calculated from E_T^{miss} and the momentum of the selected light lepton, is required in the $\tau_{\text{lep}}\tau_{\text{had}}$ channel to reject events with leptonic W decays. A requirement on the di- τ mass calculated in the collinear approximation ($m_{\tau\tau}^{\text{coll}}$) of $m_{\tau\tau}^{\text{coll}} > m_Z - 25$ GeV is introduced in the $\tau_{\text{lep}}\tau_{\text{lep}}$ channel to suppress events from $Z \rightarrow \ell\ell$ and to ensure orthogonality between this measurement and the measurement of $H \rightarrow WW^* \rightarrow \ell\nu\ell\nu$ [99], which has a similar final state.

All channels require at least one jet (j_1) with $p_T^{j_1} > 40$ GeV to select Higgs bosons produced by VBF and to suppress background from $Z \rightarrow \tau\tau$ events when selecting Higgs bosons produced through ggF. Since 2016 the di- $\tau_{\text{had-vis}}$ first-level trigger requires a jet with $p_T > 25$ GeV calibrated at trigger level with $|\eta| < 3.2$ in addition to the two $\tau_{\text{had-vis}}$ candidates. In the $\tau_{\text{had}}\tau_{\text{had}}$ channel the jet p_T requirement is thus raised to $p_T^{j_1} > 70$ GeV to achieve uniform trigger selection efficiency as a function of $p_T^{j_1}$. The trigger efficiency for the additional jet ranges from 95% to 100% for these requirements. In the $\tau_{\text{lep}}\tau_{\text{lep}}$ and $\tau_{\text{lep}}\tau_{\text{had}}$ channels, the top-quark background is suppressed by requiring that no jet with $p_T > 25$ GeV is tagged as a b -jet.

5.2 Signal, control and validation regions

To exploit signal-sensitive event topologies, a ‘VBF’ and a ‘boosted’ analysis category are defined without any overlap in phase space. The VBF category targets events with a Higgs boson produced by VBF and is characterized by the presence of a second high- p_T jet ($p_T^{j_2} > 30$ GeV). In addition, the two jets are required to be in opposite hemispheres of the detector with a large pseudorapidity separation of $|\Delta\eta_{jj}| > 3$ and their invariant mass (m_{jj}) is required to be larger than 400 GeV. The selected leptons are required to have η -values that lie between those of the two jets (‘central leptons’). Although this category is dominated by

Table 3: Summary of the event selection requirements for the three analysis channels that are applied in addition to the respective lepton p_T requirements listed in Table 2. $E_T^{\text{miss, hard}}$ is an alternative E_T^{miss} calculated only from the physics objects without the soft-track term. The transverse mass (m_T) is calculated from E_T^{miss} and the momentum of the selected light lepton. The visible momentum fractions x_1 and x_2 of the respective τ -lepton and the collinear di- τ mass ($m_{\tau\tau}^{\text{coll}}$) are calculated in the collinear approximation [98].

$e\ell/\mu\mu$	$\tau_{\text{lep}}\tau_{\text{lep}}$	$e\mu$	$\tau_{\text{lep}}\tau_{\text{had}}$	$\tau_{\text{had}}\tau_{\text{had}}$
	$N_{e/\mu}^{\text{loose}} = 2, N_{\tau_{\text{had-vis}}}^{\text{loose}} = 0$ e/μ : Medium, gradient iso.		$N_{e/\mu}^{\text{loose}} = 1, N_{\tau_{\text{had-vis}}}^{\text{loose}} = 1$ e/μ : Medium, gradient iso.	$N_{e/\mu}^{\text{loose}} = 0, N_{\tau_{\text{had-vis}}}^{\text{loose}} = 2$ $\tau_{\text{had-vis}}$: Medium
	Opposite charge $m_{\tau\tau}^{\text{coll}} > m_Z - 25 \text{ GeV}$		Opposite charge $m_T < 70 \text{ GeV}$	Opposite charge
$30 < m_{\ell\ell} < 75 \text{ GeV}$ $E_T^{\text{miss}} > 55 \text{ GeV}$ $E_T^{\text{miss, hard}} > 55 \text{ GeV}$	$30 < m_{\ell\ell} < 100 \text{ GeV}$ $E_T^{\text{miss}} > 20 \text{ GeV}$		$E_T^{\text{miss}} > 20 \text{ GeV}$	$E_T^{\text{miss}} > 20 \text{ GeV}$
	$\Delta R_{\tau\tau} < 2.0$ $ \Delta\eta_{\tau\tau} < 1.5$ $0.1 < x_1 < 1.0$ $0.1 < x_2 < 1.0$ $p_T^{j_1} > 40 \text{ GeV}$ $N_{b\text{-jets}} = 0$		$\Delta R_{\tau\tau} < 2.5$ $ \Delta\eta_{\tau\tau} < 1.5$ $0.1 < x_1 < 1.4$ $0.1 < x_2 < 1.2$ $p_T^{j_1} > 40 \text{ GeV}$ $N_{b\text{-jets}} = 0$	$0.8 < \Delta R_{\tau\tau} < 2.5$ $ \Delta\eta_{\tau\tau} < 1.5$ $0.1 < x_1 < 1.4$ $0.1 < x_2 < 1.4$ $p_T^{j_1} > 70 \text{ GeV}, \eta_{j_1} < 3.2$

VBF production, it also includes significant contributions from ggF production, amounting to up to 30% of the total expected Higgs-boson signal.

The boosted category targets events with Higgs bosons produced through ggF with additional recoiling jets, which is motivated by the harder p_T -spectrum of the $H \rightarrow \tau\tau$ signal compared to the dominant background from $Z \rightarrow \tau\tau$. It contains all events with $p_T^{\tau\tau} > 100 \text{ GeV}$ that do not pass the VBF selection. In addition to events from ggF, the boosted categories contain sizable contributions from VBF and VH production of 10–20% of the expected signal. Events that pass the event selection, detailed in Table 3, but do not fall into the VBF or boosted categories, are not used in the analysis.

Using $p_T^{\tau\tau}$, $\Delta R_{\tau\tau}$ and m_{jj} , the VBF and boosted categories, referred to as ‘inclusive’ categories, are split further into 13 exclusive signal regions with different signal-to-background ratios to improve the sensitivity. Table 4 summarizes the analysis categories and signal region definitions. Figure 1 illustrates the expected signal and background composition in the signal and control regions of all analysis channels. Figure 2 compares for each analysis channel the observed distributions with predictions, as resulting from the fit described in Section 8, for $p_T^{\tau\tau}$ in the boosted inclusive categories, and for m_{jj} in the VBF inclusive categories. The observed data agree within the given uncertainties with the background expectation described in Section 6 for all distributions.

Six control regions are defined to constrain the normalization of the dominant backgrounds in regions of phase space where their purity is high. Their definitions are summarized in Table 5. Two $Z \rightarrow \ell\ell$ CRs, which are both more than 90% pure in $Z \rightarrow \ell\ell$ events, are defined by applying the same selection as for the SF $\tau_{\text{lep}}\tau_{\text{lep}}$ VBF and boosted inclusive regions, respectively, but with the $m_{\ell\ell}$ requirement modified to $80 < m_{\ell\ell} < 100 \text{ GeV}$. The top-quark background is characterized by the presence of b -jets. Four separate CRs are defined by inverting the b -jet veto in the inclusive VBF and boosted categories for each of the

Table 4: Definition of the VBF and boosted analysis categories and of their respective signal regions (SRs). The selection criteria, which are applied in addition to those described in Table 3, are listed for each channel. The VBF high- $p_T^{\tau\tau}$ SR is only defined for the $\tau_{\text{had}}\tau_{\text{had}}$ channel, resulting in a total of seven VBF SRs and six boosted SRs. All SRs are exclusive and their yields add up to those of the corresponding VBF and boosted inclusive regions.

Signal Region		Inclusive	$\tau_{\text{lep}}\tau_{\text{lep}}$	$\tau_{\text{lep}}\tau_{\text{had}}$	$\tau_{\text{had}}\tau_{\text{had}}$
VBF	High- $p_T^{\tau\tau}$	$p_T^{j_2} > 30 \text{ GeV}$ $ \Delta\eta_{jj} > 3$ $m_{jj} > 400 \text{ GeV}$ $\eta_{j_1} \cdot \eta_{j_2} < 0$ Central leptons		—	
	Tight	$m_{jj} > 800 \text{ GeV}$		$m_{jj} > 500 \text{ GeV}$ $p_T^{\tau\tau} > 100 \text{ GeV}$	Not VBF high- $p_T^{\tau\tau}$ $m_{jj} > (1550 - 250 \cdot \Delta\eta_{jj}) \text{ GeV}$
	Loose	Not VBF tight		Not VBF high- $p_T^{\tau\tau}$ and not VBF tight	
Boosted	High- $p_T^{\tau\tau}$	Not VBF $p_T^{\tau\tau} > 100 \text{ GeV}$		$p_T^{\tau\tau} > 140 \text{ GeV}$ $\Delta R_{\tau\tau} < 1.5$	
	Low- $p_T^{\tau\tau}$			Not boosted high- $p_T^{\tau\tau}$	

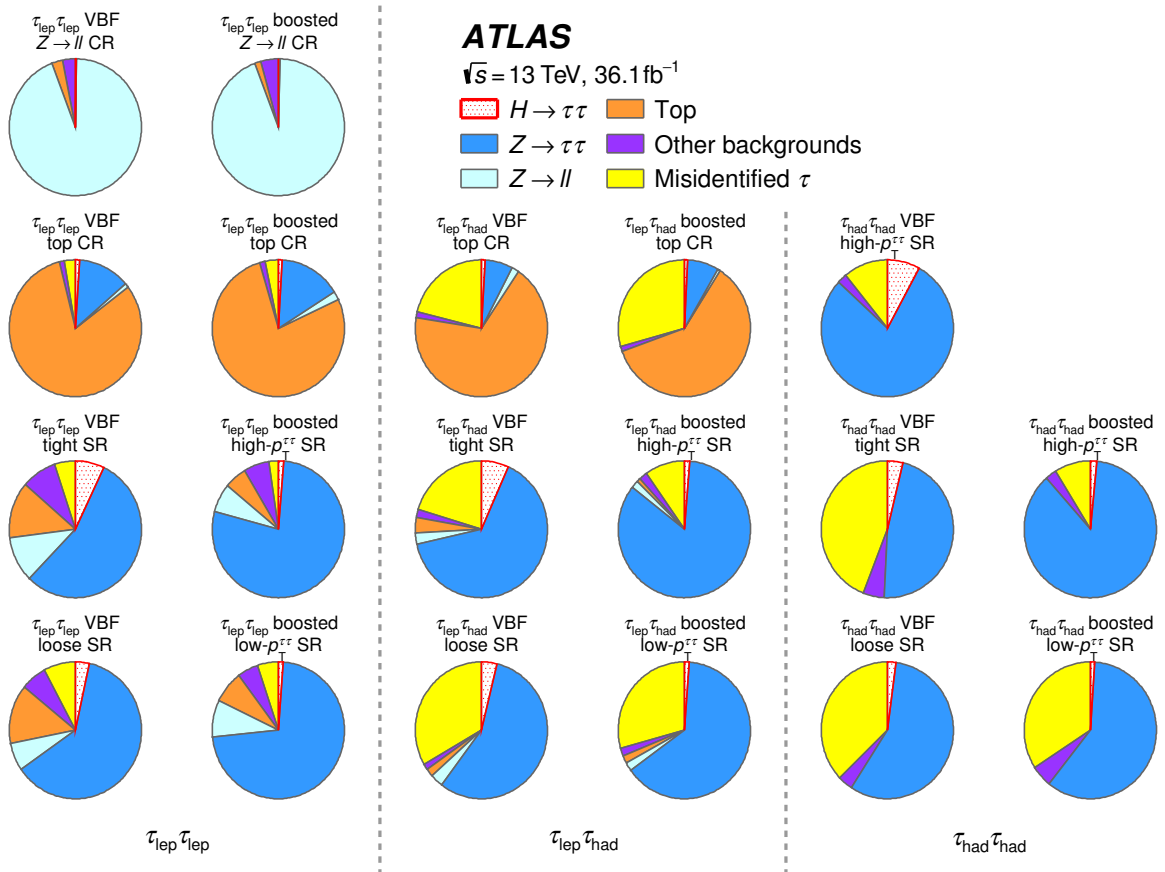


Figure 1: Expected signal and background composition in 6 control regions (CRs) and the 13 signal regions (SRs) used in the analysis.

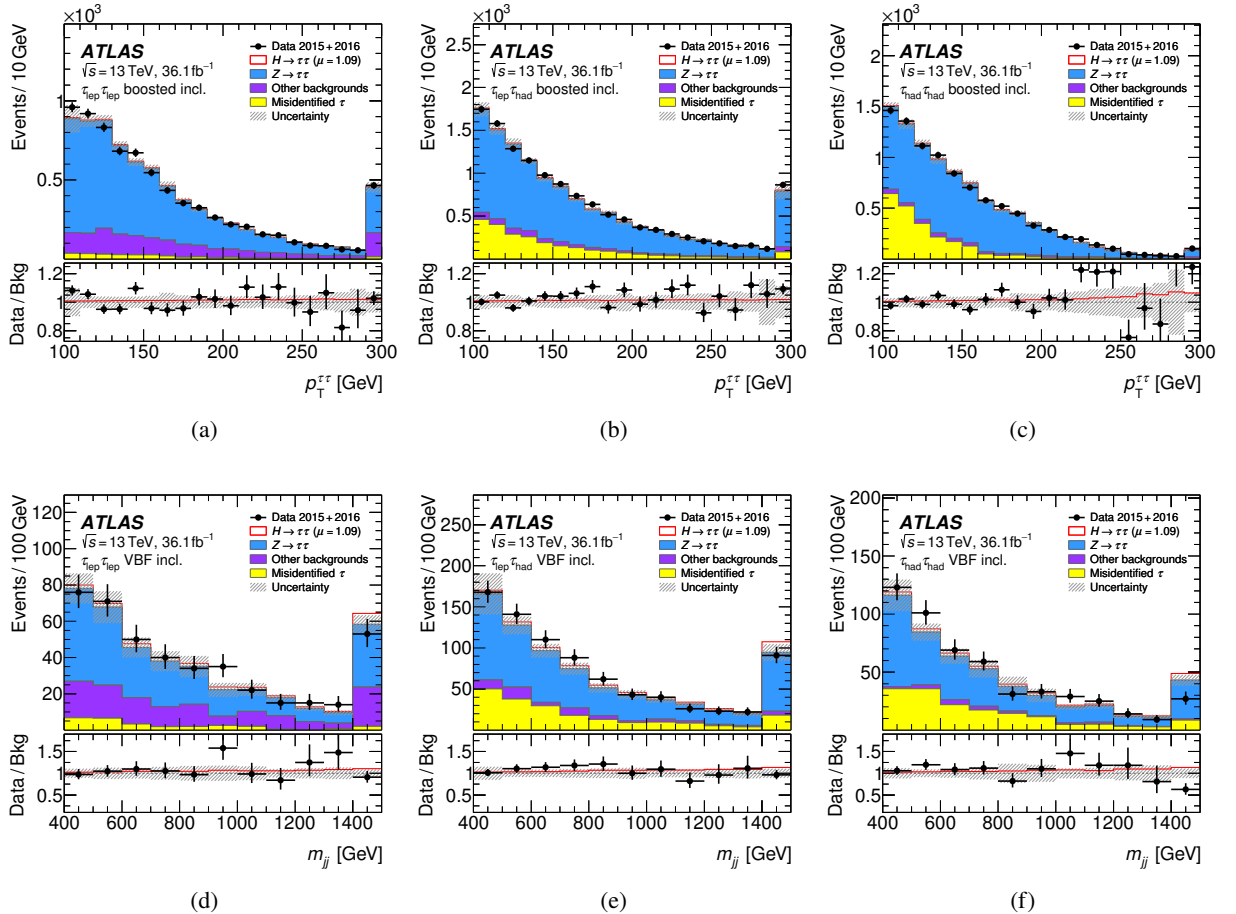


Figure 2: Comparisons between data and predictions as computed by the fit of (top) the p_T of the Higgs-boson candidate ($p_T^{\tau\tau}$) in the boosted inclusive category and (bottom) the invariant mass of the two highest- p_T jets (m_{jj}) in the VBF inclusive category for (left) the $\tau_{\text{lep}}\tau_{\text{lep}}$ channel, (center) the $\tau_{\text{lep}}\tau_{\text{had}}$ channel and (right) the $\tau_{\text{had}}\tau_{\text{had}}$ channel. The ratios of the data to the background model are shown in the lower panels. The observed Higgs-boson signal ($\mu = 1.09$) is shown with the solid red line. Entries with values that would exceed the x -axis range are shown in the last bin of each distribution. The size of the combined statistical, experimental and theoretical uncertainties in the background is indicated by the hatched bands.

Table 5: Definitions of the six control regions (CRs) used to constrain the $Z \rightarrow \ell\ell$ and top backgrounds to the event yield in data in the $\tau_{\text{lep}}\tau_{\text{lep}}$ and $\tau_{\text{lep}}\tau_{\text{had}}$ channels. ‘SF’ denotes a selection of same-flavor light leptons.

Region	Selection
$\tau_{\text{lep}}\tau_{\text{lep}}$ VBF $Z \rightarrow \ell\ell$ CR	$\tau_{\text{lep}}\tau_{\text{lep}}$ VBF incl. selection, $80 < m_{\ell\ell} < 100$ GeV, SF
$\tau_{\text{lep}}\tau_{\text{lep}}$ boosted $Z \rightarrow \ell\ell$ CR	$\tau_{\text{lep}}\tau_{\text{lep}}$ boosted incl. selection, $80 < m_{\ell\ell} < 100$ GeV, SF
$\tau_{\text{lep}}\tau_{\text{lep}}$ VBF top CR	$\tau_{\text{lep}}\tau_{\text{lep}}$ VBF incl. selection, inverted b -jet veto
$\tau_{\text{lep}}\tau_{\text{lep}}$ boosted top CR	$\tau_{\text{lep}}\tau_{\text{lep}}$ boosted incl. selection, inverted b -jet veto
$\tau_{\text{lep}}\tau_{\text{had}}$ VBF top CR	$\tau_{\text{lep}}\tau_{\text{had}}$ VBF incl. selection, inverted b -jet veto, $m_T > 40$ GeV
$\tau_{\text{lep}}\tau_{\text{had}}$ boosted top CR	$\tau_{\text{lep}}\tau_{\text{had}}$ boosted incl. selection, inverted b -jet veto, $m_T > 40$ GeV

$\tau_{\text{lep}}\tau_{\text{lep}}$ and $\tau_{\text{lep}}\tau_{\text{had}}$ channels. The top CRs in the $\tau_{\text{lep}}\tau_{\text{lep}}$ channel are about 80% pure in top-quark events. For the top CRs in the $\tau_{\text{lep}}\tau_{\text{had}}$ channel, the requirement of $m_T < 70$ GeV is replaced by $m_T > 40$ GeV to further enhance the purity to about 70% in the VBF top CR and about 60% in the boosted top CR. No such control regions are defined for the $\tau_{\text{had}}\tau_{\text{had}}$ channel since the top and $Z \rightarrow \ell\ell$ backgrounds are negligible in this case.

One validation region is defined for each signal region (‘ $Z \rightarrow \tau\tau$ VRs’) to validate the event yields and kinematic distributions of simulated $Z \rightarrow \tau\tau$ events. The $Z \rightarrow \tau\tau$ VRs are composed of $Z \rightarrow \ell\ell$ events with kinematics similar to the $Z \rightarrow \tau\tau$ background in the respective signal regions. This is achieved by starting with an event selection that is based on the SF $\tau_{\text{lep}}\tau_{\text{lep}}$ channel preselection with the following differences that account for the selection of light leptons instead of decay products from τ -leptons: The $m_{\tau\tau}^{\text{coll}}$, E_T^{miss} and $E_T^{\text{miss, hard}}$ requirements are dropped and the $m_{\ell\ell}$ requirement is inverted to $m_{\ell\ell} > 80$ GeV. The other requirements on τ -lepton decays are replaced with requirements on the two light leptons. In particular, the requirements on $p_T^{\tau\tau}$ are substituted by the p_T of the Z boson computed from the p_T of the light leptons ($p_T^{\ell\ell}$). Requirements on jets are unchanged since they define the shape of most kinematic distributions for Z -boson production similarly in the SRs and the $Z \rightarrow \tau\tau$ VRs. More than 99% of the selected events are from $Z \rightarrow \ell\ell$ in all $Z \rightarrow \tau\tau$ VRs.

6 Background estimation

The final-state topologies of the three analysis channels have different background compositions, which necessitates different strategies for the background estimation. In each SR, the expected number of background events and the associated kinematic distributions are derived from a mixture of data-driven methods and simulation.

Background contributions with $\tau_{\text{had-vis}}$, with prompt light leptons and with light leptons from τ -lepton decays are estimated from simulation. If their contribution is significant, their normalization is constrained by the observed event yields in CRs. For smaller contributions of this type, their normalization is entirely taken from the theoretical cross sections with the precision in QCD listed in Table 1. This includes di-boson processes and a small contribution from EW production of W/Z bosons from VBF. Contributions from light- and heavy-flavor jets that are misidentified as prompt, light leptons or $\tau_{\text{had-vis}}$ are estimated using data-driven methods. They are labeled as ‘fake- ℓ ’ and ‘fake- $\tau_{\text{had-vis}}$ ’ backgrounds, respectively, and

Table 6: Normalization factors for backgrounds that have their normalization constrained using data in the fit, including all statistical and systematic uncertainties described in Section 7, but without uncertainties in total simulated cross sections extrapolated to the selected phase space. Systematic uncertainties are the dominant contribution to the normalization factor uncertainties. Also shown are the analysis channels to which the normalization factors are applied.

Background	Channel	Normalization factors	
		VBF	Boosted
$Z \rightarrow \ell\ell$ (CR)	$\tau_{\text{lep}}\tau_{\text{lep}}$	$0.88^{+0.34}_{-0.30}$	$1.27^{+0.30}_{-0.25}$
Top (CR)	$\tau_{\text{lep}}\tau_{\text{lep}}$	1.19 ± 0.09	1.07 ± 0.05
Top (CR)	$\tau_{\text{lep}}\tau_{\text{had}}$	$1.53^{+0.30}_{-0.27}$	1.13 ± 0.07
Fake- $\tau_{\text{had-vis}}$ (data-driven)	$\tau_{\text{had}}\tau_{\text{had}}$		1.12 ± 0.12
$Z \rightarrow \tau\tau$ (fit in each SR)	$\tau_{\text{lep}}\tau_{\text{lep}}, \tau_{\text{lep}}\tau_{\text{had}}, \tau_{\text{had}}\tau_{\text{had}}$	$1.04^{+0.10}_{-0.09}$	1.11 ± 0.05

collectively as ‘misidentified τ ’, throughout this paper. The contamination from $H \rightarrow WW^*$ decays is treated as a background in the $\tau_{\text{lep}}\tau_{\text{lep}}$ channel, while it is negligible in other channels.

For the background sources that have their normalization constrained using data, Table 6 shows the normalization factors and their uncertainties obtained from the fit (see Section 8). For simulated backgrounds, the factors compare the background normalizations with values determined from their theoretical cross sections. The normalization factor for the data-driven fake- $\tau_{\text{had-vis}}$ background scales the event yield of the template of events that fail the opposite-charge requirement (see Section 6.4). The $Z \rightarrow \tau\tau$ normalization is constrained by data in the $m_{\tau\tau}^{\text{MMC}}$ distributions of the signal regions. Systematic uncertainties are the dominant contribution to the normalization factor uncertainties.

6.1 $Z \rightarrow \tau\tau$ background validation

The Drell–Yan process $pp \rightarrow Z/\gamma^* \rightarrow \tau\tau$ is a dominant irreducible background in all analysis categories and contributes between 50% and 90% of the total background depending on the signal region. The separation between the Drell–Yan and the $H \rightarrow \tau\tau$ signal processes is limited by the $m_{\tau\tau}^{\text{MMC}}$ resolution.

The modeling of this important background is validated using $Z \rightarrow \tau\tau$ VRs that consist of $Z \rightarrow \ell\ell$ events. In Figure 3, the observed distributions of several variables are compared with simulation normalized to the event yield in data. The selected observables correspond to either variables correlated with $m_{\tau\tau}^{\text{MMC}}$ ($p_T^{\ell_1}$ and $p_T^{\ell_2}$), or to major variables used for categorization ($p_T^{\ell\ell}, \Delta R_{\ell\ell}, \Delta\eta_{jj}$ and m_{jj}), or to variables to which different requirements are applied in each decay channel ($p_T^{j_1}$). Generally, the SHERPA simulation describes the shape of data distributions within the experimental and theoretical uncertainties (see Section 7), with the exception of a slight trend in the ratio of data to simulation as a function of $\Delta\eta_{jj}$ and m_{jj} shown in Figure 3. These trends have no impact on the modeling of $m_{\tau\tau}^{\text{MMC}}$. Reweighting the simulation with the observed m_{jj} distribution, which is an important variable for VBF categorization, has a negligible impact on the measurement. In the fit, the normalization of the $Z \rightarrow \tau\tau$ background is correlated across the decay channels and constrained by data in the $m_{\tau\tau}^{\text{MMC}}$ distributions of the signal regions associated with the boosted and VBF categories, independently. As shown in Table 6, it is constrained to $\pm 5\%$ in the boosted category and to $\pm 9\%$ in the VBF category. The relative acceptance of events among the signal regions within a category is validated by applying the corresponding event-selection criteria to the

$Z \rightarrow \tau\tau$ VRs. The expected relative acceptance from simulation agrees with data within uncertainties for all regions. Figures 8 and 9 show the good modeling of the $Z \rightarrow \tau\tau$ $m_{\tau\tau}^{\text{MMC}}$ distribution in all signal regions. Additional uncertainties in the relative acceptances and in the shape of the $m_{\tau\tau}^{\text{MMC}}$ distributions in the signal regions are evaluated from theoretical and experimental uncertainties described in Section 7.

6.2 $Z \rightarrow \ell\ell$ background

Decays of Z bosons into light leptons are a significant background for the $\tau_{\text{lep}}\tau_{\text{lep}}$ and $\tau_{\text{lep}}\tau_{\text{had}}$ channels, where mismeasured $E_{\text{T}}^{\text{miss}}$ can bias the reconstructed $m_{\tau\tau}^{\text{MMC}}$ of light-lepton pairs towards values similar to those expected for the signal. The observed event yields in the $Z \rightarrow \ell\ell$ CRs constrain the normalization of simulated $Z \rightarrow \ell\ell$ events in the $\tau_{\text{lep}}\tau_{\text{lep}}$ channel to $\pm 40\%$ in the VBF category and to $\pm 25\%$ in the boosted category, as shown in Table 6. The good modeling of the $m_{\tau\tau}^{\text{MMC}}$ distribution in the $\tau_{\text{lep}}\tau_{\text{lep}}$ VBF $Z \rightarrow \ell\ell$ CR is shown in Figure 4(a). In other channels, the contribution from $Z \rightarrow \ell\ell$ events is normalized to its theoretical cross section. In the $\tau_{\text{lep}}\tau_{\text{had}}$ channel, $Z \rightarrow \ell\ell$ background contributes primarily through $Z \rightarrow ee$ decays where an electron is misidentified as a $\tau_{\text{had-vis}}$ candidate. Due to the dedicated electron veto algorithm applied to selected 1-prong $\tau_{\text{had-vis}}$ candidates (see Section 5.1), this background is small. This and other backgrounds from light leptons misidentified as $\tau_{\text{had-vis}}$ in this channel are estimated from simulation, with the probability for electrons misidentified as $\tau_{\text{had-vis}}$ candidates scaled to match that observed in data [94].

6.3 Top-quark background

The production of $t\bar{t}$ pairs or single top quarks is a significant background ('top background') for the $\tau_{\text{lep}}\tau_{\text{lep}}$ and $\tau_{\text{lep}}\tau_{\text{had}}$ channels, due to the production of prompt light leptons with associated $E_{\text{T}}^{\text{miss}}$ in the top-quark decay chain $t \rightarrow Wb$, $W \rightarrow \ell\nu, \tau\nu$. Events where a selected τ -lepton decay product is misidentified, are estimated using data-driven methods that are discussed in Section 6.4. The remaining top background is estimated from simulation. In the $\tau_{\text{lep}}\tau_{\text{lep}}$ and $\tau_{\text{lep}}\tau_{\text{had}}$ channels the normalization of simulated top background is additionally constrained by the absolute event yields in their respective top CRs to $\pm 30\%$ in the $\tau_{\text{lep}}\tau_{\text{had}}$ VBF top CR and less than $\pm 10\%$ in the other top CRs, as shown in Table 6. Figures 4(b) and 4(c) show $m_{\tau\tau}^{\text{MMC}}$ distributions in the $\tau_{\text{lep}}\tau_{\text{lep}}$ boosted top CR and the $\tau_{\text{lep}}\tau_{\text{had}}$ VBF top CR, respectively.

6.4 Backgrounds from misidentified τ

Apart from the small contribution from light leptons misidentified as $\tau_{\text{had-vis}}$ described in Section 6.2, hadronic jets can be misidentified as $\tau_{\text{had-vis}}$, electrons and muons. These sources of background contribute up to half of the total background, depending on the signal region, and are estimated with data-driven techniques. Since the background sources depend on the event topology, specific methods are applied to each individual channel.

In the $\tau_{\text{lep}}\tau_{\text{lep}}$ channel, the main sources of the fake- ℓ background are multijets, W bosons in association with jets, and semileptonically decaying $t\bar{t}$ events. All these background sources are treated together. Fake- ℓ regions are defined in data by requiring that the light lepton with the second-highest p_{T} does not satisfy the 'gradient' isolation criterion. This is referred to as 'inverted' isolation. In addition, if the light lepton is an electron, its identification criteria are relaxed to 'loose'. Fake- ℓ templates are created

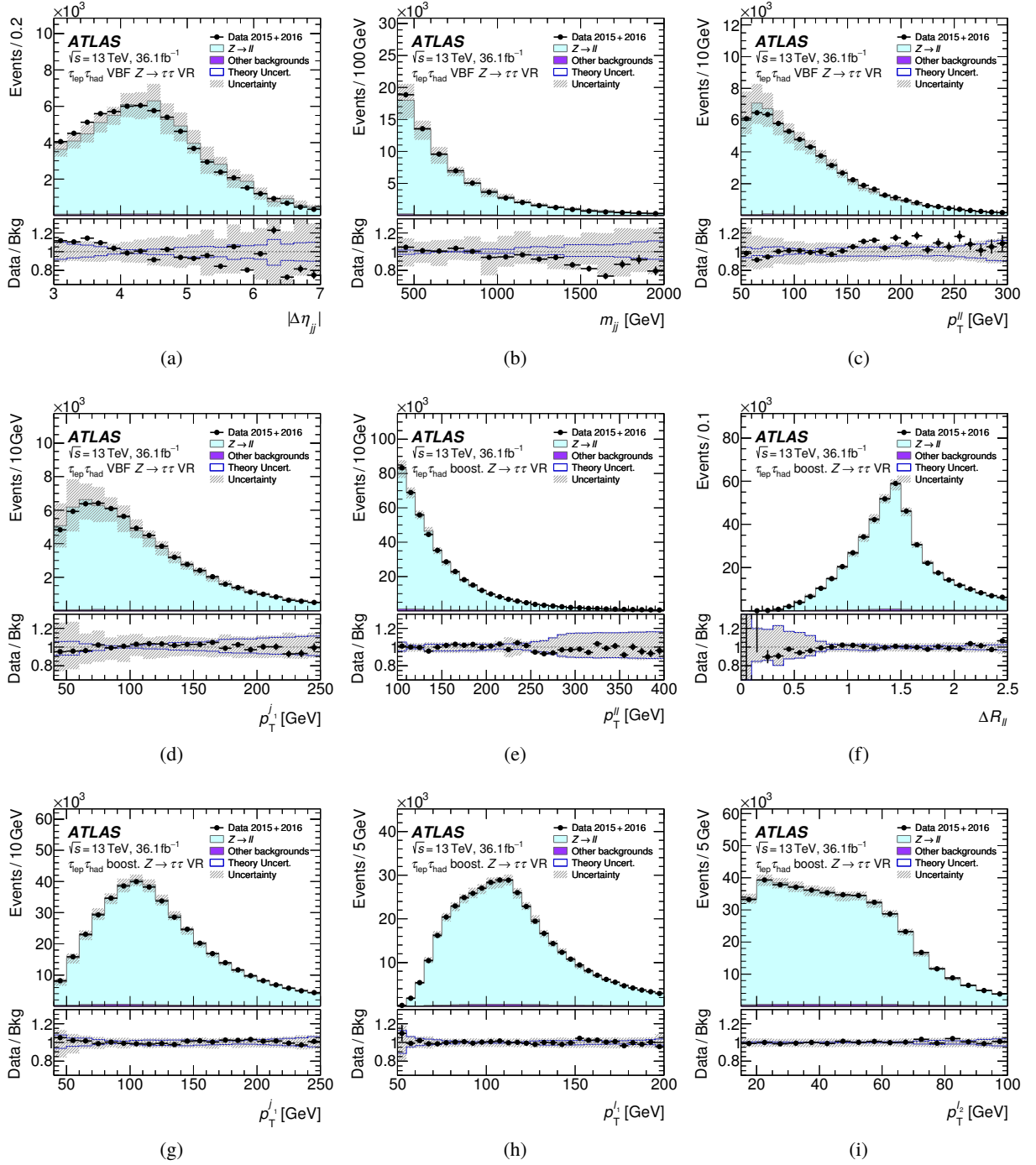


Figure 3: Observed and expected distributions in the $Z \rightarrow \tau\tau$ validation regions (VRs) corresponding to (a)–(d) the $\tau_{\text{lep}}\tau_{\text{had}}$ VBF inclusive category and (e)–(i) the $\tau_{\text{lep}}\tau_{\text{had}}$ boosted inclusive category. Shown are, in the respective region: (a) the pseudorapidity separation ($|\Delta\eta_{jj}|$) and (b) the invariant mass (m_{jj}) of the two highest- p_{T} jets; (c) and (e) the p_{T} of the di-lepton system ($p_{\text{T}}^{\ell\ell}$); (d) and (g) the p_{T} of the highest- p_{T} jet ($p_{\text{T}}^{j_1}$); (f) the angular distance between the light leptons ($\Delta R_{\ell\ell}$); (h) the p_{T} of the highest- p_{T} light lepton ($p_{\text{T}}^{\ell_1}$); and (i) the p_{T} of the second-highest- p_{T} light lepton ($p_{\text{T}}^{\ell_2}$). The predictions in these validation regions are not computed by the fit, but are simply normalized to the event yield in data. The size of the combined statistical, experimental and theoretical uncertainties is indicated by the hatched bands. The ratios of the data to the background model are shown in the lower panels together with the theoretical uncertainties in the SHERPA simulation of $Z \rightarrow \ell\ell$, which are indicated by the blue lines.

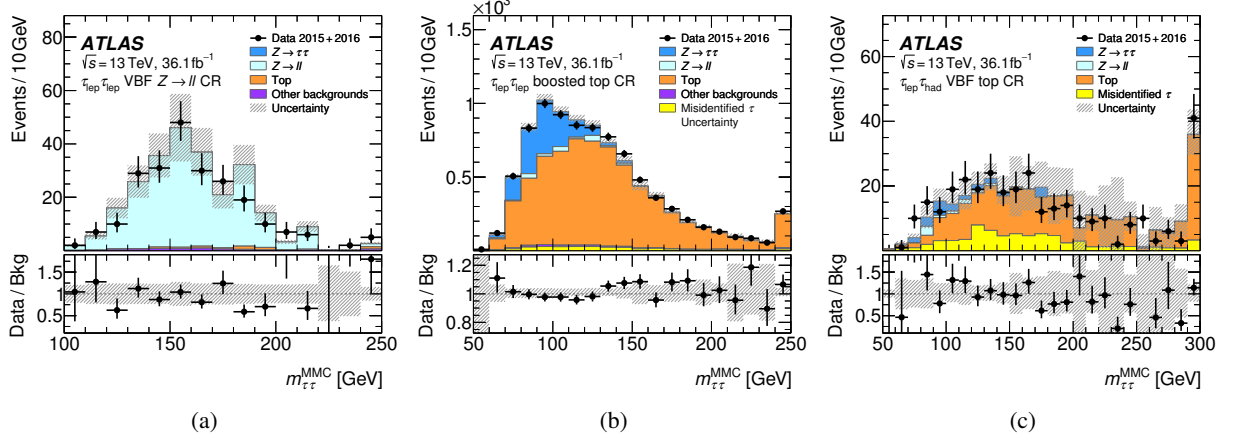


Figure 4: For the control regions (CRs) defined in Section 5, comparisons between data and predictions as computed by the fit for the reconstructed di- τ invariant mass ($m_{\tau\tau}^{\text{MMC}}$). Shown are (a) the $\tau_{\text{lep}}\tau_{\text{lep}}$ VBF $Z \rightarrow \ell\ell$ control region (CR), (b) the $\tau_{\text{lep}}\tau_{\text{lep}}$ boosted top CR and (c) the $\tau_{\text{lep}}\tau_{\text{had}}$ VBF top CR. Entries with values that would exceed the x -axis range are shown in the last bin of each distribution. The size of the combined statistical, experimental and theoretical uncertainties in the background is indicated by the hatched bands. The ratios of the data to the background model are shown in the lower panels.

from these samples by subtracting top and $Z \rightarrow \ell\ell$ backgrounds that produce real light leptons, estimated from simulation. The normalization of each template is then scaled by a factor that corrects for the inverted-isolation requirement. These correction factors are computed for each combination of lepton flavor from events that pass the $\tau_{\text{lep}}\tau_{\text{lep}}$ selection but have same-charge light leptons, subtracting simulated top and $Z \rightarrow \ell\ell$ backgrounds. Fake- ℓ background in the top-quark CRs is estimated following the same procedure.

Systematic uncertainties in the shape and normalization of the fake- ℓ background in the $\tau_{\text{lep}}\tau_{\text{lep}}$ channel depend on the p_T of the second-highest- p_T lepton and are estimated as follows. A closure test of the background estimate is performed using events where the leptons are required to have the same charge and yields an uncertainty ranging between 20% and 65%. An uncertainty in the heavy-flavor content is estimated by using isolation correction factors that are computed from samples selected with inverted b -jet requirements. This uncertainty is as large as 50%. Minor contributions come from the uncertainty in the fractional composition of the fake- ℓ background in top-quark decays, multijet events and W -boson production.

In the $\tau_{\text{lep}}\tau_{\text{had}}$ channel, a ‘fake-factor’ method is used to derive estimates for fake- $\tau_{\text{had-vis}}$ events, composed mainly of multijet events and W -boson production in association with jets. A fake-factor is defined as the ratio of the number of events where the highest- p_T jet is identified as a ‘medium’ $\tau_{\text{had-vis}}$ candidate to the number of events with a highest- p_T jet that passes a very loose $\tau_{\text{had-vis}}$ identification but fails the ‘medium’ one. Fake-factors depend on the p_T and track multiplicity of the $\tau_{\text{had-vis}}$ candidate and on the type of parton initiating the jet. Therefore, they are computed depending on the p_T and the track multiplicity, in both quark-jet-dominated ‘ W -enhanced’ and gluon-jet-dominated ‘multijet-enhanced’ regions. The W -enhanced regions are defined by inverting the $m_T < 70 \text{ GeV}$ requirement and the multijet-enhanced regions are defined by inverting the light-lepton isolation, relative to the inclusive boosted and VBF selections. Backgrounds from Z -boson production with associated jets and semileptonically decaying $t\bar{t}$ have fake-factors similar to those found in backgrounds from W bosons, and their contributions are

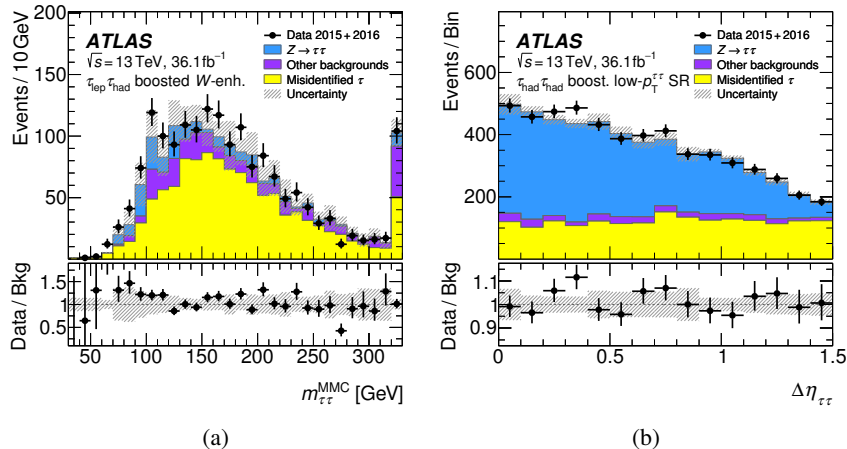


Figure 5: Observed distributions and predictions computed by the fit for (a) $m_{\tau\tau}^{\text{MMC}}$ in the W -enhanced region of the $\tau_{\text{lep}}\tau_{\text{had}}$ boosted inclusive category, and (b) $\Delta\eta$ between the two $\tau_{\text{had-vis}}$, for events in the boosted low- $p_T^{\tau\tau}$ signal region (SR) of the $\tau_{\text{had}}\tau_{\text{had}}$ channel. Entries with values that would exceed the x -axis range are shown in the last bin of each distribution. The size of the combined statistical, experimental and theoretical uncertainties in the background is indicated by the hatched bands. The ratios of the data to the background model are shown in the lower panels.

negligible. The fake-factors are in the range 0.15–0.25 for 1-prong and 0.01–0.04 for 3-prong $\tau_{\text{had-vis}}$. To obtain the fake- $\tau_{\text{had-vis}}$ background estimate for the signal regions, these fake-factors are first weighted by the multijets-to- W fraction. The weighted fake-factors are then applied to events in regions defined by the selections of the corresponding signal regions, except that the highest- p_T $\tau_{\text{had-vis}}$ candidate passes a very loose $\tau_{\text{had-vis}}$ identification and fails the ‘medium’ one (‘anti-ID’ regions). The relative multijet contribution in each anti-ID region is estimated from the yield of events that fail the light-lepton isolation requirement, multiplied by a factor that corrects for this requirement. The multijet contribution varies by more than 50% and depends on the lepton p_T and on the $\Delta\phi$ between $\tau_{\text{had-vis}}$ and E_T^{miss} . The good agreement between data and background estimates is shown in Figure 5(a) for the main discriminant of the analysis, $m_{\tau\tau}^{\text{MMC}}$, in the boosted W -enhanced region.

The dominant contribution to the uncertainties in the fake- $\tau_{\text{had-vis}}$ background in the $\tau_{\text{lep}}\tau_{\text{had}}$ channel originates from the statistical uncertainty in the individual fake-factors of up to 10% in the boosted signal regions and up to 35% in the VBF signal regions. Minor contributions originate from the statistical uncertainty in the anti-ID regions and uncertainties in the fractional size of the multijet contribution to the fake- $\tau_{\text{had-vis}}$ background.

In the $\tau_{\text{had}}\tau_{\text{had}}$ channel, the multijet background is modeled using a template extracted from data that pass the signal-region selections, but where the $\tau_{\text{had-vis}}$ candidates are allowed to have two tracks and required to fail the opposite-charge requirement (nOC region). The contribution of events with true τ -leptons from other SM processes is subtracted from this template using simulation. The template is then reweighted using scale factors dependent on the difference in ϕ between the $\tau_{\text{had-vis}}$ candidates ($\Delta\phi_{\tau\tau}$). These scale factors are derived by comparing the template from an nOC selection with a region obtained by requiring the $\tau_{\text{had-vis}}$ pair to have opposite charge and the second-highest- p_T $\tau_{\text{had-vis}}$ to fail the ‘tight’ but pass the ‘medium’ identification requirements. As the yield of events that pass these identification requirements is small, the scale factors are derived from events that pass the $\tau_{\text{had}}\tau_{\text{had}}$ selection with looser $\Delta\eta_{\tau\tau}$ and

$\Delta R_{\tau\tau}$ requirements to gain statistical power. The normalization of the multijet background is constrained in the fit by data in the $m_{\tau\tau}^{\text{MMC}}$ distribution in the signal regions. For this, a normalization factor is defined and it is correlated across all $\tau_{\text{had}}\tau_{\text{had}}$ signal regions. Figure 5(b) shows good agreement between data and background predictions in the distribution of $\Delta\eta$ between the two $\tau_{\text{had-vis}}$, which has a quite different shape for the multijets than for the $Z \rightarrow \tau\tau$ process. In this figure, events are selected that pass the $\tau_{\text{had}}\tau_{\text{had}}$ boosted low- $p_T^{\tau\tau}$ selection. Contributions from other backgrounds, such as W with associated jets, range from 2% to 5% in the $\tau_{\text{had}}\tau_{\text{had}}$ SRs.

The event yield of the multijet background in the $\tau_{\text{had}}\tau_{\text{had}}$ channel is constrained by data to $\pm 15\%$ in the signal regions as shown in Table 6. The dominant contribution to the uncertainties that affect the $m_{\tau\tau}^{\text{MMC}}$ shape originates from the statistical uncertainties in the $\Delta\phi_{\tau\tau}$ scale factors and amounts to 8%. The systematic uncertainty in these scale factors is estimated by comparing them with scale factors computed from the nOC region and a CR defined by requiring opposite-charge $\tau_{\text{had-vis}}$ to pass ‘loose’ but not ‘medium’ identification. Minor contributions arise from the uncertainty in the extrapolation from the nOC requirement and the uncertainty from the subtraction of simulated backgrounds. The combination of these uncertainties leads to a total variation in the $m_{\tau\tau}^{\text{MMC}}$ template shape by at most 10% between bins.

7 Systematic uncertainties

The expected signal and background yields in the various signal and control regions as well as the shape of the $m_{\tau\tau}^{\text{MMC}}$ distributions in the signal regions are affected by systematic uncertainties. These are discussed below, grouped into three categories: theoretical uncertainties in signal, theoretical uncertainties in background, and experimental uncertainties. The uncertainties in backgrounds from misidentified τ -leptons, which are estimated using data-driven techniques, are discussed in Section 6.4. The effects of all uncertainties are included in the fit model described in Section 8.

7.1 Theoretical uncertainties in signal

The procedures to estimate the uncertainty in the Higgs production cross sections follow the recommendations by the LHC Higgs Cross Section Working Group [100]. They are briefly summarized below. Uncertainties are evaluated separately for their impact on the total cross section, their impact on the acceptance in different SRs, and on the shape of the $m_{\tau\tau}^{\text{MMC}}$ distribution in each SR.

The cross section of ggF production in association with an exclusive number of additional jets has large uncertainties from higher-order QCD corrections [101]. In this analysis, the boosted and VBF categories almost exclusively select ggF events with one and two additional jets, respectively. To take this effect into account, nine uncertainty sources are included. Four sources account for uncertainties in the jet multiplicities due to missing higher-order corrections: Two sources account for yield uncertainties and two sources account for migration uncertainties of zero to one jets and one to at least two jets in the event, respectively, using the STWZ [102] and BLPTW [102–104] predictions as an input. Three uncertainty sources parameterize modeling uncertainties in the Higgs-boson p_T , two of which encapsulate the migration uncertainty between the intermediate and high- p_T regions of events with at least one jet, and one which encapsulates the treatment of the top-quark mass in the loop corrections, where the difference between the LO and NLO predictions is taken as an uncertainty due to missing higher-order corrections. Two sources account for the acceptance uncertainties of ggF production in the VBF phase space from

selecting exactly two and at least three jets, respectively. Their size is estimated using an extension of the Stewart–Tackmann method [105, 106]. The resulting acceptance uncertainties from these nine sources range from 1% to 10%, with the dominant uncertainties due to the modeling of the Higgs p_T distribution in all SRs, to the scale variations in the boosted SRs, and to the acceptance uncertainties in the VBF signal regions.

For VBF and VH production cross sections, the uncertainties due to missing higher-order QCD corrections are estimated by varying the factorization and renormalization scales by factors of two around the nominal scale. The resulting uncertainties in the total cross section are below 1% for VBF and WH production and below 5% for ZH production. The uncertainties in the acceptance in the different SRs are about 1% for VBF production in all categories. For VH production the relative acceptance uncertainty ranges between -10% and $+20\%$ in VBF SRs. It is below 10% in boosted SRs.

Uncertainties related to the simulation of the underlying event, hadronization and parton shower for all signal samples are estimated by comparing the acceptance when using the default UEPS model from PYTHIA 8.212 with an alternative UEPS model from HERWIG 7.0.3. The resulting acceptance uncertainties range from 2% to 26% for ggF production and from 2% to 18% for VBF production, depending on the signal region. The PDF uncertainties are estimated using 30 eigenvector variations and two α_S variations that are evaluated independently relative to the default PDF set PDF4LHC15 [42]. The total uncertainty due to these variations is 5% or less depending on the SR and the Higgs production mode. Finally, an uncertainty in the $H \rightarrow \tau\tau$ decay branching ratio of 1% [100] affects the signal rates. All sources of theoretical uncertainties in the signal expectation are correlated across SRs.

7.2 Theoretical uncertainties in backgrounds

Uncertainties from missing higher-order corrections, the PDF parameterization and the UEPS modelling are also considered for the dominant $Z \rightarrow \tau\tau$ background. The UEPS modelling uncertainties are estimated by comparing with an alternative $Z \rightarrow \tau\tau$ sample as described in Section 3. Since its overall normalization is constrained separately in the VBF and boosted SRs, variations due to these uncertainties are considered in the event migration within an analysis channel, in the $m_{\tau\tau}^{\text{MMC}}$ shape and in the relative change in acceptance between the three analysis channels. These variations are treated as uncorrelated between the VBF and boosted SRs. In addition, the first two types of variations are treated as uncorrelated between the three analysis channels. This treatment accounts for the differences in the corresponding event selections. The largest uncertainties are due to the CKKW matching [107] and are evaluated as a function of the number of true jets and the Z -boson p_T . They vary between 1% and 5% depending on the SR. The uncertainty in the measured cross section for electroweak Z production with two associated jets [108] is found to be small compared to the other uncertainties in Z -boson production.

The top-quark background normalization in the $\tau_{\text{lep}}\tau_{\text{lep}}$ and $\tau_{\text{lep}}\tau_{\text{had}}$ channels as well as the $Z \rightarrow \ell\ell$ background normalization in the $\tau_{\text{lep}}\tau_{\text{lep}}$ channel are constrained by data in dedicated CRs. All other simulated background contributions are normalized to their Monte Carlo prediction. For all simulated background contributions, other than $Z \rightarrow \tau\tau$, no theoretical uncertainties are considered, as their impact is small compared to the uncertainties in the dominant backgrounds from $Z \rightarrow \tau\tau$ and misidentified leptons.

7.3 Experimental uncertainties

Experimental systematic uncertainties result from uncertainties in efficiencies for triggering, object reconstruction and identification, as well as from uncertainties in the energy scale and resolution of jets, $\tau_{\text{had-vis}}$, light leptons and $E_{\text{T}}^{\text{miss}}$. These uncertainties affect both the event yields and the shape of the $m_{\tau\tau}^{\text{MMC}}$. The dominant experimental uncertainties in the final result are related to jet and $\tau_{\text{had-vis}}$ reconstruction. The impact of the electron- and muon-related uncertainties [86, 87, 109] on the measurement are small. Uncertainties in the integrated luminosity affect the number of predicted signal and background events, with the exception of processes that are normalized to data, see Table 6. This uncertainty is 2.1% for the combined 2015+2016 dataset. It is derived using a methodology similar to that detailed in Ref. [110], and using the LUCID-2 detector for the baseline luminosity measurements [111], from a calibration of the luminosity scale using x - y beam-separation scans.

The uncertainties of the $\tau_{\text{had-vis}}$ identification efficiency are in the range of 2–4.5% for the reconstruction efficiency [112], 3–14% for the trigger efficiency (depending on the $\tau_{\text{had-vis}} p_{\text{T}}$), 5–6% for the identification efficiency and 3–14% for the rate at which an electron is misidentified as $\tau_{\text{had-vis}}$ (depending on the $\tau_{\text{had-vis}} \eta$) [94]. The uncertainties of the b -tagging efficiencies are measured in dedicated calibration analyses [92] and are decomposed into uncorrelated components. Uncertainties in the efficiency to pass the JVT and forward JVT requirements are also considered [91, 113]. Simulated events are corrected for differences in these efficiencies between data and simulation and the associated uncertainties are propagated through the analysis.

The uncertainties of the $\tau_{\text{had-vis}}$ energy scale [94] are determined by fitting the Z -boson mass in $Z \rightarrow \tau\tau$ events, reconstructed using the visible τ decay products. The precision amounts to 2–3%, which is dominated by the uncertainty of background modeling. Additional uncertainties based on the modeling of the calorimeter response to single particles are added for $\tau_{\text{had-vis}}$ with $p_{\text{T}} > 50 \text{ GeV}$ [114]. The jet energy scale and its uncertainty are derived by combining information from test-beam data, LHC collision data and simulation [115]. The uncertainties from these measurements are factorized into eight principal components. Additional uncertainties that are considered are related to jet flavor, pileup corrections, η -dependence, and high- p_{T} jets, yielding a total of 20 independent sources. The uncertainties amount to 1–6% per jet, depending on the jet p_{T} . The jet energy resolution uncertainties [116] are divided into 11 independent components and amount to 1–6%.

Since systematic uncertainties of the energy scales of all objects affect the reconstructed $E_{\text{T}}^{\text{miss}}$, this is recalculated after each variation is applied. The scale uncertainty of $E_{\text{T}}^{\text{miss}}$ due to the energy in the calorimeter cells not associated with physics objects is also taken into account [96]. The uncertainty of the resolution of $E_{\text{T}}^{\text{miss}}$ arises from the energy resolution uncertainties of each of the $E_{\text{T}}^{\text{miss}}$ terms and the modeling of pileup and its effects on the soft term (see Section 4).

8 Results

Maximum-likelihood fits are performed on data to extract parameters of interest that probe $H \rightarrow \tau\tau$ production with increasing granularity. Firstly, a single parameter is fitted to measure the total cross section of the $H \rightarrow \tau\tau$ production processes. Then, a two-parameter cross-section fit is presented separating the ggF and VBF production processes. Finally, a three-parameter fit is performed to measure ggF production cross sections in two exclusive regions of phase space. For the small contribution from

$H \rightarrow WW^*$ decays, the measurements assume the SM predictions for production cross section and branching ratio.

A probability model is constructed that describes the $m_{\tau\tau}^{\text{MMC}}$ distributions in the 13 signal regions and the event yields in 6 control regions. The latter are included to constrain the normalizations of the dominant backgrounds. Each signal region is modeled by a product of Poisson distributions, where each such distribution describes the expected event count in intervals of $m_{\tau\tau}^{\text{MMC}}$. Each control region is modeled by a single Poisson distribution that describes the total expected event count in that region. Signal and background predictions depend on systematic uncertainties, which are parameterized as nuisance parameters and are constrained using Gaussian or log-normal probability distributions. The latter are used for normalization factors (see Table 6) to ensure that they are always positive. The dependence of the predictions on nuisance parameters related to systematic uncertainties is modeled with an interpolation approach between yields obtained at different fixed systematic uncertainty settings. A smoothing procedure is applied to remove occasional large local fluctuations in the $m_{\tau\tau}^{\text{MMC}}$ distribution templates, which encode systematic uncertainties of some background processes in certain regions. For the measurements, all theoretical uncertainties are included, except those related to the respective measured signal cross sections, and are correlated as described in Section 7.1. The experimental uncertainties are fully correlated across categories and the background modeling uncertainties are generally uncorrelated, with the exception of the normalization factors as described in Section 6. Estimates of the parameters of interest and the confidence intervals are calculated with the profile likelihood ratio [117] test statistic, whereas the test statistic \tilde{q}_0 [117] is used to compute the significances of the deviations from the background-only hypothesis.

The observed (expected) significance of the signal excess relative to the background-only hypothesis computed from the likelihood fit is 4.4 (4.1) standard deviations, compatible with a SM Higgs boson with a mass $m_H = 125$ GeV. This result is combined with the result of the search for $H \rightarrow \tau\tau$ using data at 7 and 8 TeV center-of-mass energies [15]. The combined observed (expected) significance amounts to 6.4 (5.4) standard deviations. In this combination, all nuisance parameters are treated as uncorrelated between the two analyses. In particular, the dominant $Z \rightarrow \tau\tau$ background is estimated differently, as mentioned in Section 1.

The parameter $\sigma_{H \rightarrow \tau\tau} \equiv \sigma_H \cdot \mathcal{B}(H \rightarrow \tau\tau)$ is fitted, where σ_H is the total cross section of the considered Higgs-boson production processes ggF, VBF, VH and $t\bar{t}H$, and where $\mathcal{B}(H \rightarrow \tau\tau)$ is the $H \rightarrow \tau\tau$ branching fraction. For this measurement, the relative contributions from the various Higgs production processes are assumed as predicted by the SM and the uncertainties related to the predicted total signal cross section are excluded. The measured value of $\sigma_{H \rightarrow \tau\tau}$ is $3.77^{+0.60}_{-0.59}$ (stat.) $^{+0.87}_{-0.74}$ (syst.) pb, consistent with the SM prediction, $\sigma_{H \rightarrow \tau\tau}^{\text{SM}} = 3.46 \pm 0.13$ pb [100]. The signal strength $\mu_{H \rightarrow \tau\tau}$ is defined as the ratio of the measured signal yield to the Standard Model expectation. It is computed by the fit described above, including uncertainties in the predicted signal cross section, and is evaluated to be $1.09^{+0.18}_{-0.17}$ (stat.) $^{+0.26}_{-0.22}$ (syst.) $^{+0.16}_{-0.11}$ (theory syst.).

Tables 7 to 9 summarize the expected signal and background yields computed by the fit in each signal region for the $\sigma_{H \rightarrow \tau\tau}$ measurement. The signal event yields are given separately for each production process of relevance. Within the uncertainties, good agreement is observed between the data and the predicted sum of signal and background contributions, for a SM Higgs boson of mass $m_H = 125$ GeV with the measured value of $\sigma_{H \rightarrow \tau\tau}$ reported above.

Table 10 shows a summary of the dominant uncertainties in $\sigma_{H \rightarrow \tau\tau}$, grouped by their respective sources. Figure 6 shows the systematic uncertainties with the largest impact, together with a comparison with their nominal values used as input to the fit. In both the table and the figure the shown uncertainties

Table 7: Observed event yields and predictions as computed by the fit in the $\tau_{\text{lep}}\tau_{\text{lep}}$ signal regions. Uncertainties include statistical and systematic components.

	$\tau_{\text{lep}}\tau_{\text{lep}}$ VBF		$\tau_{\text{lep}}\tau_{\text{lep}}$ boosted	
	Loose	Tight	Low- $p_T^{\tau\tau}$	High- $p_T^{\tau\tau}$
$Z \rightarrow \tau\tau$	151 \pm 13	107 \pm 12	2977 \pm 90	2687 \pm 64
$Z \rightarrow \ell\ell$	15.1 \pm 4.9	20.3 \pm 6.6	360 \pm 54	236 \pm 31
Top	33.0 \pm 6.4	25.1 \pm 4.5	321 \pm 50	189 \pm 29
VV	11.8 \pm 2.2	10.7 \pm 1.5	194.1 \pm 8.5	195.3 \pm 8.8
Misidentified τ	18.3 \pm 9.6	9.6 \pm 4.8	209 \pm 92	80 \pm 35
$ggF, H \rightarrow WW^*$	1.2 \pm 0.2	1.4 \pm 0.3	11.8 \pm 2.6	16.4 \pm 1.7
$VBF, H \rightarrow WW^*$	1.7 \pm 0.2	4.1 \pm 0.5	2.9 \pm 0.3	2.9 \pm 0.3
$ggF, H \rightarrow \tau\tau$	2.6 \pm 0.9	1.8 \pm 0.9	34.4 \pm 9.2	33.8 \pm 9.5
$VBF, H \rightarrow \tau\tau$	5.3 \pm 1.5	11.3 \pm 3.0	7.7 \pm 2.1	8.2 \pm 2.3
$WH, H \rightarrow \tau\tau$	< 0.1	< 0.1	2.5 \pm 0.7	3.1 \pm 0.9
$ZH, H \rightarrow \tau\tau$	< 0.1	< 0.1	1.3 \pm 0.4	1.6 \pm 0.4
$t\bar{t}H, H \rightarrow \tau\tau$	< 0.1	0.1 \pm 0.1	1.5 \pm 0.5	1.2 \pm 0.4
Total background	232 \pm 13	178 \pm 12	4075 \pm 61	3408 \pm 54
Total signal	8.0 \pm 2.2	13.2 \pm 3.5	47 \pm 12	48 \pm 12
Data	237	188	4124	3444

Table 8: Observed event yields and predictions as computed by the fit in the $\tau_{\text{lep}}\tau_{\text{had}}$ signal regions. Uncertainties include statistical and systematic components.

	$\tau_{\text{lep}}\tau_{\text{had}}$ VBF		$\tau_{\text{lep}}\tau_{\text{had}}$ boosted	
	Loose	Tight	Low- $p_T^{\tau\tau}$	High- $p_T^{\tau\tau}$
$Z \rightarrow \tau\tau$	178 \pm 18	323 \pm 21	4187 \pm 92	5347 \pm 82
$Z \rightarrow \ell\ell$	10.0 \pm 3.0	12.7 \pm 3.1	130 \pm 37	115 \pm 16
Top	5.8 \pm 1.6	17.9 \pm 4.6	121 \pm 20	57 \pm 10
Misidentified τ	103 \pm 16	101 \pm 15	1895 \pm 80	605 \pm 29
Other backgrounds	4.0 \pm 1.6	9.3 \pm 1.9	115.0 \pm 7.8	129.0 \pm 8.8
$ggF, H \rightarrow \tau\tau$	3.8 \pm 1.1	7.1 \pm 1.9	62 \pm 16	66 \pm 22
$VBF, H \rightarrow \tau\tau$	7.6 \pm 2.2	24.7 \pm 6.8	11.9 \pm 3.4	14.0 \pm 4.0
$WH, H \rightarrow \tau\tau$	< 0.1	0.1 \pm 0.0	3.9 \pm 1.1	5.4 \pm 1.4
$ZH, H \rightarrow \tau\tau$	< 0.1	< 0.1	1.8 \pm 0.5	2.8 \pm 0.7
$t\bar{t}H, H \rightarrow \tau\tau$	< 0.1	< 0.1	0.1 \pm 0.0	0.2 \pm 0.1
Total background	301 \pm 17	463 \pm 21	6448 \pm 81	6253 \pm 80
Total signal	11.5 \pm 3.2	32.0 \pm 8.2	80 \pm 20	89 \pm 26
Data	318	496	6556	6347

Table 9: Observed event yields and predictions as computed by the fit in the $\tau_{\text{had}}\tau_{\text{had}}$ signal regions. Uncertainties include statistical and systematic components.

	$\tau_{\text{had}}\tau_{\text{had}}$ VBF			$\tau_{\text{had}}\tau_{\text{had}}$ boosted	
	Loose	Tight	High- $p_T^{\tau\tau}$	Low- $p_T^{\tau\tau}$	High- $p_T^{\tau\tau}$
$Z \rightarrow \tau\tau$	67.3 ± 9.2	100 ± 12	141 ± 12	3250 ± 130	3582 ± 82
Misidentified τ	45.0 ± 5.4	96.4 ± 9.2	20.0 ± 2.9	1870 ± 140	364 ± 53
Other backgrounds	4.4 ± 1.4	11.6 ± 1.7	4.4 ± 0.7	281 ± 21	109.9 ± 9.2
$ggF, H \rightarrow \tau\tau$	1.1 ± 0.4	2.0 ± 0.7	3.5 ± 1.0	41 ± 11	48 ± 14
VBF, $H \rightarrow \tau\tau$	1.4 ± 0.5	6.4 ± 1.8	11.2 ± 3.0	9.0 ± 3.4	10.7 ± 2.9
$WH, H \rightarrow \tau\tau$	< 0.1	< 0.1	< 0.1	3.3 ± 0.9	4.4 ± 1.2
$ZH, H \rightarrow \tau\tau$	< 0.1	< 0.1	< 0.1	2.4 ± 0.7	2.9 ± 0.8
$t\bar{t}H, H \rightarrow \tau\tau$	< 0.1	< 0.1	< 0.1	1.6 ± 0.5	1.9 ± 0.5
Total background	116.7 ± 9.4	208 ± 12	165 ± 12	5401 ± 78	4057 ± 64
Total signal	2.6 ± 0.8	8.6 ± 2.4	14.9 ± 3.8	57 ± 15	68 ± 18
Data	121	220	179	5455	4103

Table 10: Summary of different sources of uncertainty in decreasing order of their impact on $\sigma_{H \rightarrow \tau\tau}$. Their observed and expected fractional (%) impacts, both computed by the fit, are given, relative to the $\sigma_{H \rightarrow \tau\tau}$ value. Experimental uncertainties in reconstructed objects combine efficiency and energy/momenta scale and resolution uncertainties. Background statistics includes the bin-by-bin statistical uncertainties in the simulated backgrounds as well as statistical uncertainties in misidentified τ backgrounds, which are estimated using data. Background normalization describes the combined impact of all background normalization uncertainties.

Source of uncertainty	Impact $\Delta\sigma/\sigma_{H \rightarrow \tau\tau}$ [%]	
	Observed	Expected
Theoretical uncert. in signal	+13.4 / -8.7	+12.0 / -7.8
Background statistics	+10.8 / -9.9	+10.1 / -9.7
Jets and E_T^{miss}	+11.2 / -9.1	+10.4 / -8.4
Background normalization	+6.3 / -4.4	+6.3 / -4.4
Misidentified τ	+4.5 / -4.2	+3.4 / -3.2
Theoretical uncert. in background	+4.6 / -3.6	+5.0 / -4.0
Hadronic τ decays	+4.4 / -2.9	+5.5 / -4.0
Flavor tagging	+3.4 / -3.4	+3.0 / -2.3
Luminosity	+3.3 / -2.4	+3.1 / -2.2
Electrons and muons	+1.2 / -0.9	+1.1 / -0.8
Total systematic uncert.	+23 / -20	+22 / -19
Data statistics	± 16	± 15
Total	+28 / -25	+27 / -24

are ranked by their fractional impact on the measurement of $\sigma_{H \rightarrow \tau\tau}$. To compute the impact for each nuisance parameter, a separate fit is performed again with the parameter fixed to its fitted value, and the resulting uncertainty in $\sigma_{H \rightarrow \tau\tau}$ is subtracted from the uncertainty obtained in the original fit via variance subtraction. The dominant uncertainties are related to the limited number of events in the simulated samples, the missing higher-order QCD corrections to the signal process cross sections, the jet energy resolution, the $\tau_{\text{had-vis}}$ identification and the normalizations of the $Z \rightarrow \tau\tau$ and $Z \rightarrow \ell\ell$ backgrounds. Figure 6 also shows that in most cases the fitted parameters are in agreement with the nominal values, except for the uncertainties related to jet energy resolution and scale. In the case of real di- τ events, the distribution of $m_{\tau\tau}^{\text{MMC}}$ is sensitive to the jet-related uncertainties because selected di- τ events in the VBF and boosted categories are characterized by one or more high- p_T jets that recoil against the two τ -leptons. The main contributions to E_T^{miss} are thus the neutrinos in the τ -lepton decays and the impact of the jet energy resolution when projected onto the E_T^{miss} direction. Applying both the jet energy resolution and scale uncertainties causes a shift in the mean jet p_T , which therefore translates directly into a shift of the reconstructed E_T^{miss} . This, in turn, translates into a shift of the reconstructed $m_{\tau\tau}^{\text{MMC}}$ that is constrained by data in the region of the $Z \rightarrow \tau\tau$ mass peak.

Results of the fit when only the data of an individual channel or of an individual category are used, are shown in Figure 7. Also shown is the result from the fit and the uncertainty in $\sigma_{H \rightarrow \tau\tau}^{\text{SM}}$. All results are consistent with the SM expectations. The simple combination of the individual fit results does not agree exactly with the result of the combined fit because the values of the nuisance parameters are different. The $m_{\tau\tau}^{\text{MMC}}$ distributions in all signal regions with background predictions adjusted by the likelihood fit are shown in Figures 12 and 13 in the Appendix. The $m_{\tau\tau}^{\text{MMC}}$ distributions for the predicted signal plus background are compared with the data in Figure 8, separately for the combined signal regions of $\tau_{\text{had}}\tau_{\text{had}}$, $\tau_{\text{lep}}\tau_{\text{had}}$ and $\tau_{\text{lep}}\tau_{\text{lep}}$ analysis channels, and in Figure 9, separately for the combined VBF and the combined boosted signal regions. A weighted combination of the $m_{\tau\tau}^{\text{MMC}}$ distributions in all signal regions is shown in Figure 10. The events are weighted by a factor of $\ln(1 + S/B)$ which enhances the events compatible with the signal hypothesis. Here, S/B is the expected signal-to-background ratio in the corresponding signal region.

Figure 7 illustrates that the VBF and boosted categories provide good sensitivity, respectively, to VBF and ggF Higgs-boson production. A two-parameter fit is therefore performed to determine the cross sections of these production processes by exploiting the sensitivity offered by the use of the event categories in the analysis of the three channels. Two cross-section parameters $\sigma_{H \rightarrow \tau\tau}^{\text{VBF}}$ and $\sigma_{H \rightarrow \tau\tau}^{\text{ggF}}$ are introduced and the data are fitted to these parameters, separating the vector-boson-mediated VBF process from the fermion-mediated ggF process, while the contributions from other Higgs production processes are set to their predicted SM values. The two-dimensional 68% and 95% confidence level (CL) contours in the plane of $\sigma_{H \rightarrow \tau\tau}^{\text{VBF}}$ and $\sigma_{H \rightarrow \tau\tau}^{\text{ggF}}$ are shown in Figure 11. The best-fit values are $\sigma_{H \rightarrow \tau\tau}^{\text{VBF}} = 0.28 \pm 0.09 \text{ (stat.)} {}^{+0.11}_{-0.09} \text{ (syst.) pb}$ and $\sigma_{H \rightarrow \tau\tau}^{\text{ggF}} = 3.1 \pm 1.0 \text{ (stat.)} {}^{+1.6}_{-1.3} \text{ (syst.) pb}$, in agreement with the predictions from the Standard Model of $\sigma_{\text{VBF}, H \rightarrow \tau\tau}^{\text{SM}} = 0.237 \pm 0.006 \text{ pb}$ and $\sigma_{\text{ggF}, H \rightarrow \tau\tau}^{\text{SM}} = 3.05 \pm 0.13 \text{ pb}$ [100]. The two results are strongly anti-correlated (correlation coefficient of -52%), as can be seen in Figure 11.

The ggF signal provides enough events to measure ggF cross sections in mutually exclusive regions of the ggF phase space. Two ggF regions are defined by particle-level events with at least one jet where a jet is required to have $p_T > 30 \text{ GeV}$: events with a Higgs-boson p_T of $60 < p_T^H < 120 \text{ GeV}$ and events with $p_T^H > 120 \text{ GeV}$. A cross-section parameter for each of the two ggF regions is introduced, along with a parameter for VBF production in an inclusive region, and a combined three-parameter fit is performed using the event categories in the analysis of the three channels. The particle-level definitions of all three

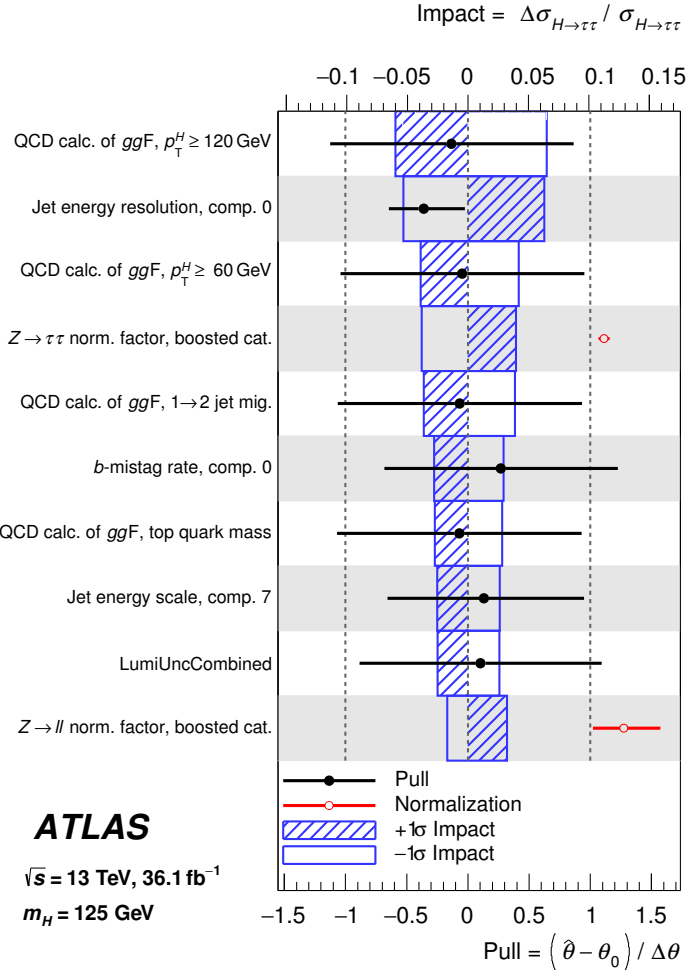


Figure 6: Fractional impact of systematic uncertainties in $\sigma_{H \rightarrow \tau\tau}$ as computed by the fit. The systematic uncertainties are listed in decreasing order of their impact on $\sigma_{H \rightarrow \tau\tau}$ on the y-axis. The hatched blue and open blue boxes show the variations of $\sigma_{H \rightarrow \tau\tau}$ referring to the top x-axis (impact), as described in the text. The filled circles, referring to the bottom x-axis, show the pulls of the fitted nuisance parameters, i.e. the deviations of the fitted parameters $\hat{\theta}$ from their nominal values θ_0 , normalized to their nominal uncertainties $\Delta\theta$. The black lines show the uncertainties of the nuisance parameters resulting from the fit. Several sources of uncertainties such as the jet energy scale and resolution as well as the b -mistag rate are described by their principal components in the fit. The open circles, also referring to the bottom x-axis, show the values of the fitted $Z \rightarrow \tau\tau$ and $Z \rightarrow \ell\ell$ normalization factors in the boosted category as listed in Table 6. Their uncertainties do not include uncertainties in total simulated cross sections extrapolated to the selected phase space.

phase-space regions closely follow the framework of simplified template cross sections [101] where the Higgs-boson rapidity y_H is required to satisfy $|y_H| < 2.5$. The ggF and VBF production cross sections outside the respective particle-level region requirements are set to the measured values reported above. Cross sections of other Higgs-boson production processes are set to their SM values. Table 11 shows the resulting cross sections along with the SM predictions in the respective particle-level region. The measurements in all regions have a precision similar to that of the inclusive ggF and VBF measurements

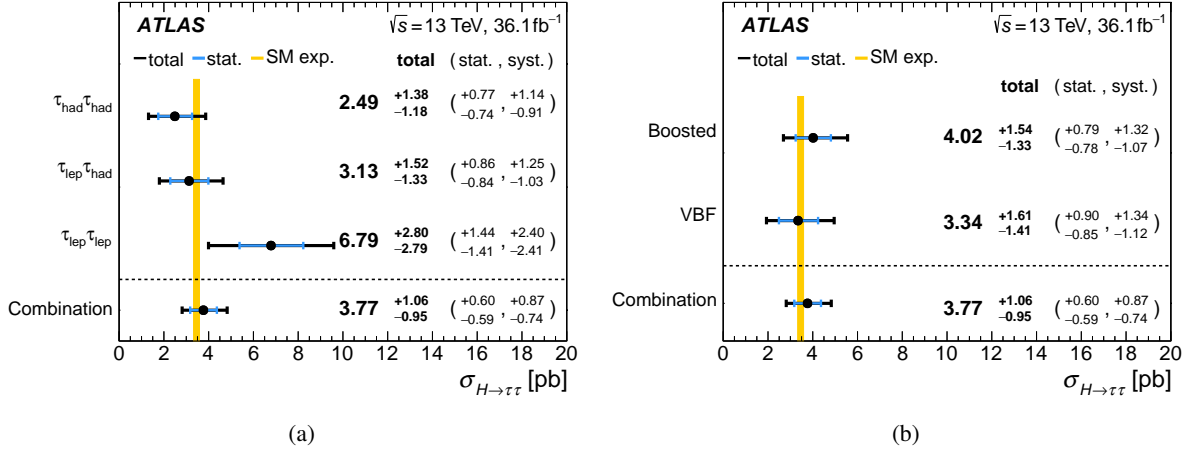


Figure 7: The measured values for $\sigma_{H \rightarrow \tau\tau}$ when only the data of (a) individual channels or (b) individual categories are used. Also shown is the result from the combined fit. The total $\pm 1\sigma$ uncertainty in the measurement is indicated by the black error bars, with the individual contribution from the statistical uncertainty in blue. The theory uncertainty in the predicted signal cross section is shown by the yellow band.

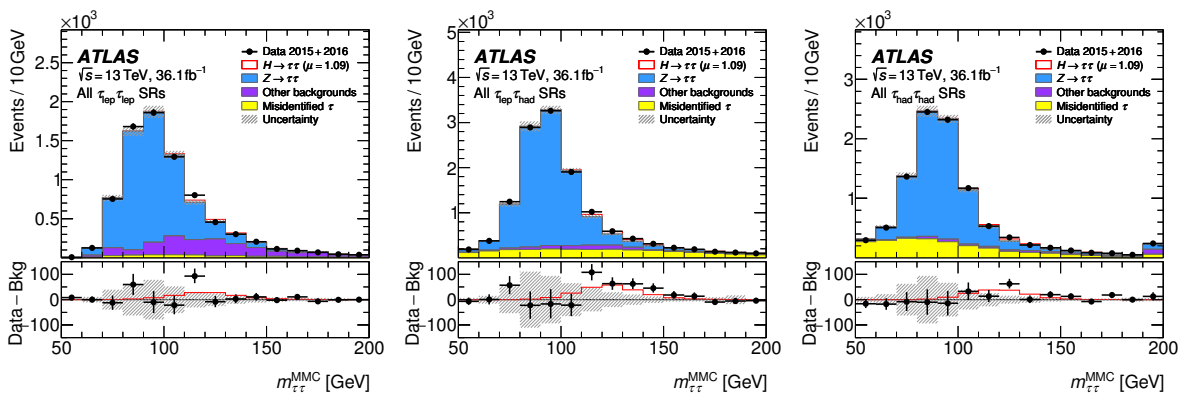


Figure 8: Distributions of the reconstructed di- τ invariant mass ($m_{\tau\tau}^{\text{MMC}}$) for the sum of (left) all $\tau_{\text{lep}}\tau_{\text{lep}}$, (center) all $\tau_{\text{lep}}\tau_{\text{had}}$ and (right) all $\tau_{\text{had}}\tau_{\text{had}}$ signal regions (SRs). The bottom panels show the differences between observed data events and expected background events (black points). The observed Higgs-boson signal ($\mu = 1.09$) is shown with the solid red line. Entries with values that would exceed the x -axis range are shown in the last bin of each distribution. The signal and background predictions are determined in the likelihood fit. The size of the combined statistical, experimental and theoretical uncertainties in the background is indicated by the hatched bands.

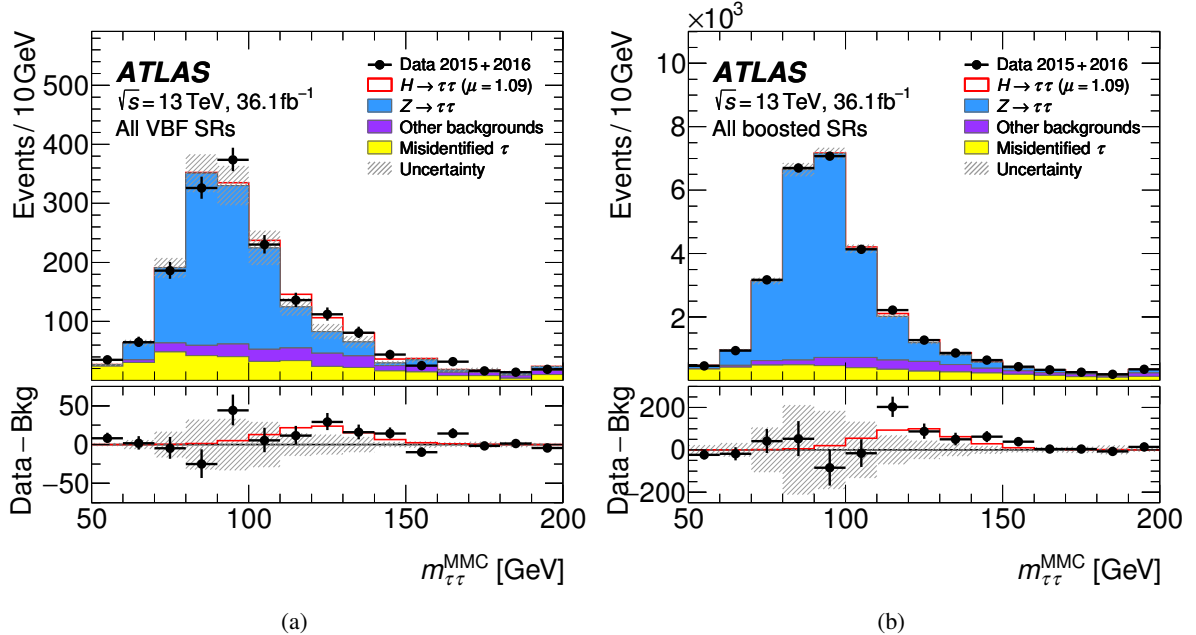


Figure 9: Distribution of the reconstructed di- τ invariant mass ($m_{\tau\tau}^{\text{MMC}}$) for the sum of (a) all VBF and (b) all boosted signal regions (SRs). The bottom panels show the differences between observed data events and expected background events (black points). The observed Higgs-boson signal ($\mu = 1.09$) is shown with the solid red line. Entries with values that would exceed the x -axis range are shown in the last bin of each distribution. The signal and background predictions are determined in the likelihood fit. The size of the combined statistical, experimental and theoretical uncertainties in the background is indicated by the hatched bands.

Table 11: Measurement of the VBF and ggF production cross sections in three mutually exclusive regions of phase space of particle-level events. The number of jets N_{jets} in ggF events comprises all jets with $p_{\text{T}} > 30 \text{ GeV}$. The cross section of ggF events that fail the particle-level requirements of the two ggF regions is set to the measured $\sigma_{H \rightarrow \tau\tau}^{\text{ggF}}$ value. Results are shown along with the SM predictions in the respective particle-level regions. The definitions of the regions closely follow the framework of simplified template cross sections [101].

Process	Particle-level selection	σ [pb]	σ^{SM} [pb]
ggF	$N_{\text{jets}} \geq 1, 60 < p_{\text{T}}^H < 120 \text{ GeV}, y_H < 2.5$	$1.79 \pm 0.53 \text{ (stat.)} \pm 0.74 \text{ (syst.)}$	0.40 ± 0.05
ggF	$N_{\text{jets}} \geq 1, p_{\text{T}}^H > 120 \text{ GeV}, y_H < 2.5$	$0.12 \pm 0.05 \text{ (stat.)} \pm 0.05 \text{ (syst.)}$	0.14 ± 0.03
VBF	$ y_H < 2.5$	$0.25 \pm 0.08 \text{ (stat.)} \pm 0.08 \text{ (syst.)}$	0.22 ± 0.01

reported above.

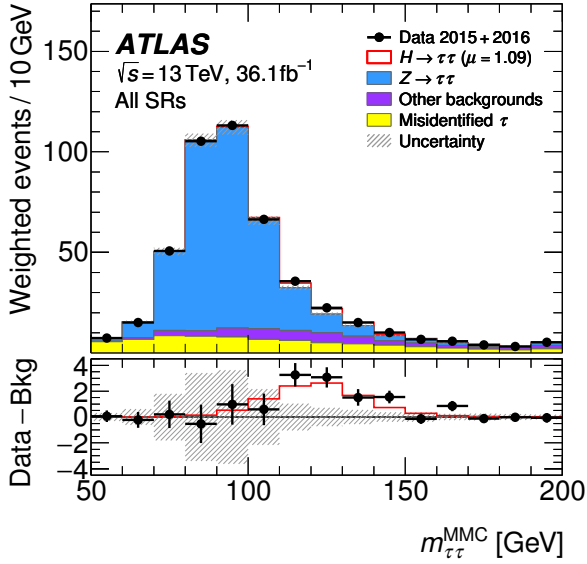


Figure 10: Distribution of the reconstructed di- τ invariant mass ($m_{\tau\tau}^{\text{MMC}}$) for the sum of all signal regions (SRs). The contributions of the different SRs are weighted by a factor of $\ln(1 + S/B)$, where S and B are the expected numbers of signal and background events in that region, respectively. The bottom panel shows the differences between observed data events and expected background events after applying the same weights (black points). The observed Higgs-boson signal ($\mu = 1.09$) is shown with the solid red line. Entries with values that would exceed the x -axis range are shown in the last bin of each distribution. The signal and background predictions are determined in the likelihood fit. The size of the combined statistical, experimental and theoretical uncertainties in the background is indicated by the hatched bands.

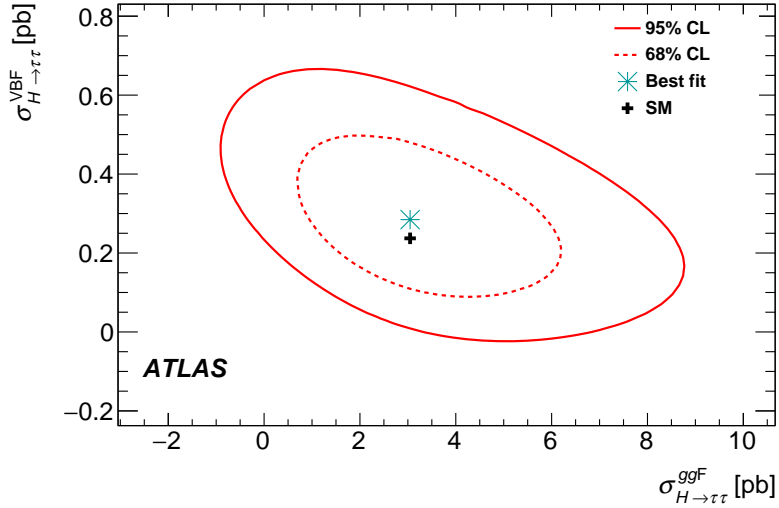


Figure 11: Likelihood contours for the combination of all channels in the $(\sigma_{H \rightarrow \tau\tau}^{\text{ggF}}, \sigma_{H \rightarrow \tau\tau}^{\text{VBF}})$ plane. The 68% and 95% CL contours are shown as dashed and solid lines, respectively, for $m_H = 125$ GeV. The SM expectation is indicated by a plus symbol and the best fit to the data is shown as a star.

9 Conclusions

A measurement of total production cross sections of the Higgs boson in proton–proton collisions is presented in the $H \rightarrow \tau\tau$ decay channel. The analysis was performed using 36.1 fb^{-1} of data recorded by the ATLAS experiment at the LHC at a center-of-mass energy of $\sqrt{s} = 13 \text{ TeV}$. All combinations of leptonic and hadronic τ decays were considered. An excess of events over the expected background from other Standard Model processes was found with an observed (expected) significance of 4.4 (4.1) standard deviations. Combined with results using data taken at \sqrt{s} of 7 and 8 TeV, the observed (expected) significance amounts to 6.4 (5.4) standard deviations and constitutes an observation of $H \rightarrow \tau\tau$ decays by the ATLAS experiment. Using the data taken at $\sqrt{s} = 13 \text{ TeV}$, the $pp \rightarrow H \rightarrow \tau\tau$ total cross section is measured to be $3.77^{+0.60}_{-0.59} \text{ (stat.)}^{+0.87}_{-0.74} \text{ (syst.) pb}$, for a Higgs boson of mass 125 GeV. A two-dimensional fit was performed to separate the vector-boson-mediated VBF process from the fermion-mediated ggF process. The cross sections of the Higgs boson decaying into two τ leptons are measured to be $\sigma_{H \rightarrow \tau\tau}^{\text{VBF}} = 0.28 \pm 0.09 \text{ (stat.)}^{+0.11}_{-0.09} \text{ (syst.) pb}$ and $\sigma_{H \rightarrow \tau\tau}^{\text{ggF}} = 3.1 \pm 1.0 \text{ (stat.)}^{+1.6}_{-1.3} \text{ (syst.) pb}$, respectively, for the two production processes. Similarly, a three-dimensional fit was performed in the framework of simplified template cross sections. Results are reported for the VBF cross section in an inclusive phase space and ggF cross sections in two exclusive regions of phase space defined by particle-level requirements on the Higgs-boson p_T . All measurements are consistent with SM predictions.

Appendix: Distributions of $m_{\tau\tau}^{\text{MMC}}$ in signal regions

Figures 12 and 13 show the $m_{\tau\tau}^{\text{MMC}}$ distributions in all signal regions with background predictions adjusted by the likelihood fit.

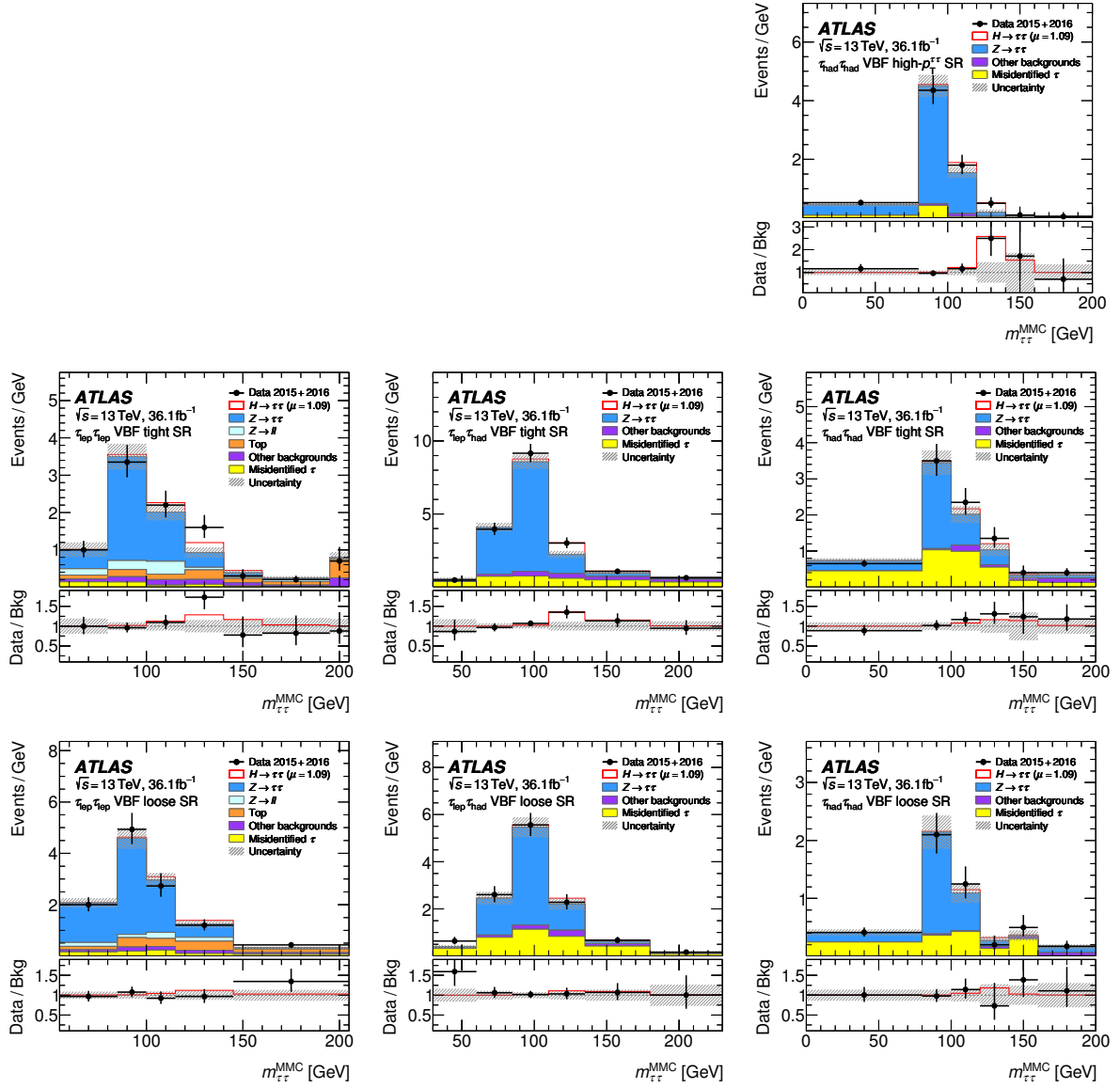


Figure 12: Observed and expected $m_{\tau\tau}^{\text{MMC}}$ distributions as used in the fit in all signal regions (SRs) in the VBF category for the $\tau_{\text{lep}}\tau_{\text{lep}}$ (left), $\tau_{\text{lep}}\tau_{\text{had}}$ (middle) and $\tau_{\text{had}}\tau_{\text{had}}$ (right) analysis channels. The bottom panels show the ratio of observed data events to expected background events (black points). The observed Higgs-boson signal ($\mu = 1.09$) is shown with the solid red line. Entries with values that would exceed the x -axis range are shown in the last bin of each distribution. The signal and background predictions are determined in the likelihood fit. The size of the combined statistical, experimental and theoretical uncertainties in the background is indicated by the hatched bands.

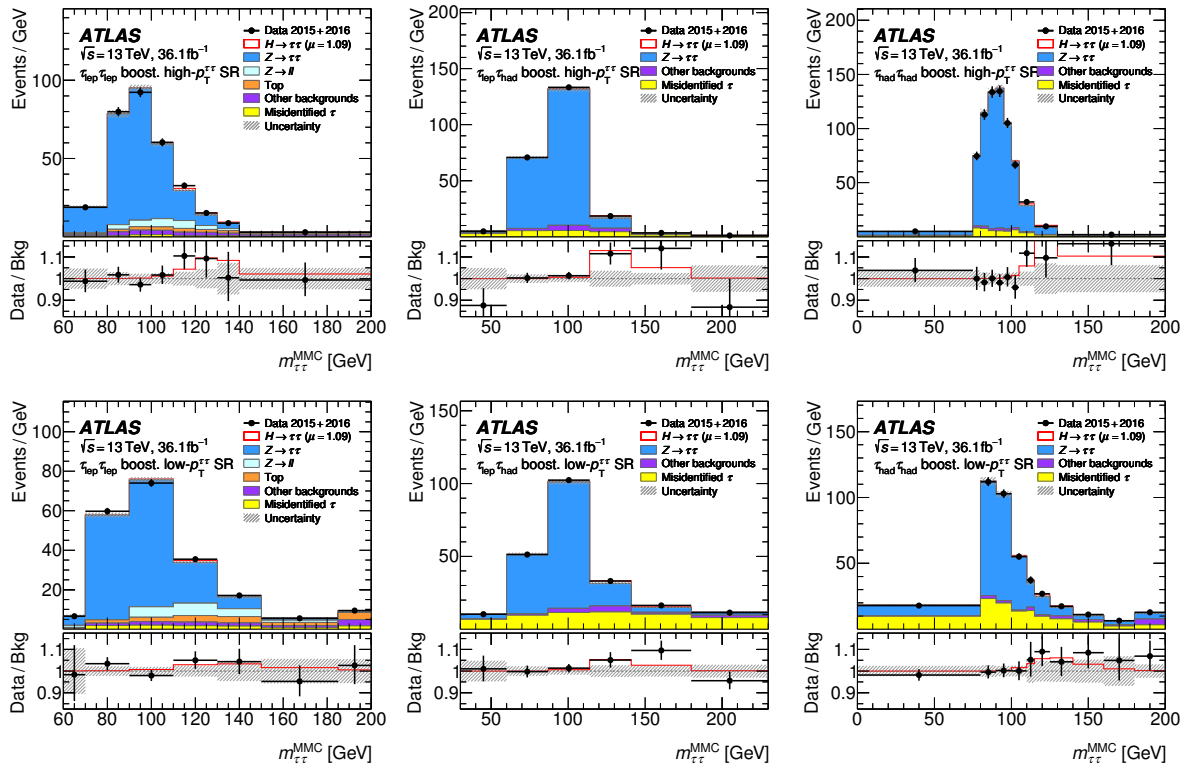


Figure 13: Observed and expected $m_{\tau\tau}^{\text{MMC}}$ distributions as used in the fit in all signal regions (SRs) in the boosted category for the $\tau_{\text{lep}}\tau_{\text{lep}}$ (left), $\tau_{\text{lep}}\tau_{\text{had}}$ (middle) and $\tau_{\text{had}}\tau_{\text{had}}$ (right) analysis channels. The bottom panels show the ratio of observed data events to expected background events (black points). The observed Higgs-boson signal ($\mu = 1.09$) is shown with the solid red line. Entries with values that would exceed the x -axis range are shown in the last bin of each distribution. The signal and background predictions are determined in the likelihood fit. The size of the combined statistical, experimental and theoretical uncertainties in the background is indicated by the hatched bands.

Acknowledgments

We thank CERN for the very successful operation of the LHC, as well as the support staff from our institutions without whom ATLAS could not be operated efficiently.

We acknowledge the support of ANPCyT, Argentina; YerPhI, Armenia; ARC, Australia; BMWFW and FWF, Austria; ANAS, Azerbaijan; SSTC, Belarus; CNPq and FAPESP, Brazil; NSERC, NRC and CFI, Canada; CERN; CONICYT, Chile; CAS, MOST and NSFC, China; COLCIENCIAS, Colombia; MSMT CR, MPO CR and VSC CR, Czech Republic; DNRF and DNSRC, Denmark; IN2P3-CNRS, CEA-DRF/IRFU, France; SRNSFG, Georgia; BMBF, HGF, and MPG, Germany; GSRT, Greece; RGC, Hong Kong SAR, China; ISF and Benoziyo Center, Israel; INFN, Italy; MEXT and JSPS, Japan; CNRST, Morocco; NWO, Netherlands; RCN, Norway; MNiSW and NCN, Poland; FCT, Portugal; MNE/IFA, Romania; MES of Russia and NRC KI, Russian Federation; JINR; MESTD, Serbia; MSSR, Slovakia; ARRS and MIZŠ, Slovenia; DST/NRF, South Africa; MINECO, Spain; SRC and Wallenberg Foundation, Sweden; SERI, SNSF and Cantons of Bern and Geneva, Switzerland; MOST, Taiwan; TAEK, Turkey; STFC, United Kingdom; DOE and NSF, United States of America. In addition, individual groups and members have received support from BCKDF, CANARIE, CRC and Compute Canada, Canada; COST, ERC, ERDF, Horizon 2020, and Marie Skłodowska-Curie Actions, European Union; Investissements d’Avenir Labex and Idex, ANR, France; DFG and AvH Foundation, Germany; Herakleitos, Thales and Aristeia programmes co-financed by EU-ESF and the Greek NSRF, Greece; BSF-NSF and GIF, Israel; CERCA Programme Generalitat de Catalunya, Spain; The Royal Society and Leverhulme Trust, United Kingdom.

The crucial computing support from all WLCG partners is acknowledged gratefully, in particular from CERN, the ATLAS Tier-1 facilities at TRIUMF (Canada), NDGF (Denmark, Norway, Sweden), CC-IN2P3 (France), KIT/GridKA (Germany), INFN-CNAF (Italy), NL-T1 (Netherlands), PIC (Spain), ASGC (Taiwan), RAL (UK) and BNL (USA), the Tier-2 facilities worldwide and large non-WLCG resource providers. Major contributors of computing resources are listed in Ref. [118].

References

- [1] ATLAS Collaboration, *Observation of a new particle in the search for the Standard Model Higgs boson with the ATLAS detector at the LHC*, *Phys. Lett. B* **716** (2012) 1, arXiv: [1207.7214 \[hep-ex\]](https://arxiv.org/abs/1207.7214).
- [2] CMS Collaboration, *Observation of a new boson at a mass of 125 GeV with the CMS experiment at the LHC*, *Phys. Lett. B* **716** (2012) 30, arXiv: [1207.7235 \[hep-ex\]](https://arxiv.org/abs/1207.7235).
- [3] S. L. Glashow, *Partial-symmetries of weak interactions*, *Nucl. Phys.* **22** (1961) 579.
- [4] S. Weinberg, *A Model of Leptons*, *Phys. Rev. Lett.* **19** (1967) 1264.
- [5] A. Salam, *Weak and Electromagnetic Interactions*, Proceedings of the 8th Nobel symposium, Ed. N. Svartholm, Almqvist & Wiksell, 1968, *Conf. Proc. C680519* (1968) 367, URL: <http://inspirehep.net/record/53083>.
- [6] F. Englert and R. Brout, *Broken Symmetry and the Mass of Gauge Vector Mesons*, *Phys. Rev. Lett.* **13** (1964) 321.

- [7] P. W. Higgs, *Broken symmetries and the masses of gauge bosons*, *Phys. Rev. Lett.* **13** (1964) 508.
- [8] G. Guralnik, C. Hagen and T. Kibble, *Global Conservation Laws and Massless Particles*, *Phys. Rev. Lett.* **13** (1964) 585.
- [9] P. W. Higgs, *Spontaneous Symmetry Breakdown without Massless Bosons*, *Phys. Rev.* **145** (1966) 1156.
- [10] T. Kibble, *Symmetry Breaking in Non-Abelian Gauge Theories*, *Phys. Rev.* **155** (1967) 1554.
- [11] ATLAS Collaboration, *Measurements of the Higgs boson production and decay rates and coupling strengths using pp collision data at $\sqrt{s} = 7$ and 8 TeV in the ATLAS experiment*, *Eur. Phys. J. C* **76** (2016) 6, arXiv: [1507.04548 \[hep-ex\]](#).
- [12] CMS Collaboration, *Precise determination of the mass of the Higgs boson and tests of compatibility of its couplings with the standard model predictions using proton collisions at 7 and 8 TeV*, *Eur. Phys. J. C* **75** (2015) 212, arXiv: [1412.8662 \[hep-ex\]](#).
- [13] ATLAS Collaboration, *Study of the spin and parity of the Higgs boson in diboson decays with the ATLAS detector*, *Eur. Phys. J. C* **75** (2015) 476, arXiv: [1506.05669 \[hep-ex\]](#), Erratum: *Eur. Phys. J. C* **76** (2016) 152.
- [14] CMS Collaboration, *Constraints on the spin-parity and anomalous HVV couplings of the Higgs boson in proton collisions at 7 and 8 TeV*, *Phys. Rev. D* **92** (2015) 012004, arXiv: [1411.3441 \[hep-ex\]](#).
- [15] ATLAS Collaboration, *Evidence for the Higgs-boson Yukawa coupling to tau leptons with the ATLAS detector*, *JHEP* **04** (2015) 117, arXiv: [1501.04943 \[hep-ex\]](#).
- [16] CMS Collaboration, *Evidence for the direct decay of the 125 GeV Higgs boson to fermions*, *Nature Phys.* **10** (2014) 557, arXiv: [1401.6527 \[hep-ex\]](#).
- [17] ATLAS and CMS Collaborations, *Measurements of the Higgs boson production and decay rates and constraints on its couplings from a combined ATLAS and CMS analysis of the LHC pp collision data at $\sqrt{s} = 7$ and 8 TeV*, *JHEP* **08** (2016) 045, arXiv: [1606.02266 \[hep-ex\]](#).
- [18] CMS Collaboration, *Observation of the Higgs boson decay to a pair of τ leptons*, *Phys. Lett. B* **779** (2018) 283, arXiv: [1708.00373 \[hep-ex\]](#).
- [19] ATLAS Collaboration, *Observation of Higgs boson production in association with a top quark pair at the LHC with the ATLAS detector*, *Phys. Lett. B* **784** (2018) 173, arXiv: [1806.00425 \[hep-ex\]](#).
- [20] CMS Collaboration, *Observation of $t\bar{t}H$ production*, *Phys. Rev. Lett.* **120** (2018) 231801, arXiv: [1804.02610 \[hep-ex\]](#).
- [21] ATLAS Collaboration, *Observation of $H \rightarrow b\bar{b}$ decays and VH production with the ATLAS detector*, *Phys. Lett. B* **786** (2018) 59, arXiv: [1808.08238 \[hep-ex\]](#).
- [22] CMS Collaboration, *Observation of Higgs Boson Decay to Bottom Quarks*, *Phys. Rev. Lett.* **121** (2018) 121801, arXiv: [1808.08242 \[hep-ex\]](#).

- [23] ATLAS Collaboration, *Search for the Dimuon Decay of the Higgs Boson in pp Collisions at $\sqrt{s} = 13$ TeV with the ATLAS Detector*, Phys. Rev. Lett. **119** (2017) 051802, arXiv: [1705.04582 \[hep-ex\]](#).
- [24] CMS Collaboration, *Search for the Higgs boson decaying to two muons in proton-proton collisions at $\sqrt{s} = 13$ TeV*, (2018), arXiv: [1807.06325 \[hep-ex\]](#).
- [25] ATLAS Collaboration, *Test of CP Invariance in vector-boson fusion production of the Higgs boson using the Optimal Observable method in the ditau decay channel with the ATLAS detector*, Eur. Phys. J. C **76** (2016) 658, arXiv: [1602.04516 \[hep-ex\]](#).
- [26] S. Berge et al., *Prospects of constraining the Higgs boson's CP nature in the tau decay channel at the LHC*, Phys. Rev. D **92** (2015) 096012, arXiv: [1510.03850 \[hep-ph\]](#).
- [27] ATLAS Collaboration, *Modelling $Z \rightarrow \tau\tau$ processes in ATLAS with τ -embedded $Z \rightarrow \mu\mu$ data*, JINST **10** (2015) P09018, arXiv: [1506.05623 \[hep-ex\]](#).
- [28] ATLAS Collaboration, *The ATLAS experiment at the CERN Large Hadron Collider*, JINST **3** (2008) S08003.
- [29] ATLAS Collaboration, *ATLAS Insertable B-Layer Technical Design Report*, CERN-LHCC-2010-013, ATLAS-TDR-19, 2010, URL: <https://cds.cern.ch/record/1291633>.
- [30] Abbott, B. and others, *Production and integration of the ATLAS Insertable B-Layer*, JINST **13** (2018) T05008, arXiv: [1803.00844 \[physics.ins-det\]](#).
- [31] ATLAS and CMS Collaborations, *Combined Measurement of the Higgs Boson Mass in pp Collisions at $\sqrt{s} = 7$ and 8 TeV with the ATLAS and CMS Experiments*, Phys. Rev. Lett. **114** (2015) 191803, arXiv: [1503.07589 \[hep-ex\]](#).
- [32] P. Nason, *A new method for combining NLO QCD with shower Monte Carlo algorithms*, JHEP **11** (2004) 040, arXiv: [hep-ph/0409146](#).
- [33] S. Frixione, P. Nason and C. Oleari, *Matching NLO QCD computations with parton shower simulations: the POWHEG method*, JHEP **11** (2007) 070, arXiv: [0709.2092 \[hep-ph\]](#).
- [34] S. Alioli et al., *A general framework for implementing NLO calculations in shower Monte Carlo programs: the POWHEG BOX*, JHEP **06** (2010) 043, arXiv: [1002.2581 \[hep-ph\]](#).
- [35] E. Bagnaschi, G. Degrassi, P. Slavich and A. Vicini, *Higgs production via gluon fusion in the POWHEG approach in the SM and in the MSSM*, JHEP **02** (2012) 088, arXiv: [1111.2854 \[hep-ph\]](#).
- [36] K. Hamilton, P. Nason, E. Re and G. Zanderighi, *NNLOPS simulation of Higgs boson production*, JHEP **10** (2013) 222, arXiv: [1309.0017 \[hep-ph\]](#).
- [37] K. Hamilton, P. Nason and G. Zanderighi, *Finite quark-mass effects in the NNLOPS POWHEG+MiNLO Higgs generator*, JHEP **05** (2015) 140, arXiv: [1501.04637 \[hep-ph\]](#).

- [38] J. Alwall, R. Frederix, S. Frixione, V. Hirschi, F. Maltoni et al.,
The automated computation of tree-level and next-to-leading order differential cross sections, and their matching to parton shower simulations, *JHEP* **07** (2014) 079,
arXiv: [1405.0301 \[hep-ph\]](#).
- [39] T. Sjöstrand, S. Mrenna and P. Z. Skands, *A brief introduction to PYTHIA 8.1*,
Comput. Phys. Commun. **178** (2008) 852, arXiv: [0710.3820 \[hep-ph\]](#).
- [40] M. Bahr et al., *Herwig++ physics and manual*, *Eur. Phys. J. C* **58** (2008) 639,
arXiv: [0803.0883 \[hep-ph\]](#).
- [41] J. Bellm et al., *Herwig 7.0/Herwig++ 3.0 release note*, *Eur. Phys. J. C* **76** (2016) 196,
arXiv: [1512.01178 \[hep-ph\]](#).
- [42] J. Butterworth et al., *PDF4LHC recommendations for LHC Run II*, *J. Phys. G* **43** (2016) 023001,
arXiv: [1510.03865 \[hep-ph\]](#).
- [43] ATLAS Collaboration, *Measurement of the Z/γ^* boson transverse momentum distribution in pp collisions at $\sqrt{s} = 7$ TeV with the ATLAS detector*, *JHEP* **09** (2014) 145,
arXiv: [1406.3660 \[hep-ex\]](#).
- [44] J. Pumplin et al.,
New generation of parton distributions with uncertainties from global QCD analysis,
JHEP **07** (2002) 012, arXiv: [hep-ph/0201195](#).
- [45] R. Ball et al., *Parton distributions for the LHC Run II*, *JHEP* **1504** (2014) 040,
arXiv: [1410.8849 \[hep-ph\]](#).
- [46] R. D. Ball et al., *Parton distributions with LHC data*, *Nucl. Phys. B* **867** (2013) 244,
arXiv: [1207.1303 \[hep-ph\]](#).
- [47] ATLAS Collaboration, *ATLAS Pythia 8 tunes to 7 TeV data*, ATL-PHYS-PUB-2014-021, 2014,
URL: <https://cds.cern.ch/record/1966419>.
- [48] N. Davidson, T. Przedzinski and Z. Was,
PHOTOS Interface in C++: Technical and Physics Documentation, (2010),
arXiv: [1011.0937 \[hep-ph\]](#).
- [49] C. Anastasiou, C. Duhr, F. Dulat, F. Herzog and B. Mistlberger,
Higgs Boson Gluon-Fusion Production in QCD at Three Loops,
Phys. Rev. Lett. **114** (2015) 212001, arXiv: [1503.06056 \[hep-ph\]](#).
- [50] C. Anastasiou et al.,
High precision determination of the gluon fusion Higgs boson cross-section at the LHC,
JHEP **05** (2016) 058, arXiv: [1602.00695 \[hep-ph\]](#).
- [51] S. Actis, G. Passarino, C. Sturm and S. Uccirati,
NLO electroweak corrections to Higgs boson production at hadron colliders,
Phys. Lett. B **670** (2008) 12, arXiv: [0809.1301 \[hep-ph\]](#).
- [52] C. Anastasiou, R. Boughezal and F. Petriello,
Mixed QCD-electroweak corrections to Higgs boson production in gluon fusion,
JHEP **04** (2009) 003, arXiv: [0811.3458 \[hep-ph\]](#).
- [53] M. Ciccolini, A. Denner and S. Dittmaier, *Strong and Electroweak Corrections to the Production of a Higgs Boson + 2 Jets via Weak Interactions at the Large Hadron Collider*,
Phys. Rev. Lett. **99** (2007) 161803, arXiv: [0707.0381 \[hep-ph\]](#).

- [54] M. Ciccolini, A. Denner and S. Dittmaier,
Electroweak and QCD corrections to Higgs production via vector-boson fusion at the LHC,
Phys. Rev. D **77** (2008) 013002, arXiv: [0710.4749 \[hep-ph\]](#).
- [55] P. Bolzoni, F. Maltoni, S.-O. Moch and M. Zaro,
Higgs Boson Production via Vector-Boson Fusion at Next-to-Next-to-Leading Order in QCD,
Phys. Rev. Lett. **105** (2010) 011801, arXiv: [1003.4451 \[hep-ph\]](#).
- [56] O. Brein, A. Djouadi and R. Harlander,
NNLO QCD corrections to the Higgs-strahlung processes at hadron colliders,
Phys. Lett. B **579** (2004) 149, arXiv: [hep-ph/0307206 \[hep-ph\]](#).
- [57] L. Altenkamp, S. Dittmaier, R. V. Harlander, H. Rzehak and T. J. E. Zirke,
Gluon-induced Higgs-strahlung at next-to-leading order QCD, *JHEP* **02** (2013) 078,
arXiv: [1211.5015 \[hep-ph\]](#).
- [58] A. Denner, S. Dittmaier, S. Kallweit and A. Muck, *Electroweak corrections to Higgs-strahlung off W/Z bosons at the Tevatron and the LHC with HAWK*, *JHEP* **03** (2012) 075,
arXiv: [1112.5142 \[hep-ph\]](#).
- [59] W. Beenakker et al., *Higgs Radiation Off Top Quarks at the Tevatron and the LHC*,
Phys. Rev. Lett. **87** (2001) 201805, arXiv: [hep-ph/0107081 \[hep-ph\]](#).
- [60] W. Beenakker et al., *NLO QCD corrections to $t\bar{t}H$ production in hadron collisions*,
Nucl. Phys. B **653** (2003) 151, arXiv: [hep-ph/0211352 \[hep-ph\]](#).
- [61] S. Dawson, L. Orr, L. Reina and D. Wackeroth,
Next-to-leading order QCD corrections to $pp \rightarrow t\bar{t}h$ at the CERN Large Hadron Collider,
Phys. Rev. D **67** (2003) 071503, arXiv: [hep-ph/0211438 \[hep-ph\]](#).
- [62] S. Dawson, C. Jackson, L. Orr, L. Reina and D. Wackeroth, *Associated Higgs boson production with top quarks at the CERN Large Hadron Collider: NLO QCD corrections*,
Phys. Rev. D **68** (2003) 034022, arXiv: [hep-ph/0305087 \[hep-ph\]](#).
- [63] Y. Zhang, W.-G. Ma, R.-Y. Zhang, C. Chen and L. Guo,
QCD NLO and EW NLO corrections to $t\bar{t}H$ production with top quark decays at hadron collider,
Phys. Lett. B **738** (2014) 1, arXiv: [1407.1110 \[hep-ph\]](#).
- [64] S. Frixione, V. Hirschi, D. Pagani, H.-S. Shao and M. Zaro,
Electroweak and QCD corrections to top-pair hadroproduction in association with heavy bosons,
JHEP **06** (2015) 184, arXiv: [1504.03446 \[hep-ph\]](#).
- [65] T. Gleisberg et al., *Event generation with SHERPA 1.1*, *JHEP* **02** (2009) 007,
arXiv: [0811.4622 \[hep-ph\]](#).
- [66] T. Gleisberg and S. Höche, *Comix, a new matrix element generator*, *JHEP* **12** (2008) 039,
arXiv: [0808.3674 \[hep-ph\]](#).
- [67] F. Cascioli, P. Maierhofer and S. Pozzorini, *Scattering Amplitudes with Open Loops*,
Phys. Rev. Lett. **108** (2012) 111601, arXiv: [1111.5206 \[hep-ph\]](#).
- [68] S. Schumann and F. Krauss,
A Parton shower algorithm based on Catani-Seymour dipole factorisation, *JHEP* **03** (2008) 038,
arXiv: [0709.1027 \[hep-ph\]](#).
- [69] S. Höche, F. Krauss, M. Schönher and F. Siegert,
QCD matrix elements + parton showers: The NLO case, *JHEP* **04** (2013) 027,
arXiv: [1207.5030 \[hep-ph\]](#).

- [70] K. Melnikov and F. Petriello,
Electroweak gauge boson production at hadron colliders through $O(\alpha_S^2)$,
Phys. Rev. D **74** (2006) 114017, arXiv: [hep-ph/0609070 \[hep-ph\]](#).
- [71] C. Anastasiou, L. J. Dixon, K. Melnikov and F. Petriello, *High precision QCD at hadron colliders: Electroweak gauge boson rapidity distributions at NNLO*,
Phys. Rev. D **69** (2004) 094008, arXiv: [hep-ph/0312266 \[hep-ph\]](#).
- [72] S. Alioli, S.-O. Moch and P. Uwer,
Hadronic top-quark pair-production with one jet and parton showering, *JHEP* **01** (2012) 137,
arXiv: [1110.5251 \[hep-ph\]](#).
- [73] M. Czakon and A. Mitov,
Top++: A program for the calculation of the top-pair cross-section at hadron colliders,
Comput. Phys. Commun. **185** (2014) 2930, arXiv: [1112.5675 \[hep-ph\]](#).
- [74] S. Alioli, P. Nason, C. Oleari and E. Re,
NLO single-top production matched with shower in POWHEG: s- and t-channel contributions,
JHEP **09** (2009) 111, arXiv: [0907.4076 \[hep-ph\]](#), Erratum: *JHEP* **02** (2010) 011.
- [75] E. Re,
Single-top Wt-channel production matched with parton showers using the POWHEG method,
Eur. Phys. J. C **71** (2011) 1547, arXiv: [1009.2450 \[hep-ph\]](#).
- [76] P. Artoisenet, R. Frederix, O. Mattelaer and R. Rietkerk,
Automatic spin-entangled decays of heavy resonances in Monte Carlo simulations,
JHEP **03** (2013) 015, arXiv: [1212.3460 \[hep-ph\]](#).
- [77] T. Sjöstrand, S. Mrenna and P. Z. Skands, *PYTHIA 6.4 physics and manual*, *JHEP* **05** (2006) 026,
arXiv: [hep-ph/0603175 \[hep-ph\]](#).
- [78] P. Z. Skands, *Tuning Monte Carlo generators: The Perugia tunes*,
Phys. Rev. D **82** (2010) 074018, arXiv: [1005.3457 \[hep-ph\]](#).
- [79] D. J. Lange, *The EvtGen particle decay simulation package*,
Nucl. Instrum. Meth. A **462** (2001) 152.
- [80] ATLAS Collaboration, *The ATLAS Simulation Infrastructure*, *Eur. Phys. J. C* **70** (2010) 823,
arXiv: [1005.4568 \[hep-ex\]](#).
- [81] GEANT4 Collaboration, S. Agostinelli et al., *Geant4 – a simulation toolkit*,
Nucl. Instrum. Meth. A **506** (2003) 250.
- [82] A. D. Martin, W. J. Stirling, R. S. Thorne and G. Watt, *Parton distributions for the LHC*,
Eur. Phys. J. C **63** (2009) 189, arXiv: [0901.0002 \[hep-ph\]](#).
- [83] ATLAS Collaboration, *Summary of ATLAS Pythia 8 tunes*, ATL-PHYS-PUB-2012-003, 2012,
URL: <https://cds.cern.ch/record/1474107>.
- [84] ATLAS Collaboration,
Electron and photon energy calibration with the ATLAS detector using LHC Run 1 data,
Eur. Phys. J. C **74** (2014) 3071, arXiv: [1407.5063 \[hep-ex\]](#).
- [85] ATLAS Collaboration, *Electron efficiency measurements with the ATLAS detector using the 2015 LHC proton–proton collision data*, ATLAS-CONF-2016-024, 2016,
URL: <https://cds.cern.ch/record/2157687>.

- [86] ATLAS Collaboration, *Performance of the ATLAS trigger system in 2015*, *Eur. Phys. J. C* **77** (2017) 317, arXiv: [1611.09661 \[hep-ex\]](#).
- [87] ATLAS Collaboration, *Muon reconstruction performance of the ATLAS detector in proton–proton collision data at $\sqrt{s} = 13$ TeV*, *Eur. Phys. J. C* **76** (2016) 292, arXiv: [1603.05598 \[hep-ex\]](#).
- [88] M. Cacciari, G. P. Salam and G. Soyez, *The anti- k_t jet clustering algorithm*, *JHEP* **04** (2008) 063, arXiv: [0802.1189 \[hep-ph\]](#).
- [89] ATLAS Collaboration, *Topological cell clustering in the ATLAS calorimeters and its performance in LHC Run 1*, *Eur. Phys. J. C* **77** (2017) 490, arXiv: [1603.02934 \[hep-ex\]](#).
- [90] ATLAS Collaboration, *Performance of pile-up mitigation techniques for jets in pp collisions at $\sqrt{s} = 8$ TeV using the ATLAS detector*, *Eur. Phys. J. C* **76** (2016) 581, arXiv: [1510.03823 \[hep-ex\]](#).
- [91] ATLAS Collaboration, *Identification and rejection of pile-up jets at high pseudorapidity with the ATLAS detector*, *Eur. Phys. J. C* **77** (2017) 580, arXiv: [1705.02211 \[hep-ex\]](#), Erratum: *Eur. Phys. J. C* **77** (2017) 712.
- [92] ATLAS Collaboration, *Performance of b-jet identification in the ATLAS experiment*, *JINST* **11** (2016) P04008, arXiv: [1512.01094 \[hep-ex\]](#).
- [93] ATLAS Collaboration, *Optimisation of the ATLAS b-tagging performance for the 2016 LHC Run*, ATL-PHYS-PUB-2016-012, 2016, URL: <https://cds.cern.ch/record/2160731>.
- [94] ATLAS Collaboration, *Measurement of the tau lepton reconstruction and identification performance in the ATLAS experiment using pp collisions at $\sqrt{s} = 13$ TeV*, ATLAS-CONF-2017-029, 2017, URL: <https://cds.cern.ch/record/2261772>.
- [95] ATLAS Collaboration, *The ATLAS Tau Trigger in Run 2*, ATLAS-CONF-2017-061, 2017, URL: <https://cds.cern.ch/record/2274201>.
- [96] ATLAS Collaboration, *Performance of missing transverse momentum reconstruction with the ATLAS detector using proton-proton collisions at $\sqrt{s} = 13$ TeV*, (2018), arXiv: [1802.08168 \[hep-ex\]](#).
- [97] A. Elagin, P. Murat, A. Pranko and A. Safonov, *A New Mass Reconstruction Technique for Resonances Decaying to $\tau\tau$* , *Nucl. Instrum. Meth. A* **654** (2011) 481, arXiv: [1012.4686 \[hep-ex\]](#).
- [98] R. Ellis et al., *Higgs decay to $\tau^+\tau^-$:A possible signature of intermediate mass Higgs bosons at high energy hadron colliders*, *Nucl. Phys. B* **297** (1998) 221.
- [99] ATLAS Collaboration, *Observation and measurement of Higgs boson decays to WW^* with the ATLAS detector*, *Phys. Rev. D* **92** (2015) 012006, arXiv: [1412.2641 \[hep-ex\]](#).
- [100] LHC Higgs Cross Section Working Group, S. Dittmaier, C. Mariotti, G. Passarino and R. Tanaka (Eds.), *Handbook of LHC Higgs Cross Sections: 1. Inclusive Observables*, CERN-2011-002 (CERN, Geneva, 2011), arXiv: [1101.0593 \[hep-ph\]](#).

- [101] LHC Higgs Cross Section Working Group et al.,
Handbook of LHC Higgs Cross Sections: 4. Deciphering the Nature of the Higgs Sector, CERN-2017-002-M (CERN, Geneva, 2016), arXiv: [1610.07922 \[hep-ph\]](#).
- [102] I. W. Stewart, F. J. Tackmann, J. R. Walsh and S. Zuberi,
Jet p_T resummation in Higgs production at NNLL' + NNLO, Phys. Rev. D **89** (2014) 054001, arXiv: [1307.1808 \[hep-ph\]](#).
- [103] X. Liu and F. Petriello,
Reducing theoretical uncertainties for exclusive Higgs-boson plus one-jet production at the LHC, Phys. Rev. D **87** (2013) 094027, arXiv: [1303.4405 \[hep-ph\]](#).
- [104] R. Boughezal, X. Liu, F. Petriello, F. J. Tackmann and J. R. Walsh,
Combining resummed Higgs predictions across jet bins, Phys. Rev. D **89** (2014) 074044, arXiv: [1312.4535 \[hep-ph\]](#).
- [105] I. W. Stewart and F. J. Tackmann,
Theory uncertainties for Higgs mass and other searches using jet bins, Phys. Rev. D **85** (2012) 034011, arXiv: [1107.2117 \[hep-ph\]](#).
- [106] S. Gangal and F. J. Tackmann,
Next-to-leading-order uncertainties in Higgs+2 jets from gluon fusion, Phys. Rev. D **87** (2013) 093008, arXiv: [1302.5437 \[hep-ph\]](#).
- [107] L. Lönnblad and S. Prestel, *Matching tree-level matrix elements with interleaved showers*, JHEP **03** (2012) 019, arXiv: [1109.4829 \[hep-ph\]](#).
- [108] ATLAS Collaboration, *Measurement of the cross-section for electroweak production of dijets in association with a Z boson in pp collisions at $\sqrt{s} = 13$ TeV with the ATLAS detector*, Phys. Lett. B **775** (2017) 206, arXiv: [1709.10264 \[hep-ex\]](#).
- [109] ATLAS Collaboration, *Electron identification measurements in ATLAS using $\sqrt{s} = 13$ TeV data with 50 ns bunch spacing*, ATL-PHYS-PUB-2015-041, 2015, URL: <https://cds.cern.ch/record/2048202>.
- [110] ATLAS Collaboration, *Luminosity determination in pp collisions at $\sqrt{s} = 8$ TeV using the ATLAS detector at the LHC*, Eur. Phys. J. C **76** (2016) 653, arXiv: [1608.03953 \[hep-ex\]](#).
- [111] G. Avoni et al., *The new LUCID-2 detector for luminosity measurement and monitoring in ATLAS*, JINST **13** (2018) P07017.
- [112] ATLAS Collaboration, *Reconstruction, Energy Calibration, and Identification of Hadronically Decaying Tau Leptons in the ATLAS Experiment for Run-2 of the LHC*, ATL-PHYS-PUB-2015-045, 2015, URL: <https://cds.cern.ch/record/2064383>.
- [113] ATLAS Collaboration, *Tagging and suppression of pileup jets with the ATLAS detector*, ATLAS-CONF-2014-018, 2014, URL: <https://cds.cern.ch/record/1700870>.
- [114] ATLAS Collaboration, *Identification and energy calibration of hadronically decaying tau leptons with the ATLAS experiment in pp collisions at $\sqrt{s} = 8$ TeV*, Eur. Phys. J. C **75** (2015) 303, arXiv: [1412.7086 \[hep-ex\]](#).
- [115] ATLAS Collaboration, *Jet energy scale measurements and their systematic uncertainties in proton-proton collisions at $\sqrt{s} = 13$ TeV with the ATLAS detector*, Phys. Rev. D **96** (2017) 072002, arXiv: [1703.09665 \[hep-ex\]](#).

- [116] ATLAS Collaboration, *Jet Calibration and Systematic Uncertainties for Jets Reconstructed in the ATLAS Detector at $\sqrt{s} = 13$ TeV*, ATL-PHYS-PUB-2015-015, 2015,
URL: <https://cds.cern.ch/record/2037613>.
- [117] G. Cowan, K. Cranmer, E. Gross and O. Vitells,
Asymptotic formulae for likelihood-based tests of new physics, Eur. Phys. J. C **71** (2011) 1554,
arXiv: [1007.1727 \[physics.data-an\]](https://arxiv.org/abs/1007.1727), Erratum: Eur. Phys. J. C **73** (2013) 2501.
- [118] ATLAS Collaboration, *ATLAS Computing Acknowledgements*, ATL-GEN-PUB-2016-002,
URL: <https://cds.cern.ch/record/2202407>.

The ATLAS Collaboration

M. Aaboud^{35d}, G. Aad¹⁰⁰, B. Abbott¹²⁷, O. Abdinov^{13,*}, B. Abeloos¹³¹, D.K. Abhayasinghe⁹², S.H. Abidi¹⁶⁶, O.S. AbouZeid⁴⁰, N.L. Abraham¹⁵⁵, H. Abramowicz¹⁶⁰, H. Abreu¹⁵⁹, Y. Abulaiti⁶, B.S. Acharya^{65a,65b,n}, S. Adachi¹⁶², L. Adam⁹⁸, C. Adam Bourdarios¹³¹, L. Adamczyk^{82a}, J. Adelman¹²⁰, M. Adersberger¹¹³, A. Adiguzel^{12c}, T. Adye¹⁴³, A.A. Affolder¹⁴⁵, Y. Afik¹⁵⁹, C. Agheorghiesei^{27c}, J.A. Aguilar-Saavedra^{139f,139a}, F. Ahmadov^{78,ad}, G. Aielli^{72a,72b}, S. Akatsuka⁸⁴, T.P.A. Åkesson⁹⁵, E. Akilli⁵³, A.V. Akimov¹⁰⁹, G.L. Alberghi^{23b,23a}, J. Albert¹⁷⁵, P. Albicocco⁵⁰, M.J. Alconada Verzini⁸⁷, S. Alderweireldt¹¹⁸, M. Aleksa³⁶, I.N. Aleksandrov⁷⁸, C. Alexa^{27b}, T. Alexopoulos¹⁰, M. Alhoob¹²⁷, B. Ali¹⁴¹, G. Alimonti^{67a}, J. Alison³⁷, S.P. Alkire¹⁴⁷, C. Allaire¹³¹, B.M.M. Allbrooke¹⁵⁵, B.W. Allen¹³⁰, P.P. Allport²¹, A. Aloisio^{68a,68b}, A. Alonso⁴⁰, F. Alonso⁸⁷, C. Alpigiani¹⁴⁷, A.A. Alshehri⁵⁶, M.I. Alstaty¹⁰⁰, B. Alvarez Gonzalez³⁶, D. Álvarez Piqueras¹⁷³, M.G. Alviggi^{68a,68b}, B.T. Amadio¹⁸, Y. Amaral Coutinho^{79b}, A. Ambler¹⁰², L. Ambroz¹³⁴, C. Amelung²⁶, D. Amidei¹⁰⁴, S.P. Amor Dos Santos^{139a,139c}, S. Amoroso⁴⁵, C.S. Amrouche⁵³, C. Anastopoulos¹⁴⁸, L.S. Ancu⁵³, N. Andari¹⁴⁴, T. Andeen¹¹, C.F. Anders^{60b}, J.K. Anders²⁰, K.J. Anderson³⁷, A. Andreazza^{67a,67b}, V. Andrei^{60a}, C.R. Anelli¹⁷⁵, S. Angelidakis³⁸, I. Angelozzi¹¹⁹, A. Angerami³⁹, A.V. Anisenkov^{121b,121a}, A. Annovi^{70a}, C. Antel^{60a}, M.T. Anthony¹⁴⁸, M. Antonelli⁵⁰, D.J.A. Antrim¹⁷⁰, F. Anulli^{71a}, M. Aoki⁸⁰, J.A. Aparisi Pozo¹⁷³, L. Aperio Bella³⁶, G. Arabidze¹⁰⁵, J.P. Araque^{139a}, V. Araujo Ferraz^{79b}, R. Araujo Pereira^{79b}, A.T.H. Arce⁴⁸, R.E. Ardell⁹², F.A. Arduh⁸⁷, J-F. Arguin¹⁰⁸, S. Argyropoulos⁷⁶, A.J. Armbruster³⁶, L.J. Armitage⁹¹, A. Armstrong¹⁷⁰, O. Arnaez¹⁶⁶, H. Arnold¹¹⁹, M. Arratia³², O. Arslan²⁴, A. Artamonov^{110,*}, G. Artoni¹³⁴, S. Artz⁹⁸, S. Asai¹⁶², N. Asbah⁵⁸, E.M. Asimakopoulou¹⁷¹, L. Asquith¹⁵⁵, K. Assamagan²⁹, R. Astalos^{28a}, R.J. Atkin^{33a}, M. Atkinson¹⁷², N.B. Atlay¹⁵⁰, K. Augsten¹⁴¹, G. Avolio³⁶, R. Avramidou^{59a}, M.K. Ayoub^{15a}, G. Azuelos^{108,ar}, A.E. Baas^{60a}, M.J. Baca²¹, H. Bachacou¹⁴⁴, K. Bachas^{66a,66b}, M. Backes¹³⁴, P. Bagnaia^{71a,71b}, M. Bahmani⁸³, H. Bahrasemani¹⁵¹, A.J. Bailey¹⁷³, J.T. Baines¹⁴³, M. Bajic⁴⁰, C. Bakalis¹⁰, O.K. Baker¹⁸², P.J. Bakker¹¹⁹, D. Bakshi Gupta⁹⁴, S. Balaji¹⁵⁶, E.M. Baldin^{121b,121a}, P. Balek¹⁷⁹, F. Balli¹⁴⁴, W.K. Balunas¹³⁶, J. Balz⁹⁸, E. Banas⁸³, A. Bandyopadhyay²⁴, Sw. Banerjee^{180,i}, A.A.E. Bannoura¹⁸¹, L. Barak¹⁶⁰, W.M. Barbe³⁸, E.L. Barberio¹⁰³, D. Barberis^{54b,54a}, M. Barbero¹⁰⁰, T. Barillari¹¹⁴, M-S. Barisits³⁶, J. Barkeloo¹³⁰, T. Barklow¹⁵², R. Barnea¹⁵⁹, S.L. Barnes^{59c}, B.M. Barnett¹⁴³, R.M. Barnett¹⁸, Z. Barnovska-Blenessy^{59a}, A. Baroncelli^{73a}, G. Barone²⁶, A.J. Barr¹³⁴, L. Barranco Navarro¹⁷³, F. Barreiro⁹⁷, J. Barreiro Guimaraes da Costa^{15a}, R. Bartoldus¹⁵², A.E. Barton⁸⁸, P. Bartos^{28a}, A. Basalaev¹³⁷, A. Bassalat^{131,al}, R.L. Bates⁵⁶, S.J. Batista¹⁶⁶, S. Batlamous^{35e}, J.R. Batley³², M. Battaglia¹⁴⁵, M. Bauce^{71a,71b}, F. Bauer¹⁴⁴, K.T. Bauer¹⁷⁰, H.S. Bawa^{31,l}, J.B. Beacham¹²⁵, T. Beau¹³⁵, P.H. Beauchemin¹⁶⁹, F. Becherer⁵¹, P. Bechtle²⁴, H.C. Beck⁵², H.P. Beck^{20,p}, K. Becker⁵¹, M. Becker⁹⁸, C. Becot⁴⁵, A. Beddall^{12d}, A.J. Beddall^{12a}, V.A. Bednyakov⁷⁸, M. Bedognetti¹¹⁹, C.P. Bee¹⁵⁴, T.A. Beermann³⁶, M. Begalli^{79b}, M. Begel²⁹, A. Behera¹⁵⁴, J.K. Behr⁴⁵, A.S. Bell⁹³, G. Bella¹⁶⁰, L. Bellagamba^{23b}, A. Bellerive³⁴, M. Bellomo¹⁵⁹, P. Bellos⁹, K. Belotskiy¹¹¹, N.L. Belyaev¹¹¹, O. Benary^{160,*}, D. Benchekroun^{35a}, M. Bender¹¹³, N. Benekos¹⁰, Y. Benhammou¹⁶⁰, E. Benhar Noccioli¹⁸², J. Benitez⁷⁶, D.P. Benjamin⁴⁸, M. Benoit⁵³, J.R. Bensinger²⁶, S. Bentvelsen¹¹⁹, L. Beresford¹³⁴, M. Beretta⁵⁰, D. Berge⁴⁵, E. Bergeaas Kuutmann¹⁷¹, N. Berger⁵, L.J. Bergsten²⁶, J. Beringer¹⁸, S. Berlendis⁷, N.R. Bernard¹⁰¹, G. Bernardi¹³⁵, C. Bernius¹⁵², F.U. Bernlochner²⁴, T. Berry⁹², P. Berta⁹⁸, C. Bertella^{15a}, G. Bertoli^{44a,44b}, I.A. Bertram⁸⁸, G.J. Besjes⁴⁰, O. Bessidskaia Bylund¹⁸¹, M. Bessner⁴⁵, N. Besson¹⁴⁴, A. Bethani⁹⁹, S. Bethke¹¹⁴, A. Betti²⁴, A.J. Bevan⁹¹, J. Beyer¹¹⁴, R.M. Bianchi¹³⁸, O. Biebel¹¹³, D. Biedermann¹⁹, R. Bielski³⁶, K. Bierwagen⁹⁸, N.V. Biesuz^{70a,70b}, M. Biglietti^{73a}, T.R.V. Billoud¹⁰⁸, M. Bindi⁵², A. Bingul^{12d}, C. Bini^{71a,71b}, S. Biondi^{23b,23a}, M. Birman¹⁷⁹, T. Bisanz⁵², J.P. Biswal¹⁶⁰, C. Bittrich⁴⁷,

D.M. Bjergaard⁴⁸, J.E. Black¹⁵², K.M. Black²⁵, T. Blazek^{28a}, I. Bloch⁴⁵, C. Blocker²⁶, A. Blue⁵⁶, U. Blumenschein⁹¹, S. Blunier^{146a}, G.J. Bobbink¹¹⁹, V.S. Bobrovnikov^{121b,121a}, S.S. Bocchetta⁹⁵, A. Bocci⁴⁸, D. Boerner¹⁸¹, D. Bogavac¹¹³, A.G. Bogdanchikov^{121b,121a}, C. Bohm^{44a}, V. Boisvert⁹², P. Bokan^{171,52}, T. Bold^{82a}, A.S. Boldyrev¹¹², A.E. Bolz^{60b}, M. Bomben¹³⁵, M. Bona⁹¹, J.S. Bonilla¹³⁰, M. Boonekamp¹⁴⁴, A. Borisov¹²², G. Borissov⁸⁸, J. Bortfeldt³⁶, D. Bortolotto¹³⁴, V. Bortolotto^{72a,72b}, D. Boscherini^{23b}, M. Bosman¹⁴, J.D. Bossio Sola³⁰, K. Bouaouda^{35a}, J. Boudreau¹³⁸, E.V. Bouhova-Thacker⁸⁸, D. Boumediene³⁸, S.K. Boutle⁵⁶, A. Boveia¹²⁵, J. Boyd³⁶, D. Boye^{33b}, I.R. Boyko⁷⁸, A.J. Bozson⁹², J. Bracinik²¹, N. Brahimi¹⁰⁰, A. Brandt⁸, G. Brandt¹⁸¹, O. Brandt^{60a}, F. Braren⁴⁵, U. Bratzler¹⁶³, B. Brau¹⁰¹, J.E. Brau¹³⁰, W.D. Breaden Madden⁵⁶, K. Brendlinger⁴⁵, L. Brenner⁴⁵, R. Brenner¹⁷¹, S. Bressler¹⁷⁹, B. Brickwedde⁹⁸, D.L. Briglin²¹, D. Britton⁵⁶, D. Britzger^{60b}, I. Brock²⁴, R. Brock¹⁰⁵, G. Brooijmans³⁹, T. Brooks⁹², W.K. Brooks^{146b}, E. Brost¹²⁰, J.H. Broughton²¹, P.A. Bruckman de Renstrom⁸³, D. Bruncko^{28b}, A. Brunni^{23b}, G. Brunni^{23b}, L.S. Brunni¹¹⁹, S. Bruno^{72a,72b}, B.H. Brunt³², M. Bruschi^{23b}, N. Bruscino¹³⁸, P. Bryant³⁷, L. Bryngemark⁴⁵, T. Buanes¹⁷, Q. Buat³⁶, P. Buchholz¹⁵⁰, A.G. Buckley⁵⁶, I.A. Budagov⁷⁸, M.K. Bugge¹³³, F. Bührer⁵¹, O. Bulekov¹¹¹, D. Bullock⁸, T.J. Burch¹²⁰, S. Burdin⁸⁹, C.D. Burgard¹¹⁹, A.M. Burger⁵, B. Burghgrave¹²⁰, K. Burka⁸³, S. Burke¹⁴³, I. Burmeister⁴⁶, J.T.P. Burr¹³⁴, V. Büscher⁹⁸, E. Buschmann⁵², P.J. Bussey⁵⁶, J.M. Butler²⁵, C.M. Buttar⁵⁶, J.M. Butterworth⁹³, P. Butti³⁶, W. Buttlinger³⁶, A. Buzatu¹⁵⁷, A.R. Buzykaev^{121b,121a}, G. Cabras^{23b,23a}, S. Cabrera Urbán¹⁷³, D. Caforio¹⁴¹, H. Cai¹⁷², V.M.M. Cairo², O. Cakir^{4a}, N. Calace⁵³, P. Calafiura¹⁸, A. Calandri¹⁰⁰, G. Calderini¹³⁵, P. Calfayan⁶⁴, G. Callea^{41b,41a}, L.P. Caloba^{79b}, S. Calvente Lopez⁹⁷, D. Calvet³⁸, S. Calvet³⁸, T.P. Calvet¹⁵⁴, M. Calvetti^{70a,70b}, R. Camacho Toro¹³⁵, S. Camarda³⁶, P. Camarri^{72a,72b}, D. Cameron¹³³, R. Caminal Armadans¹⁰¹, C. Camincher³⁶, S. Campana³⁶, M. Campanelli⁹³, A. Camplani⁴⁰, A. Campoverde¹⁵⁰, V. Canale^{68a,68b}, M. Cano Bret^{59c}, J. Cantero¹²⁸, T. Cao¹⁶⁰, Y. Cao¹⁷², M.D.M. Capeans Garrido³⁶, I. Caprini^{27b}, M. Caprini^{27b}, M. Capua^{41b,41a}, R.M. Carbone³⁹, R. Cardarelli^{72a}, F.C. Cardillo¹⁴⁸, I. Carli¹⁴², T. Carli³⁶, G. Carlino^{68a}, B.T. Carlson¹³⁸, L. Carminati^{67a,67b}, R.M.D. Carney^{44a,44b}, S. Caron¹¹⁸, E. Carquin^{146b}, S. Carrá^{67a,67b}, G.D. Carrillo-Montoya³⁶, D. Casadei^{33b}, M.P. Casado^{14,f}, A.F. Casha¹⁶⁶, D.W. Casper¹⁷⁰, R. Castelijn¹¹⁹, F.L. Castillo¹⁷³, V. Castillo Gimenez¹⁷³, N.F. Castro^{139a,139e}, A. Catinaccio³⁶, J.R. Catmore¹³³, A. Cattai³⁶, J. Caudron²⁴, V. Cavaliere²⁹, E. Cavallaro¹⁴, D. Cavalli^{67a}, M. Cavalli-Sforza¹⁴, V. Cavasinni^{70a,70b}, E. Celebi^{12b}, F. Ceradini^{73a,73b}, L. Cerdà Alberich¹⁷³, A.S. Cerqueira^{79a}, A. Cerri¹⁵⁵, L. Cerrito^{72a,72b}, F. Cerutti¹⁸, A. Cervelli^{23b,23a}, S.A. Cetin^{12b}, A. Chafaq^{35a}, D. Chakraborty¹²⁰, S.K. Chan⁵⁸, W.S. Chan¹¹⁹, Y.L. Chan^{62a}, J.D. Chapman³², B. Chargeishvili^{158b}, D.G. Charlton²¹, C.C. Chau³⁴, C.A. Chavez Barajas¹⁵⁵, S. Che¹²⁵, A. Chegwidden¹⁰⁵, S. Chekanov⁶, S.V. Chekulaev^{167a}, G.A. Chelkov^{78,aq}, M.A. Chelstowska³⁶, C. Chen^{59a}, C.H. Chen⁷⁷, H. Chen²⁹, J. Chen^{59a}, J. Chen³⁹, S. Chen¹³⁶, S.J. Chen^{15c}, X. Chen^{15b,ap}, Y. Chen⁸¹, Y-H. Chen⁴⁵, H.C. Cheng¹⁰⁴, H.J. Cheng^{15a,15d}, A. Cheplakov⁷⁸, E. Cheremushkina¹²², R. Cherkaoui El Moursli^{35e}, E. Cheu⁷, K. Cheung⁶³, L. Chevalier¹⁴⁴, V. Chiarella⁵⁰, G. Chiarelli^{70a}, G. Chiodini^{66a}, A.S. Chisholm^{36,21}, A. Chitan^{27b}, I. Chiu¹⁶², Y.H. Chiu¹⁷⁵, M.V. Chizhov⁷⁸, K. Choi⁶⁴, A.R. Chomont¹³¹, S. Chouridou¹⁶¹, Y.S. Chow¹¹⁹, V. Christodoulou⁹³, M.C. Chu^{62a}, J. Chudoba¹⁴⁰, A.J. Chuinard¹⁰², J.J. Chwastowski⁸³, L. Chytka¹²⁹, D. Cinca⁴⁶, V. Cindro⁹⁰, I.A. Cioară²⁴, A. Ciocio¹⁸, F. Cirotto^{68a,68b}, Z.H. Citron¹⁷⁹, M. Citterio^{67a}, A. Clark⁵³, M.R. Clark³⁹, P.J. Clark⁴⁹, C. Clement^{44a,44b}, Y. Coadou¹⁰⁰, M. Cobal^{65a,65c}, A. Coccaro^{54b}, J. Cochran⁷⁷, H. Cohen¹⁶⁰, A.E.C. Coimbra¹⁷⁹, L. Colasurdo¹¹⁸, B. Cole³⁹, A.P. Colijn¹¹⁹, J. Collot⁵⁷, P. Conde Muñoz^{139a}, E. Coniavitis⁵¹, S.H. Connell^{33b}, I.A. Connelly⁹⁹, S. Constantinescu^{27b}, F. Conventi^{68a,at}, A.M. Cooper-Sarkar¹³⁴, F. Cormier¹⁷⁴, K.J.R. Cormier¹⁶⁶, L.D. Corpe⁹³, M. Corradi^{71a,71b}, E.E. Corrigan⁹⁵, F. Corriveau^{102,ab}, A. Cortes-Gonzalez³⁶, M.J. Costa¹⁷³, F. Costanza⁵, D. Costanzo¹⁴⁸, G. Cottin³², G. Cowan⁹², B.E. Cox⁹⁹, J. Crane⁹⁹, K. Cranmer¹²³, S.J. Crawley⁵⁶, R.A. Creager¹³⁶, G. Cree³⁴, S. Crépé-Renaudin⁵⁷, F. Crescioli¹³⁵, M. Cristinziani²⁴, V. Croft¹²³, G. Crosetti^{41b,41a}, A. Cueto⁹⁷,

T. Cuhadar Donszelmann¹⁴⁸, A.R. Cukierman¹⁵², S. Czekierda⁸³, P. Czodrowski³⁶,
 M.J. Da Cunha Sargedas De Sousa^{59b}, C. Da Via⁹⁹, W. Dabrowski^{82a}, T. Dado^{28a,x}, S. Dahbi^{35e},
 T. Dai¹⁰⁴, F. Dallaire¹⁰⁸, C. Dallapiccola¹⁰¹, M. Dam⁴⁰, G. D'amen^{23b,23a}, J. Damp⁹⁸, J.R. Dandoy¹³⁶,
 M.F. Daneri³⁰, N.P. Dang¹⁸⁰, N.D Dann⁹⁹, M. Danninger¹⁷⁴, V. Dao³⁶, G. Darbo^{54b}, S. Darmora⁸,
 O. Dartsi⁵, A. Dattagupta¹³⁰, T. Daubney⁴⁵, S. D'Auria⁵⁶, W. Davey²⁴, C. David⁴⁵, T. Davidek¹⁴²,
 D.R. Davis⁴⁸, E. Dawe¹⁰³, I. Dawson¹⁴⁸, K. De⁸, R. De Asmundis^{68a}, A. De Benedetti¹²⁷,
 M. De Beurs¹¹⁹, S. De Castro^{23b,23a}, S. De Cecco^{71a,71b}, N. De Groot¹¹⁸, P. de Jong¹¹⁹, H. De la Torre¹⁰⁵,
 F. De Lorenzi⁷⁷, A. De Maria^{52,r}, D. De Pedis^{71a}, A. De Salvo^{71a}, U. De Sanctis^{72a,72b},
 M. De Santis^{72a,72b}, A. De Santo¹⁵⁵, K. De Vasconcelos Corga¹⁰⁰, J.B. De Vivie De Regie¹³¹,
 C. Debenedetti¹⁴⁵, D.V. Dedovich⁷⁸, N. Dehghanian³, A.M. Deiana¹⁰⁴, M. Del Gaudio^{41b,41a},
 J. Del Peso⁹⁷, Y. Delabat Diaz⁴⁵, D. Delgove¹³¹, F. Deliot¹⁴⁴, C.M. Delitzsch⁷, M. Della Pietra^{68a,68b},
 D. Della Volpe⁵³, A. Dell'Acqua³⁶, L. Dell'Asta²⁵, M. Delmastro⁵, C. Delporte¹³¹, P.A. Delsart⁵⁷,
 D.A. DeMarco¹⁶⁶, S. Demers¹⁸², M. Demichev⁷⁸, S.P. Denisov¹²², D. Denysiuk¹¹⁹, L. D'Eramo¹³⁵,
 D. Derendarz⁸³, J.E. Derkaoui^{35d}, F. Derue¹³⁵, P. Dervan⁸⁹, K. Desch²⁴, C. Deterre⁴⁵, K. Dette¹⁶⁶,
 M.R. Devesa³⁰, P.O. Deviveiros³⁶, A. Dewhurst¹⁴³, S. Dhaliwal²⁶, F.A. Di Bello⁵³, A. Di Ciaccio^{72a,72b},
 L. Di Ciaccio⁵, W.K. Di Clemente¹³⁶, C. Di Donato^{68a,68b}, A. Di Girolamo³⁶, B. Di Micco^{73a,73b},
 R. Di Nardo¹⁰¹, K.F. Di Petrillo⁵⁸, R. Di Sipio¹⁶⁶, D. Di Valentino³⁴, C. Diaconu¹⁰⁰, M. Diamond¹⁶⁶,
 F.A. Dias⁴⁰, T. Dias Do Vale^{139a}, M.A. Diaz^{146a}, J. Dickinson¹⁸, E.B. Diehl¹⁰⁴, J. Dietrich¹⁹,
 S. Díez Cornell⁴⁵, A. Dimitrievska¹⁸, J. Dingfelder²⁴, F. Dittus³⁶, F. Djama¹⁰⁰, T. Djobava^{158b},
 J.I. Djuvslund^{60a}, M.A.B. Do Vale^{79c}, M. Dobre^{27b}, D. Dodsworth²⁶, C. Doglioni⁹⁵, J. Dolejsi¹⁴²,
 Z. Dolezal¹⁴², M. Donadelli^{79d}, J. Donini³⁸, A. D'onofrio⁹¹, M. D'Onofrio⁸⁹, J. Dopke¹⁴³, A. Doria^{68a},
 M.T. Dova⁸⁷, A.T. Doyle⁵⁶, E. Drechsler⁵², E. Dreyer¹⁵¹, T. Dreyer⁵², Y. Du^{59b}, F. Dubinin¹⁰⁹,
 M. Dubovsky^{28a}, A. Dubreuil⁵³, E. Duchovni¹⁷⁹, G. Duckeck¹¹³, A. Ducourthial¹³⁵, O.A. Ducu^{108,w},
 D. Duda¹¹⁴, A. Dudarev³⁶, A.C. Dudder⁹⁸, E.M. Duffield¹⁸, L. Duflot¹³¹, M. Dührssen³⁶, C. Dülsen¹⁸¹,
 M. Dumancic¹⁷⁹, A.E. Dumitriu^{27b,d}, A.K. Duncan⁵⁶, M. Dunford^{60a}, A. Duperrin¹⁰⁰, H. Duran Yildiz^{4a},
 M. Düren⁵⁵, A. Durglishvili^{158b}, D. Duschinger⁴⁷, B. Dutta⁴⁵, D. Duvnjak¹, M. Dyndal⁴⁵, S. Dysch⁹⁹,
 B.S. Dziedzic⁸³, C. Eckardt⁴⁵, K.M. Ecker¹¹⁴, R.C. Edgar¹⁰⁴, T. Eifert³⁶, G. Eigen¹⁷, K. Einsweiler¹⁸,
 T. Ekelof¹⁷¹, M. El Kacimi^{35c}, R. El Kosseifi¹⁰⁰, V. Ellajosyula¹⁰⁰, M. Ellert¹⁷¹, F. Ellinghaus¹⁸¹,
 A.A. Elliot⁹¹, N. Ellis³⁶, J. Elmsheuser²⁹, M. Elsing³⁶, D. Emeliyanov¹⁴³, Y. Enari¹⁶², J.S. Ennis¹⁷⁷,
 M.B. Epland⁴⁸, J. Erdmann⁴⁶, A. Ereditato²⁰, S. Errede¹⁷², M. Escalier¹³¹, C. Escobar¹⁷³,
 O. Estrada Pastor¹⁷³, A.I. Etievre¹⁴⁴, E. Etzion¹⁶⁰, H. Evans⁶⁴, A. Ezhilov¹³⁷, M. Ezzi^{35e}, F. Fabbri⁵⁶,
 L. Fabbri^{23b,23a}, V. Fabiani¹¹⁸, G. Facini⁹³, R.M. Faisca Rodrigues Pereira^{139a}, R.M. Fakhrutdinov¹²²,
 S. Falciano^{71a}, P.J. Falke⁵, S. Falke⁵, J. Faltova¹⁴², Y. Fang^{15a}, M. Fanti^{67a,67b}, A. Farbin⁸, A. Farilla^{73a},
 E.M. Farina^{69a,69b}, T. Farooque¹⁰⁵, S. Farrell¹⁸, S.M. Farrington¹⁷⁷, P. Farthouat³⁶, F. Fassi^{35e},
 P. Fassnacht³⁶, D. Fassouliotis⁹, M. Faucci Giannelli⁴⁹, A. Favareto^{54b,54a}, W.J. Fawcett³², L. Fayard¹³¹,
 O.L. Fedin^{137,o}, W. Fedorko¹⁷⁴, M. Feickert⁴², S. Feigl¹³³, L. Feligioni¹⁰⁰, C. Feng^{59b}, E.J. Feng³⁶,
 M. Feng⁴⁸, M.J. Fenton⁵⁶, A.B. Fenyuk¹²², L. Feremenga⁸, J. Ferrando⁴⁵, A. Ferrari¹⁷¹, P. Ferrari¹¹⁹,
 R. Ferrari^{69a}, D.E. Ferreira de Lima^{60b}, A. Ferrer¹⁷³, D. Ferrere⁵³, C. Ferretti¹⁰⁴, F. Fiedler⁹⁸,
 A. Filipčič⁹⁰, F. Filthaut¹¹⁸, K.D. Finelli²⁵, M.C.N. Fiolhais^{139a,139c,a}, L. Fiorini¹⁷³, C. Fischer¹⁴,
 W.C. Fisher¹⁰⁵, N. Flaschel⁴⁵, I. Fleck¹⁵⁰, P. Fleischmann¹⁰⁴, R.R.M. Fletcher¹³⁶, T. Flick¹⁸¹,
 B.M. Flierl¹¹³, L.F. Flores¹³⁶, L.R. Flores Castillo^{62a}, F.M. Follega^{74a,74b}, N. Fomin¹⁷,
 G.T. Forcolin^{74a,74b}, A. Formica¹⁴⁴, F.A. Förster¹⁴, A.C. Forti⁹⁹, A.G. Foster²¹, D. Fournier¹³¹, H. Fox⁸⁸,
 S. Fracchia¹⁴⁸, P. Francavilla^{70a,70b}, M. Franchini^{23b,23a}, S. Franchino^{60a}, D. Francis³⁶, L. Franconi¹³³,
 M. Franklin⁵⁸, M. Frate¹⁷⁰, M. Fraternali^{69a,69b}, A.N. Fray⁹¹, D. Freeborn⁹³,
 S.M. Fressard-Batraneanu³⁶, B. Freund¹⁰⁸, W.S. Freund^{79b}, E.M. Freundlich⁴⁶, D.C. Frizzell¹²⁷,
 D. Froidevaux³⁶, J.A. Frost¹³⁴, C. Fukunaga¹⁶³, E. Fullana Torregrosa¹⁷³, T. Fusayasu¹¹⁵, J. Fuster¹⁷³,
 O. Gabizon¹⁵⁹, A. Gabrielli^{23b,23a}, A. Gabrielli¹⁸, G.P. Gach^{82a}, S. Gadatsch⁵³, P. Gadow¹¹⁴,

G. Gagliardi^{54b,54a}, L.G. Gagnon¹⁰⁸, C. Galea^{27b}, B. Galhardo^{139a,139c}, E.J. Gallas¹³⁴, B.J. Gallop¹⁴³,
 P. Gallus¹⁴¹, G. Galster⁴⁰, R. Gamboa Goni⁹¹, K.K. Gan¹²⁵, S. Ganguly¹⁷⁹, J. Gao^{59a}, Y. Gao⁸⁹,
 Y.S. Gao^{31,1}, C. García¹⁷³, J.E. García Navarro¹⁷³, J.A. García Pascual^{15a}, M. Garcia-Sciveres¹⁸,
 R.W. Gardner³⁷, N. Garelli¹⁵², V. Garonne¹³³, K. Gasnikova⁴⁵, A. Gaudiello^{54b,54a}, G. Gaudio^{69a},
 I.L. Gavrilenko¹⁰⁹, A. Gavrilyuk¹¹⁰, C. Gay¹⁷⁴, G. Gaycken²⁴, E.N. Gazis¹⁰, C.N.P. Gee¹⁴³, J. Geisen⁵²,
 M. Geisen⁹⁸, M.P. Geisler^{60a}, K. Gellerstedt^{44a,44b}, C. Gemme^{54b}, M.H. Genest⁵⁷, C. Geng¹⁰⁴,
 S. Gentile^{71a,71b}, S. George⁹², D. Gerbaudo¹⁴, G. Gessner⁴⁶, S. Ghasemi¹⁵⁰, M. Ghasemi Bostanabad¹⁷⁵,
 M. Ghneimat²⁴, B. Giacobbe^{23b}, S. Giagu^{71a,71b}, N. Giangiocomi^{23b,23a}, P. Giannetti^{70a},
 A. Giannini^{68a,68b}, S.M. Gibson⁹², M. Gignac¹⁴⁵, D. Gillberg³⁴, G. Gilles¹⁸¹, D.M. Gingrich^{3,ar},
 M.P. Giordani^{65a,65c}, F.M. Giorgi^{23b}, P.F. Giraud¹⁴⁴, P. Giromini⁵⁸, G. Giugliarelli^{65a,65c}, D. Giugni^{67a},
 F. Juli¹³⁴, M. Giulini^{60b}, S. Gkaitatzis¹⁶¹, I. Gkialas^{9,h}, E.L. Gkougkousis¹⁴, P. Gkountoumis¹⁰,
 L.K. Gladilin¹¹², C. Glasman⁹⁷, J. Glatzer¹⁴, P.C.F. Glaysher⁴⁵, A. Glazov⁴⁵, M. Goblirsch-Kolb²⁶,
 J. Godlewski⁸³, S. Goldfarb¹⁰³, T. Golling⁵³, D. Golubkov¹²², A. Gomes^{139a,139b}, R. Goncalves Gama^{79a},
 R. Gonçalo^{139a}, G. Gonella⁵¹, L. Gonella²¹, A. Gongadze⁷⁸, F. Gonnella²¹, J.L. Gonski⁵⁸,
 S. González de la Hoz¹⁷³, S. Gonzalez-Sevilla⁵³, L. Goossens³⁶, P.A. Gorbounov¹¹⁰, H.A. Gordon²⁹,
 B. Gorini³⁶, E. Gorini^{66a,66b}, A. Gorišek⁹⁰, A.T. Goshaw⁴⁸, C. Gössling⁴⁶, M.I. Gostkin⁷⁸,
 C.A. Gottardo²⁴, C.R. Goudet¹³¹, D. Goujdami^{35c}, A.G. Goussiou¹⁴⁷, N. Govender^{33b,b}, C. Goy⁵,
 E. Gozani¹⁵⁹, I. Grabowska-Bold^{82a}, P.O.J. Gradin¹⁷¹, E.C. Graham⁸⁹, J. Gramling¹⁷⁰, E. Gramstad¹³³,
 S. Grancagnolo¹⁹, V. Gratchev¹³⁷, P.M. Gravila^{27f}, F.G. Gravili^{66a,66b}, C. Gray⁵⁶, H.M. Gray¹⁸,
 Z.D. Greenwood⁹⁴, C. Grefe²⁴, K. Gregersen⁹⁵, I.M. Gregor⁴⁵, P. Grenier¹⁵², K. Grevtsov⁴⁵,
 N.A. Grieser¹²⁷, J. Griffiths⁸, A.A. Grillo¹⁴⁵, K. Grimm^{31,k}, S. Grinstein^{14,y}, Ph. Gris³⁸, J.-F. Grivaz¹³¹,
 S. Groh⁹⁸, E. Gross¹⁷⁹, J. Grosse-Knetter⁵², G.C. Grossi⁹⁴, Z.J. Grout⁹³, C. Grud¹⁰⁴, A. Grummer¹¹⁷,
 L. Guan¹⁰⁴, W. Guan¹⁸⁰, J. Guenther³⁶, A. Guerguichon¹³¹, F. Guescini^{167a}, D. Guest¹⁷⁰, R. Gugel⁵¹,
 B. Gui¹²⁵, T. Guillemin⁵, S. Guindon³⁶, U. Gul⁵⁶, C. Gumpert³⁶, J. Guo^{59c}, W. Guo¹⁰⁴, Y. Guo^{59a,q},
 Z. Guo¹⁰⁰, R. Gupta⁴², S. Gurbuz^{12c}, G. Gustavino¹²⁷, B.J. Gutelman¹⁵⁹, P. Gutierrez¹²⁷, C. Gutschow⁹³,
 C. Guyot¹⁴⁴, M.P. Guzik^{82a}, C. Gwenlan¹³⁴, C.B. Gwilliam⁸⁹, A. Haas¹²³, C. Haber¹⁸, H.K. Hadavand⁸,
 N. Haddad^{35e}, A. Hadef^{59a}, S. Hageböck²⁴, M. Hagihara¹⁶⁸, H. Hakobyan^{183,*}, M. Haleem¹⁷⁶,
 J. Haley¹²⁸, G. Halladjian¹⁰⁵, G.D. Hallewell¹⁰⁰, K. Hamacher¹⁸¹, P. Hamal¹²⁹, K. Hamano¹⁷⁵,
 A. Hamilton^{33a}, G.N. Hamity¹⁴⁸, K. Han^{59a,af}, L. Han^{59a}, S. Han^{15a,15d}, K. Hanagaki^{80,u}, M. Hance¹⁴⁵,
 D.M. Handl¹¹³, B. Haney¹³⁶, R. Hankache¹³⁵, P. Hanke^{60a}, E. Hansen⁹⁵, J.B. Hansen⁴⁰, J.D. Hansen⁴⁰,
 M.C. Hansen²⁴, P.H. Hansen⁴⁰, E.C. Hanson⁹⁹, K. Hara¹⁶⁸, A.S. Hard¹⁸⁰, T. Harenberg¹⁸¹,
 S. Harkusha¹⁰⁶, P.F. Harrison¹⁷⁷, N.M. Hartmann¹¹³, Y. Hasegawa¹⁴⁹, A. Hasib⁴⁹, S. Hassani¹⁴⁴,
 S. Haug²⁰, R. Hauser¹⁰⁵, L. Hauswald⁴⁷, L.B. Havener³⁹, M. Havranek¹⁴¹, C.M. Hawkes²¹,
 R.J. Hawkings³⁶, D. Hayden¹⁰⁵, C. Hayes¹⁵⁴, C.P. Hays¹³⁴, J.M. Hays⁹¹, H.S. Hayward⁸⁹,
 S.J. Haywood¹⁴³, M.P. Heath⁴⁹, V. Hedberg⁹⁵, L. Heelan⁸, S. Heer²⁴, K.K. Heidegger⁵¹, J. Heilman³⁴,
 S. Heim⁴⁵, T. Heim¹⁸, B. Heinemann^{45,am}, J.J. Heinrich¹¹³, L. Heinrich¹²³, C. Heinz⁵⁵, J. Hejbal¹⁴⁰,
 L. Helary³⁶, A. Held¹⁷⁴, S. Hellersund¹³³, S. Hellman^{44a,44b}, C. Helsens³⁶, R.C.W. Henderson⁸⁸,
 Y. Heng¹⁸⁰, S. Henkelmann¹⁷⁴, A.M. Henriques Correia³⁶, G.H. Herbert¹⁹, H. Herde²⁶, V. Herget¹⁷⁶,
 Y. Hernández Jiménez^{33c}, H. Herr⁹⁸, M.G. Herrmann¹¹³, G. Herten⁵¹, R. Hertenberger¹¹³, L. Hervas³⁶,
 T.C. Herwig¹³⁶, G.G. Hesketh⁹³, N.P. Hessey^{167a}, J.W. Hetherly⁴², S. Higashino⁸⁰,
 E. Higón-Rodríguez¹⁷³, K. Hildebrand³⁷, E. Hill¹⁷⁵, J.C. Hill³², K.K. Hill²⁹, K.H. Hiller⁴⁵, S.J. Hillier²¹,
 M. Hils⁴⁷, I. Hinchliffe¹⁸, M. Hirose¹³², D. Hirschbuehl¹⁸¹, B. Hiti⁹⁰, O. Hladík¹⁴⁰, D.R. Hlálučku^{33c},
 X. Hoad⁴⁹, J. Hobbs¹⁵⁴, N. Hod^{167a}, M.C. Hodgkinson¹⁴⁸, A. Hoecker³⁶, M.R. Hoeferkamp¹¹⁷,
 F. Hoenig¹¹³, D. Hohn²⁴, D. Hohov¹³¹, T.R. Holmes³⁷, M. Holzbock¹¹³, M. Homann⁴⁶, S. Honda¹⁶⁸,
 T. Honda⁸⁰, T.M. Hong¹³⁸, A. Hönel¹¹⁴, B.H. Hooberman¹⁷², W.H. Hopkins¹³⁰, Y. Horii¹¹⁶, P. Horn⁴⁷,
 A.J. Horton¹⁵¹, L.A. Horyn³⁷, J-Y. Hostachy⁵⁷, A. Hostiuc¹⁴⁷, S. Hou¹⁵⁷, A. Hoummada^{35a},
 J. Howarth⁹⁹, J. Hoya⁸⁷, M. Hrabovsky¹²⁹, J. Hrdinka³⁶, I. Hristova¹⁹, J. Hrvnac¹³¹, A. Hrynevich¹⁰⁷,

T. Hrynn'ova⁵, P.J. Hsu⁶³, S.-C. Hsu¹⁴⁷, Q. Hu²⁹, S. Hu^{59c}, Y. Huang^{15a}, Z. Hubacek¹⁴¹, F. Hubaut¹⁰⁰, M. Huebner²⁴, F. Huegging²⁴, T.B. Huffman¹³⁴, E.W. Hughes³⁹, M. Huhtinen³⁶, R.F.H. Hunter³⁴, P. Huo¹⁵⁴, A.M. Hupe³⁴, N. Huseynov^{78,ad}, J. Huston¹⁰⁵, J. Huth⁵⁸, R. Hyneman¹⁰⁴, G. Iacobucci⁵³, G. Iakovidis²⁹, I. Ibragimov¹⁵⁰, L. Iconomidou-Fayard¹³¹, Z. Idrissi^{35e}, P.I. Iengo³⁶, R. Ignazzi⁴⁰, O. Igonkina^{119,z}, R. Iguchi¹⁶², T. Iizawa⁵³, Y. Ikegami⁸⁰, M. Ikeno⁸⁰, D. Iliadis¹⁶¹, N. Ilic¹¹⁸, F. Iltzsche⁴⁷, G. Introzzi^{69a,69b}, M. Iodice^{73a}, K. Iordanidou³⁹, V. Ippolito^{71a,71b}, M.F. Isacson¹⁷¹, N. Ishijima¹³², M. Ishino¹⁶², M. Ishitsuka¹⁶⁴, W. Islam¹²⁸, C. Issever¹³⁴, S. Istin¹⁵⁹, F. Ito¹⁶⁸, J.M. Iturbe Ponce^{62a}, R. Iuppa^{74a,74b}, A. Ivina¹⁷⁹, H. Iwasaki⁸⁰, J.M. Izen⁴³, V. Izzo^{68a}, P. Jacka¹⁴⁰, P. Jackson¹, R.M. Jacobs²⁴, V. Jain², G. Jäkel¹⁸¹, K.B. Jakobi⁹⁸, K. Jakobs⁵¹, S. Jakobsen⁷⁵, T. Jakoubek¹⁴⁰, D.O. Jamin¹²⁸, D.K. Jana⁹⁴, R. Jansky⁵³, J. Janssen²⁴, M. Janus⁵², P.A. Janus^{82a}, G. Jarlskog⁹⁵, N. Javadov^{78,ad}, T. Javůrek³⁶, M. Javurkova⁵¹, F. Jeanneau¹⁴⁴, L. Jeanty¹⁸, J. Jejelava^{158a,ae}, A. Jelinskas¹⁷⁷, P. Jenni^{51,c}, J. Jeong⁴⁵, N. Jeong⁴⁵, S. Jézéquel⁵, H. Ji¹⁸⁰, J. Jia¹⁵⁴, H. Jiang⁷⁷, Y. Jiang^{59a}, Z. Jiang¹⁵², S. Jiggins⁵¹, F.A. Jimenez Morales³⁸, J. Jimenez Pena¹⁷³, S. Jin^{15c}, A. Jinaru^{27b}, O. Jinnouchi¹⁶⁴, H. Jivan^{33c}, P. Johansson¹⁴⁸, K.A. Johns⁷, C.A. Johnson⁶⁴, W.J. Johnson¹⁴⁷, K. Jon-And^{44a,44b}, R.W.L. Jones⁸⁸, S.D. Jones¹⁵⁵, S. Jones⁷, T.J. Jones⁸⁹, J. Jongmanns^{60a}, P.M. Jorge^{139a,139b}, J. Jovicevic^{167a}, X. Ju¹⁸, J.J. Junggeburt¹¹⁴, A. Juste Rozas^{14,y}, A. Kaczmar ska⁸³, M. Kado¹³¹, H. Kagan¹²⁵, M. Kagan¹⁵², T. Kaji¹⁷⁸, E. Kajomovitz¹⁵⁹, C.W. Kalderon⁹⁵, A. Kaluza⁹⁸, S. Kama⁴², A. Kamenshchikov¹²², L. Kanjir⁹⁰, Y. Kano¹⁶², V.A. Kantserov¹¹¹, J. Kanzaki⁸⁰, B. Kaplan¹²³, L.S. Kaplan¹⁸⁰, D. Kar^{33c}, M.J. Kareem^{167b}, E. Karentzos¹⁰, S.N. Karpov⁷⁸, Z.M. Karpova⁷⁸, V. Kartvelishvili⁸⁸, A.N. Karyukhin¹²², L. Kashif¹⁸⁰, R.D. Kass¹²⁵, A. Kastanas^{44a,44b}, Y. Kataoka¹⁶², C. Kato^{59d,59c}, J. Katzy⁴⁵, K. Kawade⁸¹, K. Kawagoe⁸⁶, T. Kawamoto¹⁶², G. Kawamura⁵², E.F. Kay⁸⁹, V.F. Kazanin^{121b,121a}, R. Keeler¹⁷⁵, R. Kehoe⁴², J.S. Keller³⁴, E. Kellermann⁹⁵, J.J. Kempster²¹, J. Kendrick²¹, O. Kepka¹⁴⁰, S. Kersten¹⁸¹, B.P. Kerševan⁹⁰, R.A. Keyes¹⁰², M. Khader¹⁷², F. Khalil-Zada¹³, A. Khanov¹²⁸, A.G. Kharlamov^{121b,121a}, T. Kharlamova^{121b,121a}, E.E. Khoda¹⁷⁴, A. Khodinov¹⁶⁵, T.J. Khoo⁵³, E. Khramov⁷⁸, J. Khubua^{158b}, S. Kido⁸¹, M. Kiehn⁵³, C.R. Kilby⁹², Y.K. Kim³⁷, N. Kimura^{65a,65c}, O.M. Kind¹⁹, B.T. King^{89,*}, D. Kirchmeier⁴⁷, J. Kirk¹⁴³, A.E. Kiryunin¹¹⁴, T. Kishimoto¹⁶², D. Kisielewska^{82a}, V. Kitali⁴⁵, O. Kiverny⁵, E. Kladiva^{28b,*}, T. Klapdor-Kleingrothaus⁵¹, M.H. Klein¹⁰⁴, M. Klein⁸⁹, U. Klein⁸⁹, K. Kleinknecht⁹⁸, P. Klimek¹²⁰, A. Klimentov²⁹, R. Klingenberg^{46,*}, T. Klingl²⁴, T. Klioutchnikova³⁶, F.F. Klitzner¹¹³, P. Kluit¹¹⁹, S. Kluth¹¹⁴, E. Kneringer⁷⁵, E.B.F.G. Knoops¹⁰⁰, A. Knue⁵¹, A. Kobayashi¹⁶², D. Kobayashi⁸⁶, T. Kobayashi¹⁶², M. Kobel⁴⁷, M. Kocian¹⁵², P. Kodys¹⁴², P.T. Koenig²⁴, T. Koffas³⁴, E. Koffeman¹¹⁹, N.M. Köhler¹¹⁴, T. Koi¹⁵², M. Kolb^{60b}, I. Koletsou⁵, T. Kondo⁸⁰, N. Kondrashova^{59c}, K. Köneke⁵¹, A.C. König¹¹⁸, T. Kono¹²⁴, R. Konoplich^{123,ai}, V. Konstantinides⁹³, N. Konstantinidis⁹³, B. Konya⁹⁵, R. Kopeliansky⁶⁴, S. Koperny^{82a}, K. Korcyl⁸³, K. Kordas¹⁶¹, G. Koren¹⁶⁰, A. Korn⁹³, I. Korolkov¹⁴, E.V. Korolkova¹⁴⁸, N. Korotkova¹¹², O. Kortner¹¹⁴, S. Kortner¹¹⁴, T. Kosek¹⁴², V.V. Kostyukhin²⁴, A. Kotwal⁴⁸, A. Koulouris¹⁰, A. Kourkoumeli-Charalampidi^{69a,69b}, C. Kourkoumelis⁹, E. Kourlitis¹⁴⁸, V. Kouskoura²⁹, A.B. Kowalewska⁸³, R. Kowalewski¹⁷⁵, T.Z. Kowalski^{82a}, C. Kozakai¹⁶², W. Kozanecki¹⁴⁴, A.S. Kozhin¹²², V.A. Kramarenko¹¹², G. Kramberger⁹⁰, D. Krasnopevtsev^{59a}, A. Krasznahorkay³⁶, D. Krauss¹¹⁴, J.A. Kremer^{82a}, J. Kretzschmar⁸⁹, P. Krieger¹⁶⁶, K. Krizka¹⁸, K. Kroeninger⁴⁶, H. Kroha¹¹⁴, J. Kroll¹⁴⁰, J. Kroll¹³⁶, J. Krstic¹⁶, U. Kruchonak⁷⁸, H. Krüger²⁴, N. Krumnack⁷⁷, M.C. Kruse⁴⁸, T. Kubota¹⁰³, S. Kuday^{4b}, J.T. Kuechler¹⁸¹, S. Kuehn³⁶, A. Kugel^{60a}, F. Kuger¹⁷⁶, T. Kuhl⁴⁵, V. Kukhtin⁷⁸, R. Kukla¹⁰⁰, Y. Kulchitsky¹⁰⁶, S. Kuleshov^{146b}, Y.P. Kulinich¹⁷², M. Kuna⁵⁷, T. Kunigo⁸⁴, A. Kupco¹⁴⁰, T. Kupfer⁴⁶, O. Kuprash¹⁶⁰, H. Kurashige⁸¹, L.L. Kurchaninov^{167a}, Y.A. Kurochkin¹⁰⁶, M.G. Kurth^{15a,15d}, E.S. Kuwertz³⁶, M. Kuze¹⁶⁴, J. Kvita¹²⁹, T. Kwan¹⁰², A. La Rosa¹¹⁴, J.L. La Rosa Navarro^{79d}, L. La Rotonda^{41b,41a}, F. La Ruffa^{41b,41a}, C. Lacasta¹⁷³, F. Lacava^{71a,71b}, J. Lacey⁴⁵, D.P.J. Lack⁹⁹, H. Lacker¹⁹, D. Lacour¹³⁵, E. Ladygin⁷⁸, R. Lafaye⁵,

B. Laforge¹³⁵, T. Lagouri^{33c}, S. Lai⁵², S. Lammers⁶⁴, W. Lampl⁷, E. Lançon²⁹, U. Landgraf⁵¹, M.P.J. Landon⁹¹, M.C. Lanfermann⁵³, V.S. Lang⁴⁵, J.C. Lange¹⁴, R.J. Langenberg³⁶, A.J. Lankford¹⁷⁰, F. Lanni²⁹, K. Lantzsch²⁴, A. Lanza^{69a}, A. Lapertosa^{54b,54a}, S. Laplace¹³⁵, J.F. Laporte¹⁴⁴, T. Lari^{67a}, F. Lasagni Manghi^{23b,23a}, M. Lassnig³⁶, T.S. Lau^{62a}, A. Laudrain¹³¹, M. Lavorgna^{68a,68b}, A.T. Law¹⁴⁵, M. Lazzaroni^{67a,67b}, B. Le¹⁰³, O. Le Dortz¹³⁵, E. Le Guirriec¹⁰⁰, E.P. Le Quilleuc¹⁴⁴, M. LeBlanc⁷, T. LeCompte⁶, F. Ledroit-Guillon⁵⁷, C.A. Lee²⁹, G.R. Lee^{146a}, L. Lee⁵⁸, S.C. Lee¹⁵⁷, B. Lefebvre¹⁰², M. Lefebvre¹⁷⁵, F. Legger¹¹³, C. Leggett¹⁸, K. Lehmann¹⁵¹, N. Lehmann¹⁸¹, G. Lehmann Miotto³⁶, W.A. Leight⁴⁵, A. Leisos^{161,v}, M.A.L. Leite^{79d}, R. Leitner¹⁴², D. Lellouch^{179,*}, B. Lemmer⁵², K.J.C. Leney⁹³, T. Lenz²⁴, B. Lenzi³⁶, R. Leone⁷, S. Leone^{70a}, C. Leonidopoulos⁴⁹, G. Lerner¹⁵⁵, C. Leroy¹⁰⁸, R. Les¹⁶⁶, A.A.J. Lesage¹⁴⁴, C.G. Lester³², M. Levchenko¹³⁷, J. Levêque⁵, D. Levin¹⁰⁴, L.J. Levinson¹⁷⁹, D. Lewis⁹¹, B. Li¹⁰⁴, C-Q. Li^{59a,ah}, H. Li^{59b}, L. Li^{59c}, M. Li^{15a}, Q. Li^{15a,15d}, Q.Y. Li^{59a}, S. Li^{59d,59c}, X. Li^{59c}, Y. Li¹⁵⁰, Z. Liang^{15a}, B. Liberti^{72a}, A. Liblong¹⁶⁶, K. Lie^{62c}, S. Liem¹¹⁹, A. Limosani¹⁵⁶, C.Y. Lin³², K. Lin¹⁰⁵, T.H. Lin⁹⁸, R.A. Linck⁶⁴, J.H. Lindon²¹, B.E. Lindquist¹⁵⁴, A.L. Lionti⁵³, E. Lipeles¹³⁶, A. Lipniacka¹⁷, M. Lisovyi^{60b}, T.M. Liss^{172,ao}, A. Lister¹⁷⁴, A.M. Litke¹⁴⁵, J.D. Little⁸, B. Liu⁷⁷, B.L. Liu⁶, H.B. Liu²⁹, H. Liu¹⁰⁴, J.B. Liu^{59a}, J.K.K. Liu¹³⁴, K. Liu¹³⁵, M. Liu^{59a}, P. Liu¹⁸, Y. Liu^{15a,15d}, Y.L. Liu^{59a}, Y.W. Liu^{59a}, M. Livan^{69a,69b}, A. Lleres⁵⁷, J. Llorente Merino^{15a}, S.L. Lloyd⁹¹, C.Y. Lo^{62b}, F. Lo Sterzo⁴², E.M. Lobodzinska⁴⁵, P. Loch⁷, T. Lohse¹⁹, K. Lohwasser¹⁴⁸, M. Lokajicek¹⁴⁰, B.A. Long²⁵, J.D. Long¹⁷², R.E. Long⁸⁸, L. Longo^{66a,66b}, K.A.Looper¹²⁵, J.A. Lopez Paz¹⁴, I. Lopez Solis¹⁴⁸, J. Lorenz¹¹³, N. Lorenzo Martinez⁵, M. Losada²², P.J. Lösel¹¹³, A. Lösle⁵¹, X. Lou⁴⁵, X. Lou^{15a}, A. Lounis¹³¹, J. Love⁶, P.A. Love⁸⁸, J.J. Lozano Bahilo¹⁷³, H. Lu^{62a}, M. Lu^{59a}, N. Lu¹⁰⁴, Y.J. Lu⁶³, H.J. Lubatti¹⁴⁷, C. Luci^{71a,71b}, A. Lucotte⁵⁷, C. Luedtke⁵¹, F. Luehring⁶⁴, I. Luise¹³⁵, L. Luminari^{71a}, B. Lund-Jensen¹⁵³, M.S. Lutz¹⁰¹, P.M. Luzi¹³⁵, D. Lynn²⁹, R. Lysak¹⁴⁰, E. Lytken⁹⁵, F. Lyu^{15a}, V. Lyubushkin⁷⁸, H. Ma²⁹, L.L. Ma^{59b}, Y. Ma^{59b}, G. Maccarrone⁵⁰, A. Macchioli¹¹⁴, C.M. Macdonald¹⁴⁸, J. Machado Miguens^{136,139b}, D. Madaffari¹⁷³, R. Madar³⁸, W.F. Mader⁴⁷, A. Madsen⁴⁵, N. Madysa⁴⁷, J. Maeda⁸¹, K. Maekawa¹⁶², S. Maeland¹⁷, T. Maeno²⁹, A.S. Maevskiy¹¹², V. Magerl⁵¹, C. Maidantchik^{79b}, T. Maier¹¹³, A. Maio^{139a,139b,139d}, O. Majersky^{28a}, S. Majewski¹³⁰, Y. Makida⁸⁰, N. Makovec¹³¹, B. Malaescu¹³⁵, Pa. Malecki⁸³, V.P. Maleev¹³⁷, F. Malek⁵⁷, U. Mallik⁷⁶, D. Malon⁶, C. Malone³², S. Maltezos¹⁰, S. Malyukov³⁶, J. Mamuzic¹⁷³, G. Mancini⁵⁰, I. Mandić⁹⁰, J. Maneira^{139a}, L. Manhaes de Andrade Filho^{79a}, J. Manjarres Ramos⁴⁷, K.H. Mankinen⁹⁵, A. Mann¹¹³, A. Manousos⁷⁵, B. Mansoulie¹⁴⁴, J.D. Mansour^{15a}, M. Mantoani⁵², S. Manzoni^{67a,67b}, A. Marantis¹⁶¹, G. Marceca³⁰, L. March⁵³, L. Marchese¹³⁴, G. Marchiori¹³⁵, M. Marcisovsky¹⁴⁰, C.A. Marin Tobon³⁶, M. Marjanovic³⁸, D.E. Marley¹⁰⁴, F. Marroquin^{79b}, Z. Marshall¹⁸, M.U.F Martensson¹⁷¹, S. Marti-Garcia¹⁷³, C.B. Martin¹²⁵, T.A. Martin¹⁷⁷, V.J. Martin⁴⁹, B. Martin dit Latour¹⁷, M. Martinez^{14,y}, V.I. Martinez Outschoorn¹⁰¹, S. Martin-Haugh¹⁴³, V.S. Martoiu^{27b}, A.C. Martyniuk⁹³, A. Marzin³⁶, L. Masetti⁹⁸, T. Mashimo¹⁶², R. Mashinistov¹⁰⁹, J. Masik⁹⁹, A.L. Maslennikov^{121b,121a}, L.H. Mason¹⁰³, L. Massa^{72a,72b}, P. Massarotti^{68a,68b}, P. Mastrandrea⁵, A. Mastroberardino^{41b,41a}, T. Masubuchi¹⁶², P. Mättig¹⁸¹, J. Maurer^{27b}, B. Maček⁹⁰, S.J. Maxfield⁸⁹, D.A. Maximov^{121b,121a}, R. Mazini¹⁵⁷, I. Maznas¹⁶¹, S.M. Mazza¹⁴⁵, N.C. Mc Fadden¹¹⁷, G. Mc Goldrick¹⁶⁶, S.P. Mc Kee¹⁰⁴, T.G. McCarthy¹¹⁴, L.I. McClymont⁹³, E.F. McDonald¹⁰³, J.A. Mcfayden³⁶, M.A. McKay⁴², K.D. McLean¹⁷⁵, S.J. McMahon¹⁴³, P.C. McNamara¹⁰³, C.J. McNicol¹⁷⁷, R.A. McPherson^{175,ab}, J.E. Mdhluli^{33c}, Z.A. Meadows¹⁰¹, S. Meehan¹⁴⁷, T. Megy⁵¹, S. Mehlhase¹¹³, A. Mehta⁸⁹, T. Meideck⁵⁷, B. Meirose⁴³, D. Melini^{173,as}, B.R. Mellado Garcia^{33c}, J.D. Mellenthin⁵², M. Melo^{28a}, F. Meloni⁴⁵, A. Melzer²⁴, S.B. Menary⁹⁹, E.D. Mendes Gouveia^{139a}, L. Meng⁸⁹, X.T. Meng¹⁰⁴, A. Mengarelli^{23b,23a}, S. Menke¹¹⁴, E. Meoni^{41b,41a}, S. Mergelmeyer¹⁹, C. Merlassino²⁰, P. Mermod⁵³, L. Merola^{68a,68b}, C. Meroni^{67a}, F.S. Merritt³⁷, A. Messina^{71a,71b}, J. Metcalfe⁶, A.S. Mete¹⁷⁰, C. Meyer¹³⁶, J. Meyer¹⁵⁹, J-P. Meyer¹⁴⁴, H. Meyer Zu Theenhausen^{60a}, F. Miano¹⁵⁵, R.P. Middleton¹⁴³, L. Mijovic⁴⁹, G. Mikenberg¹⁷⁹, M. Mikestikova¹⁴⁰, M. Mikuž⁹⁰,

M. Milesi¹⁰³, A. Milic¹⁶⁶, D.A. Millar⁹¹, D.W. Miller³⁷, A. Milov¹⁷⁹, D.A. Milstead^{44a,44b},
 A.A. Minaenko¹²², M. Miñano Moya¹⁷³, I.A. Minashvili^{158b}, A.I. Mincer¹²³, B. Mindur^{82a},
 M. Mineev⁷⁸, Y. Minegishi¹⁶², Y. Ming¹⁸⁰, L.M. Mir¹⁴, A. Mirta^{66a,66b}, K.P. Mistry¹³⁶, T. Mitani¹⁷⁸,
 J. Mitrevski¹¹³, V.A. Mitsou¹⁷³, A. Miucci²⁰, P.S. Miyagawa¹⁴⁸, A. Mizukami⁸⁰, J.U. Mjörnmark⁹⁵,
 T. Mkrtchyan¹⁸³, M. Mlynarikova¹⁴², T. Moa^{44a,44b}, K. Mochizuki¹⁰⁸, P. Mogg⁵¹, S. Mohapatra³⁹,
 S. Molander^{44a,44b}, R. Moles-Valls²⁴, M.C. Mondragon¹⁰⁵, K. Mönig⁴⁵, J. Monk⁴⁰, E. Monnier¹⁰⁰,
 A. Montalbano¹⁵¹, J. Montejo Berlingen³⁶, F. Monticelli⁸⁷, S. Monzani^{67a}, N. Morange¹³¹, D. Moreno²²,
 M. Moreno Llácer³⁶, P. Morettini^{54b}, M. Morgenstern¹¹⁹, S. Morgenstern⁴⁷, D. Mori¹⁵¹, M. Morii⁵⁸,
 M. Morinaga¹⁷⁸, V. Morisbak¹³³, A.K. Morley³⁶, G. Mornacchi³⁶, A.P. Morris⁹³, J.D. Morris⁹¹,
 L. Morvaj¹⁵⁴, P. Moschovakos¹⁰, M. Mosidze^{158b}, H.J. Moss¹⁴⁸, J. Moss^{31,m}, K. Motohashi¹⁶⁴,
 R. Mount¹⁵², E. Mountricha³⁶, E.J.W. Moyse¹⁰¹, S. Muanza¹⁰⁰, F. Mueller¹¹⁴, J. Mueller¹³⁸,
 R.S.P. Mueller¹¹³, D. Muenstermann⁸⁸, G.A. Mullier²⁰, F.J. Munoz Sanchez⁹⁹, P. Murin^{28b},
 W.J. Murray^{177,143}, A. Murrone^{67a,67b}, M. Muškinja⁹⁰, C. Mwewa^{33a}, A.G. Myagkov^{122,aj}, J. Myers¹³⁰,
 M. Myska¹⁴¹, B.P. Nachman¹⁸, O. Nackenhorst⁴⁶, K. Nagai¹³⁴, K. Nagano⁸⁰, Y. Nagasaka⁶¹, M. Nagel⁵¹,
 E. Nagy¹⁰⁰, A.M. Nairz³⁶, Y. Nakahama¹¹⁶, K. Nakamura⁸⁰, T. Nakamura¹⁶², I. Nakano¹²⁶, H. Nanjo¹³²,
 F. Napolitano^{60a}, R.F. Naranjo Garcia⁴⁵, R. Narayan¹¹, D.I. Narrias Villar^{60a}, I. Naryshkin¹³⁷,
 T. Naumann⁴⁵, G. Navarro²², R. Nayyar⁷, H.A. Neal^{104,*}, P.Y. Nechaeva¹⁰⁹, T.J. Neep¹⁴⁴, A. Negri^{69a,69b},
 M. Negrini^{23b}, S. Nektarijevic¹¹⁸, C. Nellist⁵², M.E. Nelson¹³⁴, S. Nemecek¹⁴⁰, P. Nemethy¹²³,
 M. Nessi^{36,e}, M.S. Neubauer¹⁷², M. Neumann¹⁸¹, P.R. Newman²¹, T.Y. Ng^{62c}, Y.S. Ng¹⁹,
 H.D.N. Nguyen¹⁰⁰, T. Nguyen Manh¹⁰⁸, E. Nibigira³⁸, R.B. Nickerson¹³⁴, R. Nicolaïdou¹⁴⁴,
 D.S. Nielsen⁴⁰, J. Nielsen¹⁴⁵, N. Nikiforou¹¹, V. Nikolaenko^{122,aj}, I. Nikolic-Audit¹³⁵,
 K. Nikolopoulos²¹, P. Nilsson²⁹, Y. Ninomiya⁸⁰, A. Nisati^{71a}, N. Nishu^{59c}, R. Nisius¹¹⁴, I. Nitsche⁴⁶,
 T. Nitta¹⁷⁸, T. Nobe¹⁶², Y. Noguchi⁸⁴, M. Nomachi¹³², I. Nomidis¹³⁵, M.A. Nomura²⁹, T. Nooney⁹¹,
 M. Nordberg³⁶, N. Norjoharuddeen¹³⁴, T. Novak⁹⁰, O. Novgorodova⁴⁷, R. Novotny¹⁴¹, L. Nozka¹²⁹,
 K. Ntekas¹⁷⁰, E. Nurse⁹³, F. Nuti¹⁰³, F.G. Oakham^{34,ar}, H. Oberlack¹¹⁴, T. Obermann²⁴, J. Ocariz¹³⁵,
 A. Ochi⁸¹, I. Ochoa³⁹, J.P. Ochoa-Ricoux^{146a}, K. O'Connor²⁶, S. Oda⁸⁶, S. Odaka⁸⁰, S. Oerdekk⁵²,
 A. Oh⁹⁹, S.H. Oh⁴⁸, C.C. Ohm¹⁵³, H. Oide^{54b,54a}, M.L. Ojeda¹⁶⁶, H. Okawa¹⁶⁸, Y. Okazaki⁸⁴,
 Y. Okumura¹⁶², T. Okuyama⁸⁰, A. Olariu^{27b}, L.F. Oleiro Seabra^{139a}, S.A. Olivares Pino^{146a},
 D. Oliveira Damazio²⁹, J.L. Oliver¹, M.J.R. Olsson³⁷, A. Olszewski⁸³, J. Olszowska⁸³, D.C. O'Neil¹⁵¹,
 A. Onofre^{139a,139e}, K. Onogi¹¹⁶, P.U.E. Onyisi¹¹, H. Oppen¹³³, M.J. Oreglia³⁷, G.E. Orellana⁸⁷,
 Y. Oren¹⁶⁰, D. Orestano^{73a,73b}, N. Orlando^{62b}, A.A. O'Rourke⁴⁵, R.S. Orr¹⁶⁶, B. Osculati^{54b,54a,*},
 V. O'Shea⁵⁶, R. Ospanov^{59a}, G. Otero y Garzon³⁰, H. Otono⁸⁶, M. Ouchrif^{35d}, F. Ould-Saada¹³³,
 A. Ouraou¹⁴⁴, Q. Ouyang^{15a}, M. Owen⁵⁶, R.E. Owen²¹, V.E. Ozcan^{12c}, N. Ozturk⁸, J. Pacalt¹²⁹,
 H.A. Pacey³², K. Pachal¹⁵¹, A. Pacheco Pages¹⁴, L. Pacheco Rodriguez¹⁴⁴, C. Padilla Aranda¹⁴,
 S. Pagan Griso¹⁸, M. Paganini¹⁸², G. Palacino⁶⁴, S. Palazzo^{41b,41a}, S. Palestini³⁶, M. Palka^{82b},
 D. Pallin³⁸, I. Panagoulias¹⁰, C.E. Pandini³⁶, J.G. Panduro Vazquez⁹², P. Pani³⁶, G. Panizzo^{65a,65c},
 L. Paolozzi⁵³, T.D. Papadopoulou¹⁰, K. Papageorgiou^{9,h}, A. Paramonov⁶, D. Paredes Hernandez^{62b},
 S.R. Paredes Saenz¹³⁴, B. Parida¹⁶⁵, A.J. Parker⁸⁸, K.A. Parker⁴⁵, M.A. Parker³², F. Parodi^{54b,54a},
 J.A. Parsons³⁹, U. Parzefall⁵¹, V.R. Pascuzzi¹⁶⁶, J.M.P. Pasner¹⁴⁵, E. Pasqualucci^{71a}, S. Passaggio^{54b},
 F. Pastore⁹², P. Paswan^{44a,44b}, S. Pataraia⁹⁸, J.R. Pater⁹⁹, A. Pathak¹⁸⁰, T. Pauly³⁶, B. Pearson¹¹⁴,
 M. Pedersen¹³³, L. Pedraza Diaz¹¹⁸, R. Pedro^{139a,139b}, S.V. Peleganchuk^{121b,121a}, O. Penc¹⁴⁰, C. Peng^{15a},
 H. Peng^{59a}, B.S. Peralva^{79a}, M.M. Perego¹⁴⁴, A.P. Pereira Peixoto^{139a}, D.V. Perepelitsa²⁹, F. Peri¹⁹,
 L. Perini^{67a,67b}, H. Pernegger³⁶, S. Perrella^{68a,68b}, V.D. Peshekhonov^{78,*}, K. Peters⁴⁵, R.F.Y. Peters⁹⁹,
 B.A. Petersen³⁶, T.C. Petersen⁴⁰, E. Petit⁵⁷, A. Petridis¹, C. Petridou¹⁶¹, P. Petroff¹³¹, M. Petrov¹³⁴,
 F. Petrucci^{73a,73b}, M. Pettee¹⁸², N.E. Pettersson¹⁰¹, A. Peyaud¹⁴⁴, R. Pezoa^{146b}, T. Pham¹⁰³,
 F.H. Phillips¹⁰⁵, P.W. Phillips¹⁴³, M.W. Phipps¹⁷², G. Piacquadio¹⁵⁴, E. Pianori¹⁸, A. Picazio¹⁰¹,
 M.A. Pickering¹³⁴, R.H. Pickles⁹⁹, R. Piegaia³⁰, J.E. Pilcher³⁷, A.D. Pilkington⁹⁹, M. Pinamonti^{72a,72b},

J.L. Pinfold³, M. Pitt¹⁷⁹, M.-A. Pleier²⁹, V. Pleskot¹⁴², E. Plotnikova⁷⁸, D. Pluth⁷⁷,
 P. Podberezko^{121b,121a}, R. Poettgen⁹⁵, R. Poggi⁵³, L. Poggioli¹³¹, I. Pogrebnyak¹⁰⁵, D. Pohl²⁴,
 I. Pokharel⁵², G. Polesello^{69a}, A. Poley¹⁸, A. Policicchio^{71a,71b}, R. Polifka³⁶, A. Polini^{23b}, C.S. Pollard⁴⁵,
 V. Polychronakos²⁹, D. Ponomarenko¹¹¹, L. Pontecorvo³⁶, G.A. Popeneciu^{27d}, D.M. Portillo Quintero¹³⁵,
 S. Pospisil¹⁴¹, K. Potamianos⁴⁵, I.N. Potrap⁷⁸, C.J. Potter³², H. Potti¹¹, T. Poulsen⁹⁵, J. Poveda³⁶,
 T.D. Powell¹⁴⁸, M.E. Pozo Astigarraga³⁶, P. Pralavorio¹⁰⁰, S. Prell⁷⁷, D. Price⁹⁹, M. Primavera^{66a},
 S. Prince¹⁰², N. Proklova¹¹¹, K. Prokofiev^{62c}, F. Prokoshin^{146b}, S. Protopopescu²⁹, J. Proudfoot⁶,
 M. Przybycien^{82a}, A. Puri¹⁷², P. Puzo¹³¹, J. Qian¹⁰⁴, Y. Qin⁹⁹, A. Quadt⁵², M. Queitsch-Maitland⁴⁵,
 A. Qureshi¹, P. Rados¹⁰³, F. Ragusa^{67a,67b}, G. Rahal⁹⁶, J.A. Raine⁵³, S. Rajagopalan²⁹,
 A. Ramirez Morales⁹¹, T. Rashid¹³¹, S. Raspopov⁵, M.G. Ratti^{67a,67b}, D.M. Rauch⁴⁵, F. Rauscher¹¹³,
 S. Rave⁹⁸, B. Ravina¹⁴⁸, I. Ravinovich¹⁷⁹, J.H. Rawling⁹⁹, M. Raymond³⁶, A.L. Read¹³³, N.P. Readoff⁵⁷,
 M. Reale^{66a,66b}, D.M. Rebuzzi^{69a,69b}, A. Redelbach¹⁷⁶, G. Redlinger²⁹, R. Reece¹⁴⁵, R.G. Reed^{33c},
 K. Reeves⁴³, L. Rehnisch¹⁹, J. Reichert¹³⁶, D. Reikher¹⁶⁰, A. Reiss⁹⁸, C. Rembser³⁶, H. Ren^{15a},
 M. Rescigno^{71a}, S. Resconi^{67a}, E.D. Resseguei¹³⁶, S. Rettie¹⁷⁴, E. Reynolds²¹, O.L. Rezanova^{121b,121a},
 P. Reznicek¹⁴², E. Ricci^{74a,74b}, R. Richter¹¹⁴, S. Richter⁴⁵, E. Richter-Was^{82b}, O. Ricken²⁴, M. Ridel¹³⁵,
 P. Rieck¹¹⁴, C.J. Riegel¹⁸¹, O. Rifki⁴⁵, M. Rijssenbeek¹⁵⁴, A. Rimoldi^{69a,69b}, M. Rimoldi²⁰,
 L. Rinaldi^{23b}, G. Ripellino¹⁵³, B. Ristic⁸⁸, E. Ritsch³⁶, I. Riu¹⁴, J.C. Rivera Vergara^{146a},
 F. Rizatdinova¹²⁸, E. Rizvi⁹¹, C. Rizzi¹⁴, R.T. Roberts⁹⁹, S.H. Robertson^{102,ab}, D. Robinson³²,
 J.E.M. Robinson⁴⁵, A. Robson⁵⁶, E. Rocco⁹⁸, C. Roda^{70a,70b}, Y. Rodina¹⁰⁰, S. Rodriguez Bosca¹⁷³,
 A. Rodriguez Perez¹⁴, D. Rodriguez Rodriguez¹⁷³, A.M. Rodríguez Vera^{167b}, S. Roe³⁶, C.S. Rogan⁵⁸,
 O. Røhne¹³³, R. Röhrlig¹¹⁴, C.P.A. Roland⁶⁴, J. Roloff⁵⁸, A. Romaniouk¹¹¹, M. Romano^{23b,23a},
 N. Rompotis⁸⁹, M. Ronzani¹²³, L. Roos¹³⁵, S. Rosati^{71a}, K. Rosbach⁵¹, P. Rose¹⁴⁵, N-A. Rosien⁵²,
 B.J. Rosser¹³⁶, E. Rossi⁴⁵, E. Rossi^{73a,73b}, E. Rossi^{68a,68b}, L.P. Rossi^{54b}, L. Rossini^{67a,67b},
 J.H.N. Rosten³², R. Rosten¹⁴, M. Rotaru^{27b}, J. Rothberg¹⁴⁷, B. Rottler⁵¹, D. Rousseau¹³¹, D. Roy^{33c},
 A. Rozanov¹⁰⁰, Y. Rozen¹⁵⁹, X. Ruan^{33c}, F. Rubbo¹⁵², F. Rühr⁵¹, A. Ruiz-Martinez¹⁷³, Z. Rurikova⁵¹,
 N.A. Rusakovich⁷⁸, H.L. Russell¹⁰², J.P. Rutherford⁷, E.M. Rüttinger^{45,j}, Y.F. Ryabov¹³⁷, M. Rybar¹⁷²,
 G. Rybkin¹³¹, S. Ryu⁶, A. Ryzhov¹²², G.F. Rzehorzh⁵², P. Sabatini⁵², G. Sabato¹¹⁹, S. Sacerdoti¹³¹,
 H.F-W. Sadrozinski¹⁴⁵, R. Sadykov⁷⁸, F. Safai Tehrani^{71a}, P. Saha¹²⁰, M. Sahinsoy^{60a}, A. Sahu¹⁸¹,
 M. Saimpert⁴⁵, M. Saito¹⁶², T. Saito¹⁶², H. Sakamoto¹⁶², A. Sakharov^{123,ai}, D. Salamani⁵³,
 G. Salamanna^{73a,73b}, J.E. Salazar Loyola^{146b}, P.H. Sales De Bruin¹⁷¹, D. Salihagic^{114,*}, A. Salnikov¹⁵²,
 J. Salt¹⁷³, D. Salvatore^{41b,41a}, F. Salvatore¹⁵⁵, A. Salvucci^{62a,62b,62c}, A. Salzburger³⁶, J. Samarati³⁶,
 D. Sammel⁵¹, D. Sampsonidis¹⁶¹, D. Sampsonidou¹⁶¹, J. Sánchez¹⁷³, A. Sanchez Pineda^{65a,65c},
 H. Sandaker¹³³, C.O. Sander⁴⁵, M. Sandhoff¹⁸¹, C. Sandoval²², D.P.C. Sankey¹⁴³, M. Sannino^{54b,54a},
 Y. Sano¹¹⁶, A. Sansoni⁵⁰, C. Santoni³⁸, H. Santos^{139a}, I. Santoyo Castillo¹⁵⁵, A. Santra¹⁷³,
 A. Sapronov⁷⁸, J.G. Saraiva^{139a,139d}, O. Sasaki⁸⁰, K. Sato¹⁶⁸, F. Sauerburger⁵¹, E. Sauvan⁵,
 P. Savard^{166,ar}, N. Savic¹¹⁴, R. Sawada¹⁶², C. Sawyer¹⁴³, L. Sawyer^{94,ag}, C. Sbarra^{23b}, A. Sbrizzi^{23a},
 T. Scanlon⁹³, J. Schaarschmidt¹⁴⁷, P. Schacht¹¹⁴, B.M. Schachtner¹¹³, D. Schaefer³⁷, L. Schaefer¹³⁶,
 J. Schaeffer⁹⁸, S. Schaepe³⁶, U. Schäfer⁹⁸, A.C. Schaffer¹³¹, D. Schaille¹¹³, R.D. Schamberger¹⁵⁴,
 N. Scharmberg⁹⁹, V.A. Schegelsky¹³⁷, D. Scheirich¹⁴², F. Schenck¹⁹, M. Schernau¹⁷⁰, C. Schiavi^{54b,54a},
 S. Schier¹⁴⁵, L.K. Schildgen²⁴, Z.M. Schillaci²⁶, E.J. Schioppa³⁶, M. Schioppa^{41b,41a}, K.E. Schleicher⁵¹,
 S. Schlenker³⁶, K.R. Schmidt-Sommerfeld¹¹⁴, K. Schmieden³⁶, C. Schmitt⁹⁸, S. Schmitt⁴⁵, S. Schmitz⁹⁸,
 J.C. Schmoeckel⁴⁵, U. Schnoor⁵¹, L. Schoeffel¹⁴⁴, A. Schoening^{60b}, E. Schopf¹³⁴, M. Schott⁹⁸,
 J.F.P. Schouwenberg¹¹⁸, J. Schovancova³⁶, S. Schramm⁵³, A. Schulte⁹⁸, H-C. Schultz-Coulon^{60a},
 M. Schumacher⁵¹, B.A. Schumm¹⁴⁵, Ph. Schune¹⁴⁴, A. Schwartzman¹⁵², T.A. Schwarz¹⁰⁴,
 Ph. Schwemling¹⁴⁴, R. Schwienhorst¹⁰⁵, A. Sciandra²⁴, G. Sciolla²⁶, M. Scornajenghi^{41b,41a}, F. Scuri^{70a},
 F. Scutti¹⁰³, L.M. Scyboz¹¹⁴, J. Searcy¹⁰⁴, C.D. Sebastiani^{71a,71b}, P. Seema¹⁹, S.C. Seidel¹¹⁷,
 A. Seiden¹⁴⁵, T. Seiss³⁷, J.M. Seixas^{79b}, G. Sekhniaidze^{68a}, K. Sekhon¹⁰⁴, S.J. Sekula⁴²,

N. Semprini-Cesari^{23b,23a}, S. Sen⁴⁸, S. Senkin³⁸, C. Serfon¹³³, L. Serin¹³¹, L. Serkin^{65a,65b}, M. Sessa^{59a}, H. Severini¹²⁷, F. Sforza¹⁶⁹, A. Sfyrla⁵³, E. Shabalina⁵², J.D. Shahinian¹⁴⁵, N.W. Shaikh^{44a,44b}, L.Y. Shan^{15a}, R. Shang¹⁷², J.T. Shank²⁵, M. Shapiro¹⁸, A. Sharma¹³⁴, A.S. Sharma¹, P.B. Shatalov¹¹⁰, K. Shaw¹⁵⁵, S.M. Shaw⁹⁹, A. Shcherbakova¹³⁷, Y. Shen¹²⁷, N. Sherafati³⁴, A.D. Sherman²⁵, P. Sherwood⁹³, L. Shi^{157,an}, S. Shimizu⁸⁰, C.O. Shimmin¹⁸², M. Shimojima¹¹⁵, I.P.J. Shipsey¹³⁴, S. Shirabe⁸⁶, M. Shiyakova⁷⁸, J. Shlomi¹⁷⁹, A. Shmeleva¹⁰⁹, D. Shoaleh Saadi¹⁰⁸, M.J. Shochet³⁷, S. Shojaii¹⁰³, D.R. Shope¹²⁷, S. Shrestha¹²⁵, E. Shulga¹¹¹, P. Sicho¹⁴⁰, A.M. Sickles¹⁷², P.E. Sidebo¹⁵³, E. Sideras Haddad^{33c}, O. Sidiropoulou³⁶, A. Sidoti^{23b,23a}, F. Siegert⁴⁷, Dj. Sijacki¹⁶, J. Silva^{139a}, M. Silva Jr.¹⁸⁰, M.V. Silva Oliveira^{79a}, S.B. Silverstein^{44a}, S. Simion¹³¹, E. Simioni⁹⁸, M. Simon⁹⁸, R. Simoniello⁹⁸, P. Sinervo¹⁶⁶, N.B. Sinev¹³⁰, M. Sioli^{23b,23a}, G. Siragusa¹⁷⁶, I. Siral¹⁰⁴, S.Yu. Sivoklokov¹¹², J. Sjölin^{44a,44b}, P. Skubic¹²⁷, M. Slater²¹, T. Slavicek¹⁴¹, M. Slawinska⁸³, K. Sliwa¹⁶⁹, R. Slovak¹⁴², V. Smakhtin¹⁷⁹, B.H. Smart⁵, J. Smiesko^{28a}, N. Smirnov¹¹¹, S.Yu. Smirnov¹¹¹, Y. Smirnov¹¹¹, L.N. Smirnova^{112,s}, O. Smirnova⁹⁵, J.W. Smith⁵², M.N.K. Smith³⁹, M. Smizanska⁸⁸, K. Smolek¹⁴¹, A. Smykiewicz⁸³, A.A. Snesarev¹⁰⁹, I.M. Snyder¹³⁰, S. Snyder²⁹, R. Sobie^{175,ab}, A.M. Soffa¹⁷⁰, A. Soffer¹⁶⁰, A. Søgaard⁴⁹, D.A. Soh¹⁵⁷, G. Sokhrannyi⁹⁰, C.A. Solans Sanchez³⁶, M. Solar¹⁴¹, E.Yu. Soldatov¹¹¹, U. Soldevila¹⁷³, A.A. Solodkov¹²², A. Soloshenko⁷⁸, O.V. Solovyanov¹²², V. Solovyev¹³⁷, P. Sommer¹⁴⁸, H. Son¹⁶⁹, W. Song¹⁴³, W.Y. Song^{167b}, A. Sopczak¹⁴¹, F. Sopkova^{28b}, C.L. Sotropoulou^{70a,70b}, S. Sottocornola^{69a,69b}, R. Soualah^{65a,65c,g}, A.M. Soukharev^{121b,121a}, D. South⁴⁵, B.C. Sowden⁹², S. Spagnolo^{66a,66b}, M. Spalla¹¹⁴, M. Spangenberg¹⁷⁷, F. Spanò⁹², D. Sperlich¹⁹, F. Spettel¹¹⁴, T.M. Spieker^{60a}, R. Spighi^{23b}, G. Spigo³⁶, L.A. Spiller¹⁰³, D.P. Spiteri⁵⁶, M. Spousta¹⁴², A. Stabile^{67a,67b}, R. Stamen^{60a}, S. Stamm¹⁹, E. Stanecka⁸³, R.W. Stanek⁶, C. Stanescu^{73a}, B. Stanislaus¹³⁴, M.M. Stanitzki⁴⁵, B. Stapf¹¹⁹, S. Stapnes¹³³, E.A. Starchenko¹²², G.H. Stark³⁷, J. Stark⁵⁷, S.H. Stark⁴⁰, P. Staroba¹⁴⁰, P. Starovoitov^{60a}, S. Stärz³⁶, R. Staszewski⁸³, M. Stegler⁴⁵, P. Steinberg²⁹, B. Stelzer¹⁵¹, H.J. Stelzer³⁶, O. Stelzer-Chilton^{167a}, H. Stenzel⁵⁵, T.J. Stevenson¹⁵⁵, G.A. Stewart³⁶, M.C. Stockton¹³⁰, G. Stoica^{27b}, P. Stolte⁵², S. Stonjek¹¹⁴, A. Straessner⁴⁷, J. Strandberg¹⁵³, S. Strandberg^{44a,44b}, M. Strauss¹²⁷, P. Strizenec^{28b}, R. Ströhmer¹⁷⁶, D.M. Strom¹³⁰, R. Stroynowski⁴², A. Strubig⁴⁹, S.A. Stucci²⁹, B. Stugu¹⁷, J. Stupak¹²⁷, N.A. Styles⁴⁵, D. Su¹⁵², J. Su¹³⁸, S. Suchek^{60a}, Y. Sugaya¹³², M. Suk¹⁴¹, V.V. Sulin¹⁰⁹, M.J. Sullivan⁸⁹, D.M.S. Sultan⁵³, S. Sultansoy^{4c}, T. Sumida⁸⁴, S. Sun¹⁰⁴, X. Sun³, K. Suruliz¹⁵⁵, C.J.E. Suster¹⁵⁶, M.R. Sutton¹⁵⁵, S. Suzuki⁸⁰, M. Svatos¹⁴⁰, M. Swiatlowski³⁷, S.P. Swift², A. Sydorenko⁹⁸, I. Sykora^{28a}, T. Sykora¹⁴², D. Ta⁹⁸, K. Tackmann⁴⁵, J. Taenzer¹⁶⁰, A. Taffard¹⁷⁰, R. Tafirout^{167a}, E. Tahirovic⁹¹, N. Taiblum¹⁶⁰, H. Takai²⁹, R. Takashima⁸⁵, E.H. Takasugi¹¹⁴, K. Takeda⁸¹, T. Takeshita¹⁴⁹, Y. Takubo⁸⁰, M. Talby¹⁰⁰, A.A. Talyshev^{121b,121a}, J. Tanaka¹⁶², M. Tanaka¹⁶⁴, R. Tanaka¹³¹, B.B. Tannenwald¹²⁵, S. Tapia Araya^{146b}, S. Tapprogge⁹⁸, A. Tarek Abouelfadl Mohamed¹³⁵, S. Tarem¹⁵⁹, G. Tarna^{27b,d}, G.F. Tartarelli^{67a}, P. Tas¹⁴², M. Tasevsky¹⁴⁰, T. Tashiro⁸⁴, E. Tassi^{41b,41a}, A. Tavares Delgado^{139a,139b}, Y. Tayalati^{35e}, A.C. Taylor¹¹⁷, A.J. Taylor⁴⁹, G.N. Taylor¹⁰³, P.T.E. Taylor¹⁰³, W. Taylor^{167b}, A.S. Tee⁸⁸, P. Teixeira-Dias⁹², H. Ten Kate³⁶, P.K. Teng¹⁵⁷, J.J. Teoh¹¹⁹, S. Terada⁸⁰, K. Terashi¹⁶², J. Terron⁹⁷, S. Terzo¹⁴, M. Testa⁵⁰, R.J. Teuscher^{166,ab}, S.J. Thais¹⁸², T. Theveneaux-Pelzer⁴⁵, F. Thiele⁴⁰, D.W. Thomas⁹², J.P. Thomas²¹, A.S. Thompson⁵⁶, P.D. Thompson²¹, L.A. Thomsen¹⁸², E. Thomson¹³⁶, Y. Tian³⁹, R.E. Ticse Torres⁵², V.O. Tikhomirov^{109,ak}, Yu.A. Tikhonov^{121b,121a}, S. Timoshenko¹¹¹, P. Tipton¹⁸², S. Tisserant¹⁰⁰, K. Todome¹⁶⁴, S. Todorova-Nova⁵, S. Todt⁴⁷, J. Tojo⁸⁶, S. Tokár^{28a}, K. Tokushuku⁸⁰, E. Tolley¹²⁵, K.G. Tomiwa^{33c}, M. Tomoto¹¹⁶, L. Tompkins¹⁵², K. Toms¹¹⁷, B. Tong⁵⁸, P. Tornambe⁵¹, E. Torrence¹³⁰, H. Torres⁴⁷, E. Torró Pastor¹⁴⁷, C. Tosciri¹³⁴, J. Toth^{100,aa}, F. Touchard¹⁰⁰, D.R. Tovey¹⁴⁸, C.J. Treado¹²³, T. Trefzger¹⁷⁶, F. Tresoldi¹⁵⁵, A. Tricoli²⁹, I.M. Trigger^{167a}, S. Trineaz-Duvoid¹³⁵, M.F. Tripiana¹⁴, W. Trischuk¹⁶⁶, B. Trocmé⁵⁷, A. Trofymov¹³¹, C. Troncon^{67a}, M. Trovatelli¹⁷⁵, F. Trovato¹⁵⁵, L. Truong^{33b}, M. Trzebinski⁸³, A. Trzupek⁸³, F. Tsai⁴⁵, J.C.-L. Tseng¹³⁴, P.V. Tsiareshka¹⁰⁶,

A. Tsirigotis¹⁶¹, N. Tsirintanis⁹, V. Tsiskaridze¹⁵⁴, E.G. Tskhadadze^{158a}, I.I. Tsukerman¹¹⁰, V. Tsulaia¹⁸, S. Tsuno⁸⁰, D. Tsybychev¹⁵⁴, Y. Tu^{62b}, A. Tudorache^{27b}, V. Tudorache^{27b}, T.T. Tulbure^{27a}, A.N. Tuna⁵⁸, S. Turchikhin⁷⁸, D. Turgeman¹⁷⁹, I. Turk Cakir^{4b,t}, R.T. Turra^{67a}, P.M. Tuts³⁹, E. Tzovara⁹⁸, G. Ucchielli^{23b,23a}, I. Ueda⁸⁰, M. Ughetto^{44a,44b}, F. Ukegawa¹⁶⁸, G. Unal³⁶, A. Undrus²⁹, G. Unel¹⁷⁰, F.C. Ungaro¹⁰³, Y. Unno⁸⁰, K. Uno¹⁶², J. Urban^{28b}, P. Urquijo¹⁰³, P. Urrejola⁹⁸, G. Usai⁸, J. Usui⁸⁰, L. Vacavant¹⁰⁰, V. Vacek¹⁴¹, B. Vachon¹⁰², K.O.H. Vadla¹³³, A. Vaidya⁹³, C. Valderanis¹¹³, E. Valdes Santurio^{44a,44b}, M. Valente⁵³, S. Valentineti^{23b,23a}, A. Valero¹⁷³, L. Valéry⁴⁵, R.A. Vallance²¹, A. Vallier⁵, J.A. Valls Ferrer¹⁷³, T.R. Van Daalen¹⁴, H. Van der Graaf¹¹⁹, P. Van Gemmeren⁶, J. Van Nieuwkoop¹⁵¹, I. Van Vulpen¹¹⁹, M. Vanadia^{72a,72b}, W. Vandelli³⁶, A. Vaniachine¹⁶⁵, P. Vankov¹¹⁹, R. Vari^{71a}, E.W. Varnes⁷, C. Varni^{54b,54a}, T. Varol⁴², D. Varouchas¹³¹, K.E. Varvell¹⁵⁶, G.A. Vasquez^{146b}, J.G. Vasquez¹⁸², F. Vazeille³⁸, D. Vazquez Furelos¹⁴, T. Vazquez Schroeder¹⁰², J. Veatch⁵², V. Vecchio^{73a,73b}, L.M. Veloce¹⁶⁶, F. Veloso^{139a,139c}, S. Veneziano^{71a}, A. Ventura^{66a,66b}, M. Venturi¹⁷⁵, N. Venturi³⁶, V. Vercesi^{69a}, M. Verducci^{73a,73b}, C.M. Vergel Infante⁷⁷, C. Vergis²⁴, W. Verkerke¹¹⁹, A.T. Vermeulen¹¹⁹, J.C. Vermeulen¹¹⁹, M.C. Vetterli^{151,ar}, N. Viaux Maira^{146b}, M. Vicente Barreto Pinto⁵³, I. Vichou^{172,*}, T. Vickey¹⁴⁸, O.E. Vickey Boeriu¹⁴⁸, G.H.A. Viehhauser¹³⁴, S. Viel¹⁸, L. Vigani¹³⁴, M. Villa^{23b,23a}, M. Villaplana Perez^{67a,67b}, E. Vilucchi⁵⁰, M.G. Vincter³⁴, V.B. Vinogradov⁷⁸, A. Vishwakarma⁴⁵, C. Vittori^{23b,23a}, I. Vivarelli¹⁵⁵, S. Vlachos¹⁰, M. Vogel¹⁸¹, P. Vokac¹⁴¹, G. Volpi¹⁴, S.E. von Buddenbrock^{33c}, E. Von Toerne²⁴, V. Vorobel¹⁴², K. Vorobev¹¹¹, M. Vos¹⁷³, J.H. Vossebeld⁸⁹, N. Vranjes¹⁶, M. Vranjes Milosavljevic¹⁶, V. Vrba¹⁴¹, M. Vreeswijk¹¹⁹, T. Šfiligoj⁹⁰, R. Vuillermet³⁶, I. Vukotic³⁷, T. Ženiš^{28a}, L. Živković¹⁶, P. Wagner²⁴, W. Wagner¹⁸¹, J. Wagner-Kuhr¹¹³, H. Wahlberg⁸⁷, S. Wahrmund⁴⁷, K. Wakamiya⁸¹, V.M. Walbrecht¹¹⁴, J. Walder⁸⁸, R. Walker¹¹³, S.D. Walker⁹², W. Walkowiak¹⁵⁰, V. Wallangen^{44a,44b}, A.M. Wang⁵⁸, C. Wang^{59b,d}, F. Wang¹⁸⁰, H. Wang¹⁸, H. Wang³, J. Wang¹⁵⁶, J. Wang^{60b}, P. Wang⁴², Q. Wang¹²⁷, R.-J. Wang¹³⁵, R. Wang^{59a}, R. Wang⁶, S.M. Wang¹⁵⁷, W.T. Wang^{59a}, W. Wang^{15c,ac}, W.X. Wang^{59a,ac}, Y. Wang^{59a,ah}, Z. Wang^{59c}, C. Wanotayaroj⁴⁵, A. Warburton¹⁰², C.P. Ward³², D.R. Wardrope⁹³, A. Washbrook⁴⁹, P.M. Watkins²¹, A.T. Watson²¹, M.F. Watson²¹, G. Watts¹⁴⁷, S. Watts⁹⁹, B.M. Waugh⁹³, A.F. Webb¹¹, S. Webb⁹⁸, C. Weber¹⁸², M.S. Weber²⁰, S.A. Weber³⁴, S.M. Weber^{60a}, A.R. Weidberg¹³⁴, B. Weinert⁶⁴, J. Weingarten⁴⁶, M. Weirich⁹⁸, C. Weiser⁵¹, P.S. Wells³⁶, T. Wenaus²⁹, T. Wengler³⁶, S. Wenig³⁶, N. Wermes²⁴, M.D. Werner⁷⁷, P. Werner³⁶, M. Wessels^{60a}, T.D. Weston²⁰, K. Whalen¹³⁰, N.L. Whallon¹⁴⁷, A.M. Wharton⁸⁸, A.S. White¹⁰⁴, A. White⁸, M.J. White¹, R. White^{146b}, D. Whiteson¹⁷⁰, B.W. Whitmore⁸⁸, F.J. Wicksens¹⁴³, W. Wiedenmann¹⁸⁰, M. Wielers¹⁴³, C. Wiglesworth⁴⁰, L.A.M. Wiik-Fuchs⁵¹, F. Wilk⁹⁹, H.G. Wilkens³⁶, L.J. Wilkins⁹², H.H. Williams¹³⁶, S. Williams³², C. Willis¹⁰⁵, S. Willocq¹⁰¹, J.A. Wilson²¹, I. Wingerter-Seez⁵, E. Winkels¹⁵⁵, F. Winklmeier¹³⁰, O.J. Winston¹⁵⁵, B.T. Winter²⁴, M. Wittgen¹⁵², M. Wobisch⁹⁴, A. Wolf⁹⁸, T.M.H. Wolf¹¹⁹, R. Wolff¹⁰⁰, M.W. Wolter⁸³, H. Wolters^{139a,139c}, V.W.S. Wong¹⁷⁴, N.L. Woods¹⁴⁵, S.D. Worm²¹, B.K. Wosiek⁸³, K.W. Woźniak⁸³, K. Wraith⁵⁶, M. Wu³⁷, S.L. Wu¹⁸⁰, X. Wu⁵³, Y. Wu^{59a}, T.R. Wyatt⁹⁹, B.M. Wynne⁴⁹, S. Xella⁴⁰, Z. Xi¹⁰⁴, L. Xia¹⁷⁷, D. Xu^{15a}, H. Xu^{59a,d}, L. Xu²⁹, T. Xu¹⁴⁴, W. Xu¹⁰⁴, B. Yabsley¹⁵⁶, S. Yacoob^{33a}, K. Yajima¹³², D.P. Yallup⁹³, D. Yamaguchi¹⁶⁴, Y. Yamaguchi¹⁶⁴, A. Yamamoto⁸⁰, T. Yamanaka¹⁶², F. Yamane⁸¹, M. Yamatani¹⁶², T. Yamazaki¹⁶², Y. Yamazaki⁸¹, Z. Yan²⁵, H.J. Yang^{59c,59d}, H.T. Yang¹⁸, S. Yang⁷⁶, Y. Yang¹⁶², Z. Yang¹⁷, W-M. Yao¹⁸, Y.C. Yap⁴⁵, Y. Yasu⁸⁰, E. Yatsenko^{59c,59d}, J. Ye⁴², S. Ye²⁹, I. Yeletskikh⁷⁸, E. Yigitbasi²⁵, E. Yildirim⁹⁸, K. Yorita¹⁷⁸, K. Yoshihara¹³⁶, C.J.S. Young³⁶, C. Young¹⁵², J. Yu⁷⁷, J. Yu⁸, X. Yue^{60a}, S.P.Y. Yuen²⁴, B. Zabinski⁸³, G. Zacharis¹⁰, E. Zaffaroni⁵³, R. Zaidan¹⁴, A.M. Zaitsev^{122,aj}, T. Zakareishvili^{158b}, N. Zakharchuk³⁴, J. Zalieckas¹⁷, S. Zambito⁵⁸, D. Zanzi³⁶, D.R. Zaripovas⁵⁶, S.V. Zeißner⁴⁶, C. Zeitnitz¹⁸¹, G. Zemaityte¹³⁴, J.C. Zeng¹⁷², Q. Zeng¹⁵², O. Zenin¹²², D. Zerwas¹³¹, M. Zgubič¹³⁴, D.F. Zhang^{59b}, D. Zhang¹⁰⁴, F. Zhang¹⁸⁰, G. Zhang^{59a}, H. Zhang^{15c}, J. Zhang⁶, L. Zhang^{15c}, L. Zhang^{59a}, M. Zhang¹⁷², P. Zhang^{15c}, R. Zhang^{59a}, R. Zhang²⁴, X. Zhang^{59b}, Y. Zhang¹³¹, Z. Zhang⁴⁸, P. Zhao⁴², X. Zhao⁴²,

Y. Zhao^{59b,131,af}, Z. Zhao^{59a}, A. Zhemchugov⁷⁸, Z. Zheng¹⁰⁴, D. Zhong¹⁷², B. Zhou¹⁰⁴, C. Zhou¹⁸⁰, L. Zhou⁴², M.S. Zhou^{15a,15d}, M. Zhou¹⁵⁴, N. Zhou^{59c}, Y. Zhou⁷, C.G. Zhu^{59b}, H.L. Zhu^{59a}, H. Zhu^{15a}, J. Zhu¹⁰⁴, Y. Zhu^{59a}, X. Zhuang^{15a}, K. Zhukov¹⁰⁹, V. Zhulanov^{121b,121a}, A. Zibell¹⁷⁶, D. Ziemska⁶⁴, N.I. Zimine⁷⁸, S. Zimmermann⁵¹, Z. Zinonos¹¹⁴, M. Zinser⁹⁸, M. Ziolkowski¹⁵⁰, G. Zobernig¹⁸⁰, A. Zoccoli^{23b,23a}, K. Zoch⁵², T.G. Zorbas¹⁴⁸, R. Zou³⁷, M. Zur Nedden¹⁹, L. Zwalski³⁶.

¹Department of Physics, University of Adelaide, Adelaide; Australia.

²Physics Department, SUNY Albany, Albany NY; United States of America.

³Department of Physics, University of Alberta, Edmonton AB; Canada.

^{4(a)}Department of Physics, Ankara University, Ankara; ^(b)Istanbul Aydin University, Istanbul; ^(c)Division of Physics, TOBB University of Economics and Technology, Ankara; Turkey.

⁵LAPP, Université Grenoble Alpes, Université Savoie Mont Blanc, CNRS/IN2P3, Annecy; France.

⁶High Energy Physics Division, Argonne National Laboratory, Argonne IL; United States of America.

⁷Department of Physics, University of Arizona, Tucson AZ; United States of America.

⁸Department of Physics, University of Texas at Arlington, Arlington TX; United States of America.

⁹Physics Department, National and Kapodistrian University of Athens, Athens; Greece.

¹⁰Physics Department, National Technical University of Athens, Zografou; Greece.

¹¹Department of Physics, University of Texas at Austin, Austin TX; United States of America.

^{12(a)}Bahcesehir University, Faculty of Engineering and Natural Sciences, Istanbul; ^(b)Istanbul Bilgi University, Faculty of Engineering and Natural Sciences, Istanbul; ^(c)Department of Physics, Bogazici University, Istanbul; ^(d)Department of Physics Engineering, Gaziantep University, Gaziantep; Turkey.

¹³Institute of Physics, Azerbaijan Academy of Sciences, Baku; Azerbaijan.

¹⁴Institut de Física d'Altes Energies (IFAE), Barcelona Institute of Science and Technology, Barcelona; Spain.

^{15(a)}Institute of High Energy Physics, Chinese Academy of Sciences, Beijing; ^(b)Physics Department, Tsinghua University, Beijing; ^(c)Department of Physics, Nanjing University, Nanjing; ^(d)University of Chinese Academy of Science (UCAS), Beijing; China.

¹⁶Institute of Physics, University of Belgrade, Belgrade; Serbia.

¹⁷Department for Physics and Technology, University of Bergen, Bergen; Norway.

¹⁸Physics Division, Lawrence Berkeley National Laboratory and University of California, Berkeley CA; United States of America.

¹⁹Institut für Physik, Humboldt Universität zu Berlin, Berlin; Germany.

²⁰Albert Einstein Center for Fundamental Physics and Laboratory for High Energy Physics, University of Bern, Bern; Switzerland.

²¹School of Physics and Astronomy, University of Birmingham, Birmingham; United Kingdom.

²²Facultad de Ciencias y Centro de Investigaciones, Universidad Antonio Nariño, Bogota; Colombia.

^{23(a)}INFN Bologna and Universita' di Bologna, Dipartimento di Fisica; ^(b)INFN Sezione di Bologna; Italy.

²⁴Physikalisches Institut, Universität Bonn, Bonn; Germany.

²⁵Department of Physics, Boston University, Boston MA; United States of America.

²⁶Department of Physics, Brandeis University, Waltham MA; United States of America.

^{27(a)}Transilvania University of Brasov, Brasov; ^(b)Horia Hulubei National Institute of Physics and Nuclear Engineering, Bucharest; ^(c)Department of Physics, Alexandru Ioan Cuza University of Iasi, Iasi; ^(d)National Institute for Research and Development of Isotopic and Molecular Technologies, Physics Department, Cluj-Napoca; ^(e)University Politehnica Bucharest, Bucharest; ^(f)West University in Timisoara, Timisoara; Romania.

^{28(a)}Faculty of Mathematics, Physics and Informatics, Comenius University, Bratislava; ^(b)Department of

Subnuclear Physics, Institute of Experimental Physics of the Slovak Academy of Sciences, Kosice; Slovak Republic.

²⁹Physics Department, Brookhaven National Laboratory, Upton NY; United States of America.

³⁰Departamento de Física, Universidad de Buenos Aires, Buenos Aires; Argentina.

³¹California State University, CA; United States of America.

³²Cavendish Laboratory, University of Cambridge, Cambridge; United Kingdom.

^{33(a)}Department of Physics, University of Cape Town, Cape Town;^(b)Department of Mechanical Engineering Science, University of Johannesburg, Johannesburg;^(c)School of Physics, University of the Witwatersrand, Johannesburg; South Africa.

³⁴Department of Physics, Carleton University, Ottawa ON; Canada.

^{35(a)}Faculté des Sciences Ain Chock, Réseau Universitaire de Physique des Hautes Energies - Université Hassan II, Casablanca;^(b)Faculté des Sciences, Université Ibn-Tofail, Kénitra;^(c)Faculté des Sciences Semlalia, Université Cadi Ayyad, LPHEA-Marrakech;^(d)Faculté des Sciences, Université Mohamed Premier and LPTPM, Oujda;^(e)Faculté des sciences, Université Mohammed V, Rabat; Morocco.

³⁶CERN, Geneva; Switzerland.

³⁷Enrico Fermi Institute, University of Chicago, Chicago IL; United States of America.

³⁸LPC, Université Clermont Auvergne, CNRS/IN2P3, Clermont-Ferrand; France.

³⁹Nevis Laboratory, Columbia University, Irvington NY; United States of America.

⁴⁰Niels Bohr Institute, University of Copenhagen, Copenhagen; Denmark.

^{41(a)}Dipartimento di Fisica, Università della Calabria, Rende;^(b)INFN Gruppo Collegato di Cosenza, Laboratori Nazionali di Frascati; Italy.

⁴²Physics Department, Southern Methodist University, Dallas TX; United States of America.

⁴³Physics Department, University of Texas at Dallas, Richardson TX; United States of America.

^{44(a)}Department of Physics, Stockholm University;^(b)Oskar Klein Centre, Stockholm; Sweden.

⁴⁵Deutsches Elektronen-Synchrotron DESY, Hamburg and Zeuthen; Germany.

⁴⁶Lehrstuhl für Experimentelle Physik IV, Technische Universität Dortmund, Dortmund; Germany.

⁴⁷Institut für Kern- und Teilchenphysik, Technische Universität Dresden, Dresden; Germany.

⁴⁸Department of Physics, Duke University, Durham NC; United States of America.

⁴⁹SUPA - School of Physics and Astronomy, University of Edinburgh, Edinburgh; United Kingdom.

⁵⁰INFN e Laboratori Nazionali di Frascati, Frascati; Italy.

⁵¹Physikalisches Institut, Albert-Ludwigs-Universität Freiburg, Freiburg; Germany.

⁵²II. Physikalisches Institut, Georg-August-Universität Göttingen, Göttingen; Germany.

⁵³Département de Physique Nucléaire et Corpusculaire, Université de Genève, Genève; Switzerland.

^{54(a)}Dipartimento di Fisica, Università di Genova, Genova;^(b)INFN Sezione di Genova; Italy.

⁵⁵II. Physikalisches Institut, Justus-Liebig-Universität Giessen, Giessen; Germany.

⁵⁶SUPA - School of Physics and Astronomy, University of Glasgow, Glasgow; United Kingdom.

⁵⁷LPSC, Université Grenoble Alpes, CNRS/IN2P3, Grenoble INP, Grenoble; France.

⁵⁸Laboratory for Particle Physics and Cosmology, Harvard University, Cambridge MA; United States of America.

^{59(a)}Department of Modern Physics and State Key Laboratory of Particle Detection and Electronics, University of Science and Technology of China, Hefei;^(b)Institute of Frontier and Interdisciplinary Science and Key Laboratory of Particle Physics and Particle Irradiation (MOE), Shandong University, Qingdao;^(c)School of Physics and Astronomy, Shanghai Jiao Tong University, KLPPAC-MoE, SKLPPC, Shanghai;^(d)Tsung-Dao Lee Institute, Shanghai; China.

^{60(a)}Kirchhoff-Institut für Physik, Ruprecht-Karls-Universität Heidelberg, Heidelberg;^(b)Physikalisch Institut, Ruprecht-Karls-Universität Heidelberg, Heidelberg; Germany.

⁶¹Faculty of Applied Information Science, Hiroshima Institute of Technology, Hiroshima; Japan.

- ^{62(a)}Department of Physics, Chinese University of Hong Kong, Shatin, N.T., Hong Kong; ^(b)Department of Physics, University of Hong Kong, Hong Kong; ^(c)Department of Physics and Institute for Advanced Study, Hong Kong University of Science and Technology, Clear Water Bay, Kowloon, Hong Kong; China.
⁶³Department of Physics, National Tsing Hua University, Hsinchu; Taiwan.
⁶⁴Department of Physics, Indiana University, Bloomington IN; United States of America.
^{65(a)}INFN Gruppo Collegato di Udine, Sezione di Trieste, Udine; ^(b)ICTP, Trieste; ^(c)Dipartimento Politecnico di Ingegneria e Architettura, Università di Udine, Udine; Italy.
^{66(a)}INFN Sezione di Lecce; ^(b)Dipartimento di Matematica e Fisica, Università del Salento, Lecce; Italy.
^{67(a)}INFN Sezione di Milano; ^(b)Dipartimento di Fisica, Università di Milano, Milano; Italy.
^{68(a)}INFN Sezione di Napoli; ^(b)Dipartimento di Fisica, Università di Napoli, Napoli; Italy.
^{69(a)}INFN Sezione di Pavia; ^(b)Dipartimento di Fisica, Università di Pavia, Pavia; Italy.
^{70(a)}INFN Sezione di Pisa; ^(b)Dipartimento di Fisica E. Fermi, Università di Pisa, Pisa; Italy.
^{71(a)}INFN Sezione di Roma; ^(b)Dipartimento di Fisica, Sapienza Università di Roma, Roma; Italy.
^{72(a)}INFN Sezione di Roma Tor Vergata; ^(b)Dipartimento di Fisica, Università di Roma Tor Vergata, Roma; Italy.
^{73(a)}INFN Sezione di Roma Tre; ^(b)Dipartimento di Matematica e Fisica, Università Roma Tre, Roma; Italy.
^{74(a)}INFN-TIFPA; ^(b)Università degli Studi di Trento, Trento; Italy.
⁷⁵Institut für Astro- und Teilchenphysik, Leopold-Franzens-Universität, Innsbruck; Austria.
⁷⁶University of Iowa, Iowa City IA; United States of America.
⁷⁷Department of Physics and Astronomy, Iowa State University, Ames IA; United States of America.
⁷⁸Joint Institute for Nuclear Research, Dubna; Russia.
^{79(a)}Departamento de Engenharia Elétrica, Universidade Federal de Juiz de Fora (UFJF), Juiz de Fora; ^(b)Universidade Federal do Rio De Janeiro COPPE/EE/IF, Rio de Janeiro; ^(c)Universidade Federal de São João del Rei (UFSJ), São João del Rei; ^(d)Instituto de Física, Universidade de São Paulo, São Paulo; Brazil.
⁸⁰KEK, High Energy Accelerator Research Organization, Tsukuba; Japan.
⁸¹Graduate School of Science, Kobe University, Kobe; Japan.
^{82(a)}AGH University of Science and Technology, Faculty of Physics and Applied Computer Science, Krakow; ^(b)Marian Smoluchowski Institute of Physics, Jagiellonian University, Krakow; Poland.
⁸³Institute of Nuclear Physics Polish Academy of Sciences, Krakow; Poland.
⁸⁴Faculty of Science, Kyoto University, Kyoto; Japan.
⁸⁵Kyoto University of Education, Kyoto; Japan.
⁸⁶Research Center for Advanced Particle Physics and Department of Physics, Kyushu University, Fukuoka ; Japan.
⁸⁷Instituto de Física La Plata, Universidad Nacional de La Plata and CONICET, La Plata; Argentina.
⁸⁸Physics Department, Lancaster University, Lancaster; United Kingdom.
⁸⁹Oliver Lodge Laboratory, University of Liverpool, Liverpool; United Kingdom.
⁹⁰Department of Experimental Particle Physics, Jožef Stefan Institute and Department of Physics, University of Ljubljana, Ljubljana; Slovenia.
⁹¹School of Physics and Astronomy, Queen Mary University of London, London; United Kingdom.
⁹²Department of Physics, Royal Holloway University of London, Egham; United Kingdom.
⁹³Department of Physics and Astronomy, University College London, London; United Kingdom.
⁹⁴Louisiana Tech University, Ruston LA; United States of America.
⁹⁵Fysiska institutionen, Lunds universitet, Lund; Sweden.
⁹⁶Centre de Calcul de l’Institut National de Physique Nucléaire et de Physique des Particules (IN2P3),

Villeurbanne; France.

⁹⁷Departamento de Física Teorica C-15 and CIAFF, Universidad Autónoma de Madrid, Madrid; Spain.

⁹⁸Institut für Physik, Universität Mainz, Mainz; Germany.

⁹⁹School of Physics and Astronomy, University of Manchester, Manchester; United Kingdom.

¹⁰⁰CPPM, Aix-Marseille Université, CNRS/IN2P3, Marseille; France.

¹⁰¹Department of Physics, University of Massachusetts, Amherst MA; United States of America.

¹⁰²Department of Physics, McGill University, Montreal QC; Canada.

¹⁰³School of Physics, University of Melbourne, Victoria; Australia.

¹⁰⁴Department of Physics, University of Michigan, Ann Arbor MI; United States of America.

¹⁰⁵Department of Physics and Astronomy, Michigan State University, East Lansing MI; United States of America.

¹⁰⁶B.I. Stepanov Institute of Physics, National Academy of Sciences of Belarus, Minsk; Belarus.

¹⁰⁷Research Institute for Nuclear Problems of Byelorussian State University, Minsk; Belarus.

¹⁰⁸Group of Particle Physics, University of Montreal, Montreal QC; Canada.

¹⁰⁹P.N. Lebedev Physical Institute of the Russian Academy of Sciences, Moscow; Russia.

¹¹⁰Institute for Theoretical and Experimental Physics of the National Research Centre Kurchatov Institute, Moscow; Russia.

¹¹¹National Research Nuclear University MEPhI, Moscow; Russia.

¹¹²D.V. Skobeltsyn Institute of Nuclear Physics, M.V. Lomonosov Moscow State University, Moscow; Russia.

¹¹³Fakultät für Physik, Ludwig-Maximilians-Universität München, München; Germany.

¹¹⁴Max-Planck-Institut für Physik (Werner-Heisenberg-Institut), München; Germany.

¹¹⁵Nagasaki Institute of Applied Science, Nagasaki; Japan.

¹¹⁶Graduate School of Science and Kobayashi-Maskawa Institute, Nagoya University, Nagoya; Japan.

¹¹⁷Department of Physics and Astronomy, University of New Mexico, Albuquerque NM; United States of America.

¹¹⁸Institute for Mathematics, Astrophysics and Particle Physics, Radboud University Nijmegen/Nikhef, Nijmegen; Netherlands.

¹¹⁹Nikhef National Institute for Subatomic Physics and University of Amsterdam, Amsterdam; Netherlands.

¹²⁰Department of Physics, Northern Illinois University, DeKalb IL; United States of America.

^{121(a)}Budker Institute of Nuclear Physics and NSU, SB RAS, Novosibirsk;^(b)Novosibirsk State University Novosibirsk; Russia.

¹²²Institute for High Energy Physics of the National Research Centre Kurchatov Institute, Protvino; Russia.

¹²³Department of Physics, New York University, New York NY; United States of America.

¹²⁴Ochanomizu University, Otsuka, Bunkyo-ku, Tokyo; Japan.

¹²⁵Ohio State University, Columbus OH; United States of America.

¹²⁶Faculty of Science, Okayama University, Okayama; Japan.

¹²⁷Homer L. Dodge Department of Physics and Astronomy, University of Oklahoma, Norman OK; United States of America.

¹²⁸Department of Physics, Oklahoma State University, Stillwater OK; United States of America.

¹²⁹Palacký University, RCPTM, Joint Laboratory of Optics, Olomouc; Czech Republic.

¹³⁰Center for High Energy Physics, University of Oregon, Eugene OR; United States of America.

¹³¹LAL, Université Paris-Sud, CNRS/IN2P3, Université Paris-Saclay, Orsay; France.

¹³²Graduate School of Science, Osaka University, Osaka; Japan.

¹³³Department of Physics, University of Oslo, Oslo; Norway.

- ¹³⁴Department of Physics, Oxford University, Oxford; United Kingdom.
- ¹³⁵LPNHE, Sorbonne Université, Paris Diderot Sorbonne Paris Cité, CNRS/IN2P3, Paris; France.
- ¹³⁶Department of Physics, University of Pennsylvania, Philadelphia PA; United States of America.
- ¹³⁷Konstantinov Nuclear Physics Institute of National Research Centre "Kurchatov Institute", PNPI, St. Petersburg; Russia.
- ¹³⁸Department of Physics and Astronomy, University of Pittsburgh, Pittsburgh PA; United States of America.
- ^{139(a)}Laboratório de Instrumentação e Física Experimental de Partículas - LIP;^(b)Departamento de Física, Faculdade de Ciências, Universidade de Lisboa, Lisboa;^(c)Departamento de Física, Universidade de Coimbra, Coimbra;^(d)Centro de Física Nuclear da Universidade de Lisboa, Lisboa;^(e)Departamento de Física, Universidade do Minho, Braga;^(f)Universidad de Granada, Granada (Spain);^(g)Dep Física and CEFITEC of Faculdade de Ciências e Tecnologia, Universidade Nova de Lisboa, Caparica; Portugal.
- ¹⁴⁰Institute of Physics of the Czech Academy of Sciences, Prague; Czech Republic.
- ¹⁴¹Czech Technical University in Prague, Prague; Czech Republic.
- ¹⁴²Charles University, Faculty of Mathematics and Physics, Prague; Czech Republic.
- ¹⁴³Particle Physics Department, Rutherford Appleton Laboratory, Didcot; United Kingdom.
- ¹⁴⁴IRFU, CEA, Université Paris-Saclay, Gif-sur-Yvette; France.
- ¹⁴⁵Santa Cruz Institute for Particle Physics, University of California Santa Cruz, Santa Cruz CA; United States of America.
- ^{146(a)}Departamento de Física, Pontificia Universidad Católica de Chile, Santiago;^(b)Departamento de Física, Universidad Técnica Federico Santa María, Valparaíso; Chile.
- ¹⁴⁷Department of Physics, University of Washington, Seattle WA; United States of America.
- ¹⁴⁸Department of Physics and Astronomy, University of Sheffield, Sheffield; United Kingdom.
- ¹⁴⁹Department of Physics, Shinshu University, Nagano; Japan.
- ¹⁵⁰Department Physik, Universität Siegen, Siegen; Germany.
- ¹⁵¹Department of Physics, Simon Fraser University, Burnaby BC; Canada.
- ¹⁵²SLAC National Accelerator Laboratory, Stanford CA; United States of America.
- ¹⁵³Physics Department, Royal Institute of Technology, Stockholm; Sweden.
- ¹⁵⁴Departments of Physics and Astronomy, Stony Brook University, Stony Brook NY; United States of America.
- ¹⁵⁵Department of Physics and Astronomy, University of Sussex, Brighton; United Kingdom.
- ¹⁵⁶School of Physics, University of Sydney, Sydney; Australia.
- ¹⁵⁷Institute of Physics, Academia Sinica, Taipei; Taiwan.
- ^{158(a)}E. Andronikashvili Institute of Physics, Iv. Javakhishvili Tbilisi State University, Tbilisi;^(b)High Energy Physics Institute, Tbilisi State University, Tbilisi; Georgia.
- ¹⁵⁹Department of Physics, Technion, Israel Institute of Technology, Haifa; Israel.
- ¹⁶⁰Raymond and Beverly Sackler School of Physics and Astronomy, Tel Aviv University, Tel Aviv; Israel.
- ¹⁶¹Department of Physics, Aristotle University of Thessaloniki, Thessaloniki; Greece.
- ¹⁶²International Center for Elementary Particle Physics and Department of Physics, University of Tokyo, Tokyo; Japan.
- ¹⁶³Graduate School of Science and Technology, Tokyo Metropolitan University, Tokyo; Japan.
- ¹⁶⁴Department of Physics, Tokyo Institute of Technology, Tokyo; Japan.
- ¹⁶⁵Tomsk State University, Tomsk; Russia.
- ¹⁶⁶Department of Physics, University of Toronto, Toronto ON; Canada.
- ^{167(a)}TRIUMF, Vancouver BC;^(b)Department of Physics and Astronomy, York University, Toronto ON; Canada.
- ¹⁶⁸Division of Physics and Tomonaga Center for the History of the Universe, Faculty of Pure and

- Applied Sciences, University of Tsukuba, Tsukuba; Japan.
- ¹⁶⁹Department of Physics and Astronomy, Tufts University, Medford MA; United States of America.
- ¹⁷⁰Department of Physics and Astronomy, University of California Irvine, Irvine CA; United States of America.
- ¹⁷¹Department of Physics and Astronomy, University of Uppsala, Uppsala; Sweden.
- ¹⁷²Department of Physics, University of Illinois, Urbana IL; United States of America.
- ¹⁷³Instituto de Física Corpuscular (IFIC), Centro Mixto Universidad de Valencia - CSIC, Valencia; Spain.
- ¹⁷⁴Department of Physics, University of British Columbia, Vancouver BC; Canada.
- ¹⁷⁵Department of Physics and Astronomy, University of Victoria, Victoria BC; Canada.
- ¹⁷⁶Fakultät für Physik und Astronomie, Julius-Maximilians-Universität Würzburg, Würzburg; Germany.
- ¹⁷⁷Department of Physics, University of Warwick, Coventry; United Kingdom.
- ¹⁷⁸Waseda University, Tokyo; Japan.
- ¹⁷⁹Department of Particle Physics, Weizmann Institute of Science, Rehovot; Israel.
- ¹⁸⁰Department of Physics, University of Wisconsin, Madison WI; United States of America.
- ¹⁸¹Fakultät für Mathematik und Naturwissenschaften, Fachgruppe Physik, Bergische Universität Wuppertal, Wuppertal; Germany.
- ¹⁸²Department of Physics, Yale University, New Haven CT; United States of America.
- ¹⁸³Yerevan Physics Institute, Yerevan; Armenia.
- ^a Also at Borough of Manhattan Community College, City University of New York, New York NY; United States of America.
- ^b Also at Centre for High Performance Computing, CSIR Campus, Rosebank, Cape Town; South Africa.
- ^c Also at CERN, Geneva; Switzerland.
- ^d Also at CPPM, Aix-Marseille Université, CNRS/IN2P3, Marseille; France.
- ^e Also at Département de Physique Nucléaire et Corpusculaire, Université de Genève, Genève; Switzerland.
- ^f Also at Departament de Fisica de la Universitat Autònoma de Barcelona, Barcelona; Spain.
- ^g Also at Department of Applied Physics and Astronomy, University of Sharjah, Sharjah; United Arab Emirates.
- ^h Also at Department of Financial and Management Engineering, University of the Aegean, Chios; Greece.
- ⁱ Also at Department of Physics and Astronomy, University of Louisville, Louisville, KY; United States of America.
- ^j Also at Department of Physics and Astronomy, University of Sheffield, Sheffield; United Kingdom.
- ^k Also at Department of Physics, California State University, East Bay; United States of America.
- ^l Also at Department of Physics, California State University, Fresno; United States of America.
- ^m Also at Department of Physics, California State University, Sacramento; United States of America.
- ⁿ Also at Department of Physics, King's College London, London; United Kingdom.
- ^o Also at Department of Physics, St. Petersburg State Polytechnical University, St. Petersburg; Russia.
- ^p Also at Department of Physics, University of Fribourg, Fribourg; Switzerland.
- ^q Also at Department of Physics, University of Michigan, Ann Arbor MI; United States of America.
- ^r Also at Dipartimento di Fisica E. Fermi, Università di Pisa, Pisa; Italy.
- ^s Also at Faculty of Physics, M.V. Lomonosov Moscow State University, Moscow; Russia.
- ^t Also at Giresun University, Faculty of Engineering, Giresun; Turkey.
- ^u Also at Graduate School of Science, Osaka University, Osaka; Japan.
- ^v Also at Hellenic Open University, Patras; Greece.
- ^w Also at Horia Hulubei National Institute of Physics and Nuclear Engineering, Bucharest; Romania.
- ^x Also at II. Physikalisches Institut, Georg-August-Universität Göttingen, Göttingen; Germany.

^y Also at Institutio Catalana de Recerca i Estudis Avancats, ICREA, Barcelona; Spain.

^z Also at Institute for Mathematics, Astrophysics and Particle Physics, Radboud University Nijmegen/Nikhef, Nijmegen; Netherlands.

^{aa} Also at Institute for Particle and Nuclear Physics, Wigner Research Centre for Physics, Budapest; Hungary.

^{ab} Also at Institute of Particle Physics (IPP); Canada.

^{ac} Also at Institute of Physics, Academia Sinica, Taipei; Taiwan.

^{ad} Also at Institute of Physics, Azerbaijan Academy of Sciences, Baku; Azerbaijan.

^{ae} Also at Institute of Theoretical Physics, Ilia State University, Tbilisi; Georgia.

^{af} Also at LAL, Université Paris-Sud, CNRS/IN2P3, Université Paris-Saclay, Orsay; France.

^{ag} Also at Louisiana Tech University, Ruston LA; United States of America.

^{ah} Also at LPNHE, Sorbonne Université, Paris Diderot Sorbonne Paris Cité, CNRS/IN2P3, Paris; France.

^{ai} Also at Manhattan College, New York NY; United States of America.

^{aj} Also at Moscow Institute of Physics and Technology State University, Dolgoprudny; Russia.

^{ak} Also at National Research Nuclear University MEPhI, Moscow; Russia.

^{al} Also at Physics Department, An-Najah National University, Nablus; Palestine.

^{am} Also at Physikalisches Institut, Albert-Ludwigs-Universität Freiburg, Freiburg; Germany.

^{an} Also at School of Physics, Sun Yat-sen University, Guangzhou; China.

^{ao} Also at The City College of New York, New York NY; United States of America.

^{ap} Also at The Collaborative Innovation Center of Quantum Matter (CICQM), Beijing; China.

^{aq} Also at Tomsk State University, Tomsk, and Moscow Institute of Physics and Technology State University, Dolgoprudny; Russia.

^{ar} Also at TRIUMF, Vancouver BC; Canada.

^{as} Also at Universidad de Granada, Granada (Spain); Spain.

^{at} Also at Universita di Napoli Parthenope, Napoli; Italy.

* Deceased